GIS-BIM BASED REGIONAL SEISMIC RISK ASSESSMENT FOR DUBAI, UAE

by

Ahmed Mansour Maky

A Thesis presented to the Faculty of the
American University of Sharjah
College of Engineering
In Partial Fulfilment
of the Requirements
for the Degree of

Master of Science in
Civil Engineering

Sharjah, United Arab Emirates

May 2023

Declaration of Authorship

I declare that this thesis is my own work and, to the best of my knowledge and belief, it does not contain material published or written by a third party, except where permission has been obtained and/or appropriately cited through full and accurate referencing.

Signed……………………Ahmed Mansour Maky………………….

Date…………………………03 October 2023………………………………

Approval Signatures

We, the undersigned, approve the Masters Thesis written by: Ahmed Mansour Maky

Thesis Title: GIS-BIM Based Regional Seismic Risk Assessment For Dubai, UAE

Date of Defence: 23 May 2023

Name, Title and Affiliation	Signature
Dr. Mohammad AlHamaydeh Professor Department of Civil Engineering Thesis Advisor	
Dr. Ahmed El-Kady Lecturer in Structural Engineering Department of Civil Engineering, University of Southhampton Thesis Co-advisor	
Dr. Tarig Ali Professor Department of Civil Engineering Thesis Examiner (Internal)	
Dr. Ra'afat Abu-Rukba Assistant Professor Department of Computer Science Thesis Examiner (Internal)	

Accepted by:

Dr. Fadi Aloul
Dean
College of Engineering

Dr. Mohamed El-Tarhuni
Vice Provost for Research and Graduate Studies
Office of Research and Graduate Studies

Abstract

In the last two decades, the construction sector in UAE has been expanded to include a high range of tall and supertall buildings. Geographically, this region is surrounded by multiple earthquakes, such as the Zagros Fold and Thrust Belt. Additionally, the Makran Subduction Zone shows an activity source indicating a relatively high seismic risk. A similar situation motivated a research trend in China to simulate an earthquake on a city scale. The research objectives cover developing programming architecture to adapt to parallel computing concepts. Moreover, it targets creating simplified models that can indicate behavior key parameters with fewer DOFs. Both directions pushed into estimating the losses of the simulated hazard within moderate computers. However, the computational complexity of nonlinear simulations was not the only obstacle. The uncertainty in/among the problem modules; (ground motions intensity, structure simulations, damage analysis, and losses estimations) represents another significant concern. In 1995, the structural engineering community established performance-based engineering principles as a probabilistic design process instead of the traditional deterministic philosophy. Additionally, the Computational Modeling and Simulation Center (SimCenter) adopted this methodology into a software platform divided into microprograms. This architecture was designed to be generic to fit different problems according to the type of hazard, simulation, or data availability variation. In 2010, the Regional Resilience Determination (R2D) was released to provide a software package automating this methodology using a graphical user interface. A research plan is proposed to produce a step forward for realistic seismic simulation that includes the conclusion of previous studies and custom development for the UAE location. The objective is to produce an example of an end-to-end framework for seismic risk assessments that integrate with digital transformation trends such as Building Information Modelling (BIM) and the Geographic Information System (GIS). The scope of this investigation is a virtual dataset for RC tall buildings on a dense grid map that considers the variation in building location, material properties, building height, and seismic activity source.

Keywords: Seismic damage, High-fidelity structural model city-scale, Regional seismic, Parallel computing simulation, Tall buildings, Loss estimation, Nonlinear time history analysis.

Table of Contents

List of Figures

List of Tables

List of Abbreviations

ACI	American Concrete Institute
ANN	Artificial Neural Network
BIM	Building Information Modelling
BRAILS	Building Recognition using Artificial Intelligence at a Large Scale
C_d	Deflection Amplification Factor
CPU	Central Processing Unit
CTBUH	Council on Tall Buildings and Urban Habitat
CUDA	Compute Unified Device Architecture
DL	Damage Loss
DLL	Dynamic Link Library
DM	Damage Measures
DOF	Degree-Of-Freedom
DSN	Dubai Seismic Network
DV	Decision Variables
EDP	Engineering Demand Parameters
FE	Finite Element
GA	Genetic Algorithm
GIS	Geographic Information System
GPGPU	General-Purpose Computing on GPU
GPU	Graphics Processing Unit
GSHAP	Global Seismic Hazard Map Project
HPC	High-Performance Computer
HSC	High Strength Concrete
IDA	Incremental Dynamic Analysis
IFC	Industry Foundation Classes

IM	Intensity Measures
JSON	JavaScript Object Notation
MCS	Multistory Concentrated-Mass Shear
NHE	Natural Hazard Engineering
NHERI	Natural Hazards Engineering Research Infrastructure
NMFS	Nonlinear MDOF Flexural-Shear
NSF	The National Science Foundation
MDUES	Multidimensional Urban Earthquake Impact Simulation
MSE	Mean Squared Error
OPENSEES	Open System for Earthquake Engineering Simulation
PBED	Performance-Based Earthquake Design
PBEE	Performance-Based Earthquake Engineering
PC	Personal Computer
PEER	Pacific Earthquake Engineering Research Center
PGA	Peak Ground Acceleration
PGV	Peak Ground Velocity
POE	Probability of Exceedance
PRSA	Probabilistic seismic risk assessment
R	Response Modification Factor
R2D	Regional Resilience Determination
RC	Reinforced Concrete
SAM	Structural Analysis Model
SEAOC	Structural Engineers Association of California
SHA	Seismic Hazard Analysis
SimCenter	Computational Modeling and Simulation Center
SMRF	Special Moment Resisting Frames
SOE	System of Equations

SRSS	the square root of the sum of the squares
SSFI	Soil Structure Foundation Interaction
S_S	The mapped Maximum Considered Earthquake spectral response acceleration parameter at short periods
S_1	The mapped Maximum Considered Earthquake spectral response acceleration parameter a period of 1 second.
THA	Time-History Analysis
UBC	Uniform Building Code
UHPC	Ultra-High Performance Concrete
UI	User Interface
Ω_0	the System Over-strength Factor

Chapter 1: Introduction and Background

1.1 Introduction

In recent years, the real estate sector in UAE witnessed a significant development in the construction of tall buildings and iconic structures. Unfortunately, this area lacks data regarding seismic events and definitions of structural design considerations to be applied. Generally, the UAE is subjected to relatively high seismic risks, according to **Table 1** and **Figure 1**. Several studies indicate that, on average, three seismic events per year affect UAE based on observations from 2000-2006. For example, a moderate earthquake (M_b=5) shook a vast area in the North-East of UAE on March 11, 2002, and was accompanied by smaller foreshocks and aftershocks [1]. On November 27, 2005, and September 10, 2008, more complex earthquakes with magnitudes of M_b=5.9 and 6 started at the Qeshm Island region in the Hormozgan province of Southern Iran. Their impacts extended and were widely felt in Northern UAE, leading to the evacuation of some areas. In addition, two local earthquakes (with M_b=3.7 and 3.9) occurred in the Eastern region of UAE on March 10 and September 13, 2007, respectively. In 2018, a Seismic Hazard Analysis (SHA) study obtained many of UAE's geophysical parameters; PGA, soil type, geology, slope, and fault line distance [2].
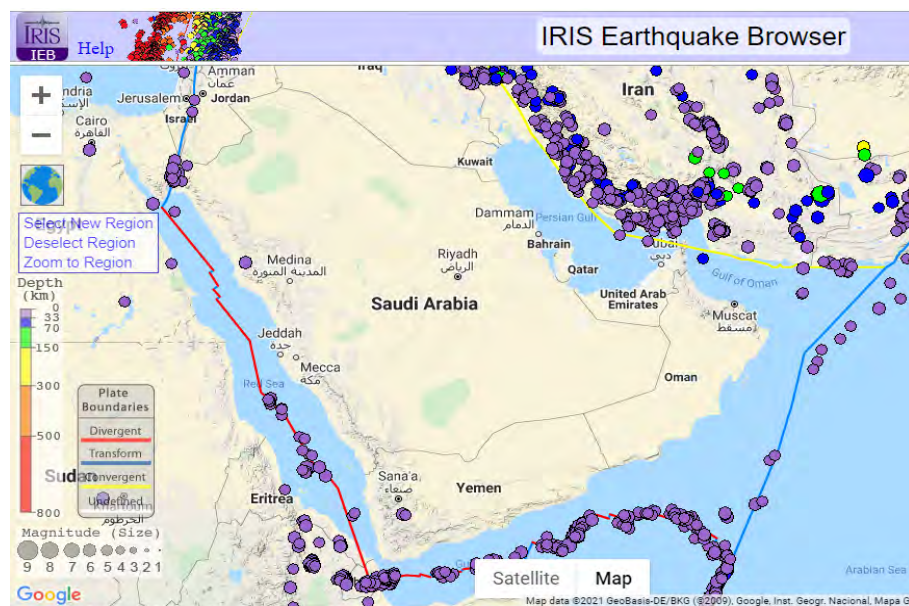
Figure 1: A map of Mb~4 to Mb~9 earthquakes in the Arabian plate since 1970 [3].

Table 1: The primary seismic risk sources in the UAE [4], [5].

Seismic Risk Source	Description
The Zagros Fold and Thrust Belt	A series of major blind thrust faults capable of generating $M_b\sim7$ earthquakes.
The Makran Subduction Zone	Shallow dipping seismic source ~6° that steepens to ~19° South of Iran's coastline. It produced an Ms=8 earthquake in 1945.
The Zendan-Minab Fault System	A complex faulting system was created by the Makran subduction zone joining the Zagros fold and thrust belt. It is capable of generating moderate/large earthquakes.
The Sabzevaran Jiroft Fault System	Has a similar seismogenic potential to the Zendan-Minab fault system, located further East.
Oman Mountains and the Dibba Line	A region is exhibiting features of faulting and a history of active tectonics. The 2002 Masafi earthquake originated in this region.
The West Coast Fault	Crosses the cities of Dubai and Abu Dhabi and passes very close to Ra's Al Khaymah. There is limited information about its activity (debatable existence).

This research aims to establish a robust, scalable, and intelligent framework for seismic risk assessment and damage estimation in some UAE regions/cities. Moreover, the framework will be compatible with trending civil engineering technologies: BIM and GIS. In addition, it will utilize the collected data in a machine-learning application. The concept of BIM was first introduced by a not-for-profit organization called **BuildingSMART**. It can simply be defined as a standard for proceeding with engineering projects, where there is a centralized data model instead of many files with different formats, and all project stages are reflected in it. This concept allows more collaboration among owners, designers, contractors, and stockholders. Moreover, it facilitates tracking of the project's progress, coordination, early clash detection, and facility management. Technically, **BuildingSMART** published Industry Foundation Classes (**IFC**) in an open international standard (ISO 16739-1:2018) format that can digitally describe the whole building assets. Additionally, it enables interoperability among different software. On the other hand, GIS is recognized as a framework for gathering, visualizing, and analyzing spatial data as an integration between geography science and data analysis. Many types of data are organized into multi-layers, then visualized into maps and 3D scenes. Analyzing data can better understand some patterns and allow for better decisions. GIS concepts were prolific for many engineering

problems, specifically infrastructure designs and urban planning. In smart/digital city simulations, the integrated GIS/BIM solutions retrieve and reuse vital data through each stage of the structure's life cycle. Thus, merging BIM and GIS data provides more efficient workflows and can be helpful on many scales, as explained in **Figure 2**. GIS data is necessary for planning operations regarding infrastructures, such as rail networks, airports, bridges, and roads. In post-construction, BIM models can provide specific data for GIS layers regarding building, facility management, and GIS visualization for 3D scenes. In this study, both BIM and GIS are used to provide data for seismic risk analysis as another application of GIS/BIM integration.
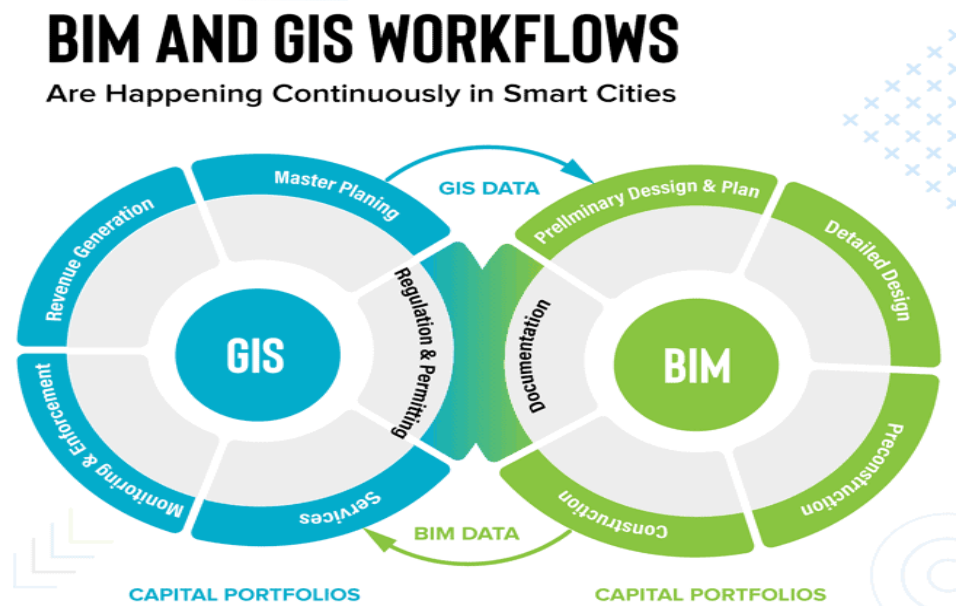
Figure 2: Benefits of GIS/BIM integration in smart cities [6].

1.2 Problem Statement

The UAE region represents a crucial case where a growing construction sector, including many mega and iconic buildings, is subjected to various distant and local earthquake sources, causing high seismicity levels. The main problem here is caused due to the wide diversity in estimating seismic levels, followed by an ambiguity among structure designers to agree on the design response spectrum. According to the Uniform Building Code (UBC'97), Dubai has been classified to be in zone zero (with no seismic requirements), with an estimated PGA, based on 475 years return period, of 0.15g. In 2013, the local authorities raised these requirements to zone 2B for buildings higher than nine stories and 2A for other buildings, based on Dubai Seismic Network (DSN).

Thus, some of the existing structures could be designed for underestimated seismic conditions.

Moreover, previous studies for this region mostly focused on comparing the performance of different structural systems using parametric studies of reference archetypes and earthquake records. However, a city-scale risk assessment study is urgently required to evaluate the effect of the previous variation regarding seismicity levels on the existing structures. But, in the meanwhile, regional seismic simulations have highly complex and computationally challenging problems. The aspects of complexity can be listed as follows:

- Data Collection: a dense amount of data is required to start this simulation. The required GIS data are for seismic resources and buildings' locations. Additionally, the attributes required for the adopted loss and damage analysis methodology. Usually, extensive work is required to build these databases from different resources and may be from different formats.

- Computational cost: The number of required nonlinear structural analyses equals the number of buildings multiplied by the number of seismic events. This number requires a huge computational capacity for storage and processing.

- Uncertainties: Conceptually, the structure performance can be assessed into four modules: hazard analysis, structure analysis, damage analysis, and loss analysis. According to this methodology, each module develops a certain margin of error, leading to accumulative expected error for outputted values.

1.3 Research Significance

The GIS-based risk assessment study for Dubai by [7] could be considered the first step in UAE regional simulations. Heavy work was included in the data collection aspect, where Dubai was divided into several neighborhoods, and the dominating usage classified each area. Also, the number of buildings in each neighborhood was estimated approximately according to the population density. However, a more profound methodology will be implemented in this research as another advanced step toward fully realistic city-scale simulation. Many significant changes are determined through all performance-based stages: hazard, structural, damage, and loss analyses. The research significance of the proposed study can be summarized as follows:

- An "Earthquake Scenario Simulation "will be performed for the hazard analysis stage instead of using reference records. This change would incorporate the effect of the location on the input ground motions for structural analysis. The region would be divided into 2D grids, and an input ground motion would be generated for each grid according to an earthquake prediction equation, as shown in **Figure 3**.

- A wider range of archetypes will be included in the structural analysis stage. Seventeen archetypes will be adopted with a high variation in building height from low-rise to high-rise (from single story to 50 stories) and other building properties, such as occupancy.

- Investigating calibrated models concept for the structural analysis to achieve simulations with personal computer capabilities. The MCS model will simulate low-rise and mid-rise archetypes, while the NFMS model will be utilized for high-rise buildings.

- Implementing PEER PBEE methodology and following HAZUS-MH 2.1 manual [8] to determine the collapse probability and DL parameters (like monetary loss and injuries) for included assets.
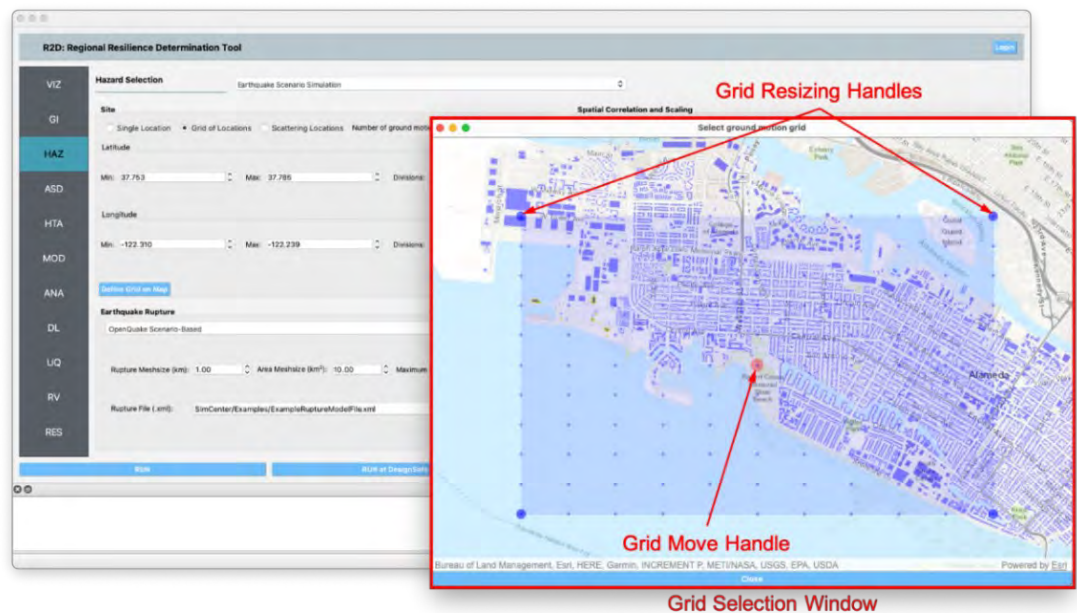
Figure 3: Earthquake scenario simulation based on a user-defined grid map.

1.4 Objectives

The main objectives of this research are:

1. Performing an **"Earthquake Scenario simulation"** to investigate the effect of asset location on the involved earthquake record based on ground motion prediction equations.

2. Development of an archetype building portfolio for Dubai, UAE, and associated special geographic distribution in a GIS-compatible format [GIS maps].

3. Perform a regional seismic simulation for the Dubai region that handles computational and uncertainties challenges.

4. Quantification of the expected losses in Dubai, UAE, under seismic hazard; Precisely, probability of collapse, economic losses for repair (or reconstruction), and expected injuries.

5. Identify critical building types, locations, structural types, and heights for various seismic hazard intensities.

1.5 Scope

The scope of the proposed research can be defined as follows:

1. The research is dedicated to estimating damage and losses due to seismic disasters only. Other risk resources not included like; wind, floods, .etc.

2. The study will be based in Dubai, so the collected GIS Buildings database is expected to reflect the demographic properties of this region. Also, the required "Earthquake Scenario Simulation" is limited to region location.

3. Seventeen reference buildings that vary according to height and occupancy were selected to reflect common structures in the region. Their properties are shown in **Tables 5** and **6**.

4. The R2D [9] software package will be utilized to perform a regional simulation. It utilizes Opensees [10] in nonlinear structure analyses, Dakota [11] for UQ modules, and HAZUS-MH 2.1 manual [8] for DL analyses and also contains an embedded package for "Earthquake Scenario Simulation."

1.6 Methodology

This research extensively reviews the literature about UAE seismicity, the effects of seismicity, performance-based earthquake engineering, and computing regional earthquake frameworks. The study's main aim is to perform a virtual example on a city scale using 17 reference models. The MCS model will be utilized for low-rise and medium-rise structures. The designed tall building models will be calibrated to an

equivalent NMFS model to facilitate several simulations within regular PC capabilities. The R2D [9] software package will be utilized to perform a GIS investigation. This package provides a GUI for an end-to-end regional earthquake framework that includes all stages of a PBED process. It will be used to perform an earthquake scenario simulation for each grid in the UAE region to select the most likely earthquake record. The primary outputs are the damage cost and probability of collapse for each asset in the virtual database. As shown in **Figure 4**, The workflow can be organized into three major phases;

- Earthquake scenario simulation: the studied region will be divided into grids, and an input ground motion will be assigned to each grid. Studied earthquake sources can be filtered according to the maximum distance and minimum and maximum magnitude. The ground motion record at each record is formulated from included resources based on a "Ground motion prediction equation" such as Abrahamson, Silva & Kamai (2014) [12].

- Assuming buildings database: many reference buildings should be selected according to the required variation. A high-fidelity FEM should be determined for nonlinear analyses. These archetypes will be distributed on the map to simulate neighbors' usage.

- Regional simulation: a nonlinear dynamic analysis will perform for each asset in the database by assigning the input ground motion in the closet earthquake grid. Then, damage and loss analysis will be performed to relate collapse probability, economic losses, and injuries to EDPs. All estimated data will be visualized in a GIS map to deduce relationships between building parameters and loss outputs.

Tables 2 and **3** demonstrate the parameters of adopted reference buildings, where the cost of archetypes was estimated according to [13]. They classified them into five Low-rise buildings, three Mid-rise buildings, and nine High-rise buildings. The detailed FE element model is required to deduct the MCS model for low-rise and medium-rise. Instead, a procedure was proposed by [14] to estimate the hysteresis parameters of each floor and implemented in R2D [9]. Three different elastic design response spectrums were selected to simulate ambiguity in defining seismicity level. These spectrums were defined by [15], and their key parameters are (S_s = 0.18 g, 0.42 g, and 1.65 g) and (S_1 = 0.06 g, 0.17 g, and 0.65g) for low, medium, and high seismicity levels. The chosen

models show a variation in structure systems, usage, and design seismic level according to the common types in the UAE region. On the other hand, a detailed FE is required to calibrate the NMFS model for high-rise buildings [16]. Nine tall buildings are assumed as commercial construction, with RC shear walls, for years from 2000 to 2010.
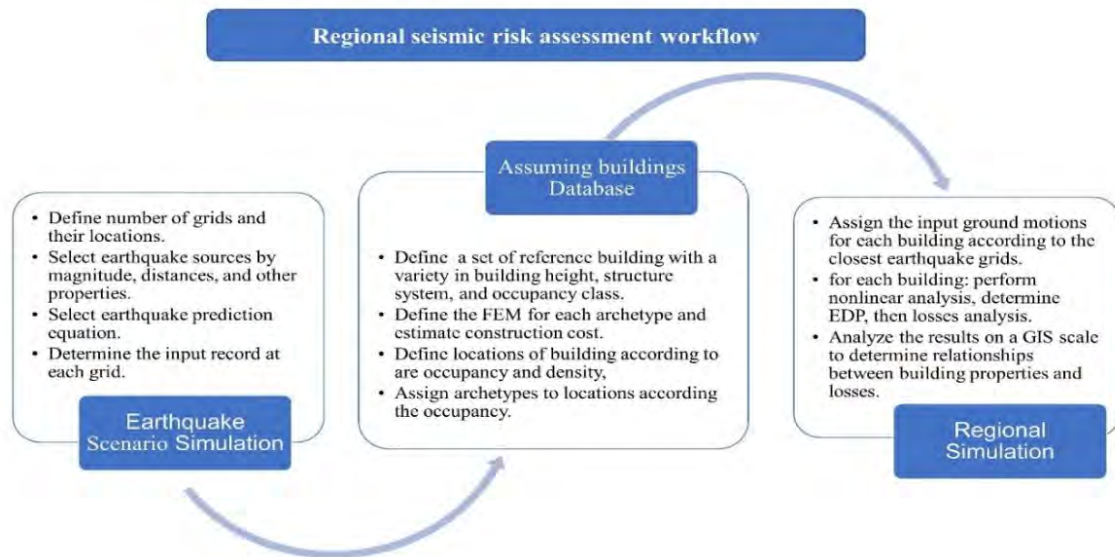
Figure 4: Flowchart for regional earthquake workflow.

Table 2: Parameters of low-rise and medium-rise archetypes.

Label	Number of Stories	Year built	Occupancy Class	Structure Type	Plan Area (Ft²)	Cost (AED K)	Seismic Level
LR_RES_F1	1	1981	RES1	RM1L	1615	675	Low
LR_RES_F2	2	1995	RES3	C1L	2690	2025	Low
LR_RES_F3	3	2000	RES3	C2L	4300	4850	Low
MR_RES_F5	5	2002	RES3	C1L	5382	14500	Middle
LR_COM_F3	3	1990	COM2	C1L	5920	7012	Low
MR_COM_F6	6	2005	COM1	C1L	5382	16120	Middle
MR_COM_F7	7	2010	COM1	C2L	5382	18805	Middle
LR_IND_F1	1	2003	IND2	S1L	10764	4500	Middle

NOTE: RES refers to Residential Occupancy; RES1 is for a single-family and RES3 is for multiple families. COM refers to Commercial Occupancy; COM1 and COM2 are for Retail Trade and Wholesale Trade. IND2 means light industrial factory. RM1L, C1L, C2L, and S1L are representing Reinforced Masonry Bearing Walls, Concrete Moment Frames, Concrete Shear Walls, and Steel Moment Frames for structure types.

Table 3: Parameters of high-rise archetypes.

Label	Number of Stories	Cost (AED)	Year built	Material properties Fc' (MPa)	Fy (MPa)	Plan Area (Ft²)	Seismic Level
HR_ COM _F10	10	58485					
HR_ COM _F15	15	87727	2000	50	420		
HR_ COM _F20	20	115970					
HR_ COM _F25	25	146211					
HR_ COM _F30	30	175454	2005	60	420	9685	High
HR_ COM _F35	35	204696					
HR_ COM _F40	40	233939					
HR_ COM _F45	45	263181	2010	70	500		
HR_ COM _F50	50	292423					

NOTE: The occupancy class is COM4 and the structure type is C2L for all high rise archetypes .COM refers to Commercial Occupancy; COM4 is for Professional/Technical Services. C2L are representing structures with Concrete Shear Walls.
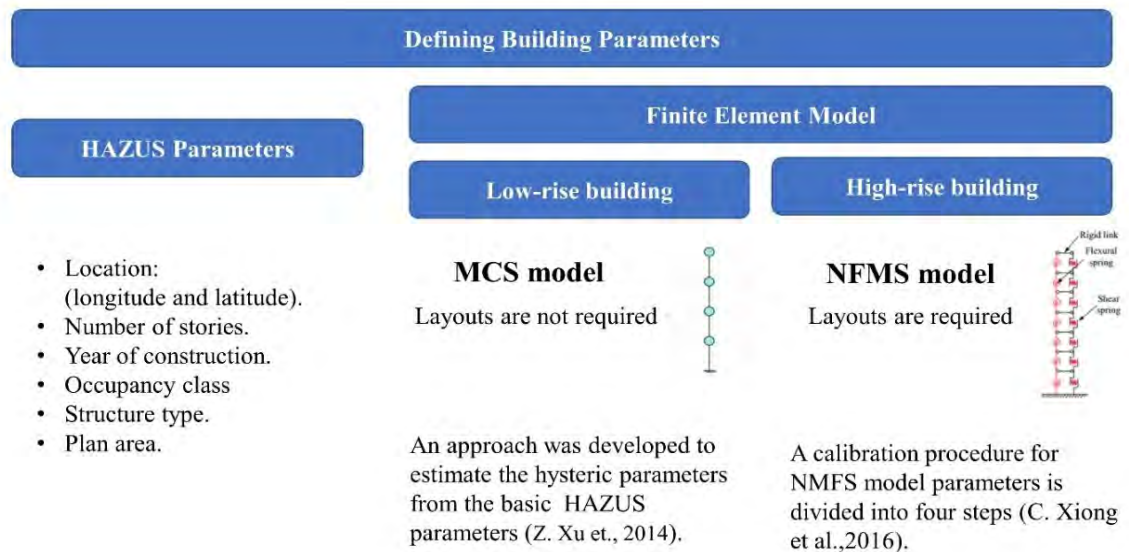
Figure 5: Flowchart for the required data to define a building.

The reference buildings will be distributed in Dubai neighbors according to the usage and population density, and these data are available and published by [7]. The selected earthquake records for each grid will be selected according to the scenario simulation component in R2D [9]. A series of regional simulations will be executed for a differently designed model. The outputs can be represented in the form of GIS maps

for collapse probability and economic loss. According to the parameters of total height and shear wall strength, these maps will be a heuristic reference for designers. This research will represent a first-step stage of regional simulations in UAE, where the distant goal is to collect and digitalize an actual building inventory database.

1.7 Thesis Organization

The thesis is organized into six chapters, described as followings:

- **Chapter 1: Introduction.** Presents a general introduction of the research background, importance, main objectives, scope, and methodology.

- **Chapter 2: Literature Review.** Provides an extensive review of accomplished research studies for performing regional simulations and overcoming computational obstacles. Additionally, it includes a brief description of performance-based earthquake engineering and the uncertainty in Dubai Seismicity.

- **Chapter 3: Design of Tall Buildings Archetypes.** It provides the applied loads' definitions and the resulting designed section for all structural elements.

- **Chapter 4: Calibrating NMFS Models for Tall Buildings Archetypes.** Describes the process of calibrating NMFS models from the designed archetypes. Also, it provides the properties of calibrated models and the accuracy in their pushover results relative to the FE models.

- **Chapter 5: GIS Databases for Building, Ground Motions, and Risk Assessment Results.** Presents the properties of included building and ground motions databases, the assumptions used to generate these data, and the final generated results and maps.

- **Chapter 6: Conclusions and Recommendations.** It contains a summary of regional results and the effects of building properties on the damage and loss estimation outputs.

Chapter 2: Literature Review

2.1 Challenges and Research Aspects

Since the beginning of 2010, there have been approximately 120 super high-rise buildings higher than 300 m, based on a statistic inventory by CTBUH. This survey included either completed or under-construction tall buildings and obtained that they are mainly located in regions with rapid economic development, namely: China, UAE, and the USA (there are 47 in China, 28 in the UAE, and 18 in the USA). However, most developing cities are threatened by severe seismic disasters. This risk created a critical and motivational need to develop a scientific prediction of seismic damage platform, providing early warning of potential seismic risks. The main challenges were; (1) achieving precise flexural-shear deformations for each building with efficient computational techniques that could consume limited time, practical computational demand, and storage resources, and (2) implementing a performance-based engineering framework that includes all uncertainties and probabilistic inputs and present stakeholders' outputs like injuries and economic losses. The following paragraphs contain the progress achieved by several studies on related objectives, such as implementing a more brilliant programming architecture to minimize computational costs; developing simplified numerical models to accurately reflect the inter-story earthquake damage with fewer DOFs.

2.2 GPU-Based High-Performance Computing

Generally, computers have two main processing units, the CPU and the GPU. The essential, fast, and versatile processing component is the CPU. It is composed of a few cores with lots of cache memory that can handle some software threads at a time. In contrast, the GPU was originally designed for high-performance computer graphics visualization, costing much less than a traditional CPU platform. Although the performance of a single GPU core is relatively weak compared to a CPU core, the total parallel and float computing capabilities of the GPU are much higher. The GPU contains hundreds of cores that break complex problems into thousands or millions of separate tasks and work them out at once. Thus, the concept of GPGPU was subsequently proposed to perform high-performance computing tasks in addition to visualization. In 2006, NVIDIA Corporation released CUDA, a GPGPU platform. It depends on utilizing the CPU for serial processing and GPU for parallel processing.

This innovation significantly reduced programming difficulties and enhanced its computational performance. As shown in **Figure 6**, the CUDA processing flow is: (1) Copy data from main memory to GPU memory, (2) CPU initializes the GPU compute kernel, (3) GPU's CUDA cores execute the kernel in parallel, and (4) Retrieve results from GPU memory back into main memory. The computing capacity of each GPU core is relatively weak, and the data exchange between different GPU cores is very time-consuming. This makes the flow only suitable for some tasks having specific characteristics: (1) the computing task can be divided into many relatively short subtasks, (2) each subtask has a moderate computing workload and can be individually implemented on a single GPU core, and (3) different subtasks do not require data exchange throughout their life-cycle.
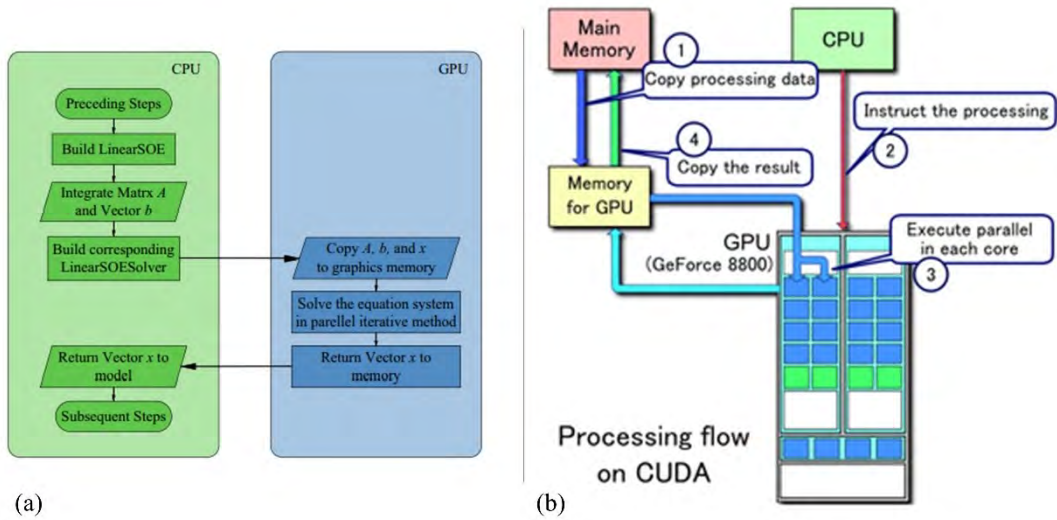
Figure 6: Typical processing flow on CUDA [17].

Although OpenSees [10] is a well-known computational tool that has been widely used in earthquake engineering research, it is not computationally efficient in cases of tall and supertall buildings [10]. For large structures with hundreds of DOFs, a nonlinear time-history analysis is very time-consuming (may take several weeks to complete), and most of this time is consumed by SOE solving. For this scale of structures with beam and shell elements, the stiffness matrix, mass matrix, and damping matrix (if the classical Rayleigh damping is adopted) usually exhibit significant sparse characteristics. Although, the existing framework of OpenSees implements three sparse SOEs: SuperLU SOE, UmfPack SOE, and SparseSYM SOE. Direct methods, such as triangular and elimination decomposition, are integrated into these solvers. However, these methods are not suitable for GPU-based parallel computing. In 2016, a GPU-

based SOE solver, named CuSP solver, was developed to be compatible with the existing software architecture [17] . This development was based on: (1) Using iterative algorithms, such as the conjugate gradient (CG) algorithm, Bi-CG algorithm, and generalized minimal residual (GMRES) algorithm. These algorithms can be implemented in a parallel processing logic; (2) Building a solver class that inherits from the LinearSOESolver class of OpenSees. The kernel algorithm of the solver is packaged in a DLL form to achieve compatibility. The corresponding scripts of CuSP are provided as obtained herein [18]. A case study was conducted to compare the performance of a CPU-based solver to a GPU-based solver with almost the same price for Hardware platforms. Two benchmark models were selected. The first was the Building 2N model, a 141.8 m height model based on a frame-core tube building. It contained 23,945 nodes, 23,024 fiber-beam elements, and 16,032 multi-layer shell elements. The second model was 632 m in height, called the Shanghai Tower model. It contained 53,006 nodes, 48,774 fiber-beam elements, and 39,315 multi-layer shell elements. The study included performing THA, adopted from the El-Centro EW ground motion, with 1000 cm/s^2 and 400 cm/s^2 PGA values for the Building 2N and Shanghai Tower models, respectively. Results of the speed-up ratios indicated that using the two GPU-based solvers is up to 9–15 times faster than using the CPU-based solver.

Logically, seismic damage simulation for a dataset of buildings can be a suitable task for a GPGPU processing workflow if each building is a subtask and is simulated with macro models (e.g., concentrated-mass story model). In this case, the application will meet the previously mentioned characteristics as the computing workload of each subtask is sufficiently small for a single GPU core. Additionally, there should be little interaction between different buildings during an earthquake. A program architecture was developed for this problem [19]. Its main concept was utilizing the parallel computing capacity of GPU for the nonlinear time-history computing of individual buildings. Moreover, the CPU was used for data reading, computational tasks, and copying data between the two memories inside the CPU and GPU. Also, the communication between the CPU and GPU was reduced to prevent communication delays. The efficiency of this procedure was measured and compared to the default CPU processing flow with a similar price platform. The inputted test case was 100 six-story buildings with the same parameters. The bilinear hysteretic model was selected for the inter-story hysteretic model, and the nonlinear contained 8000 steps. In conclusion, when a single building is computed, the CPU computing time is 7% of the GPU

computing time. Such a result is expected because of the difference in performance between a single CPU core and a single GPU core. However, as the number of buildings increases, the CPU computing time increases significantly, corresponding with a less increase in GPU computing time due to parallelization. As a result, when 1000 buildings are computed, the GPU computing time can be 1/40 of the CPU computing time.

2.3 High-Fidelity Computational Models for Earthquake Disaster Simulation of Tall Buildings

The collapse simulation of complex buildings can be achieved based on the FE method using the proper element models, constitutive material laws, and elemental-failure criteria. For example, a study for collapse simulation of the Shanghai Tower subjected to extremely strong earthquakes was conducted by [20]. Shanghai Tower, located in Lujiazui, Shanghai, is a multi-functional office building containing 124 stories and is ranked as the second tallest building globally. The total height of the central tower is 632 m, while its structural height is 580 m. The structural design implemented a hybrid lateral-force-resisting system named "mega-column/core-tube/outrigger."
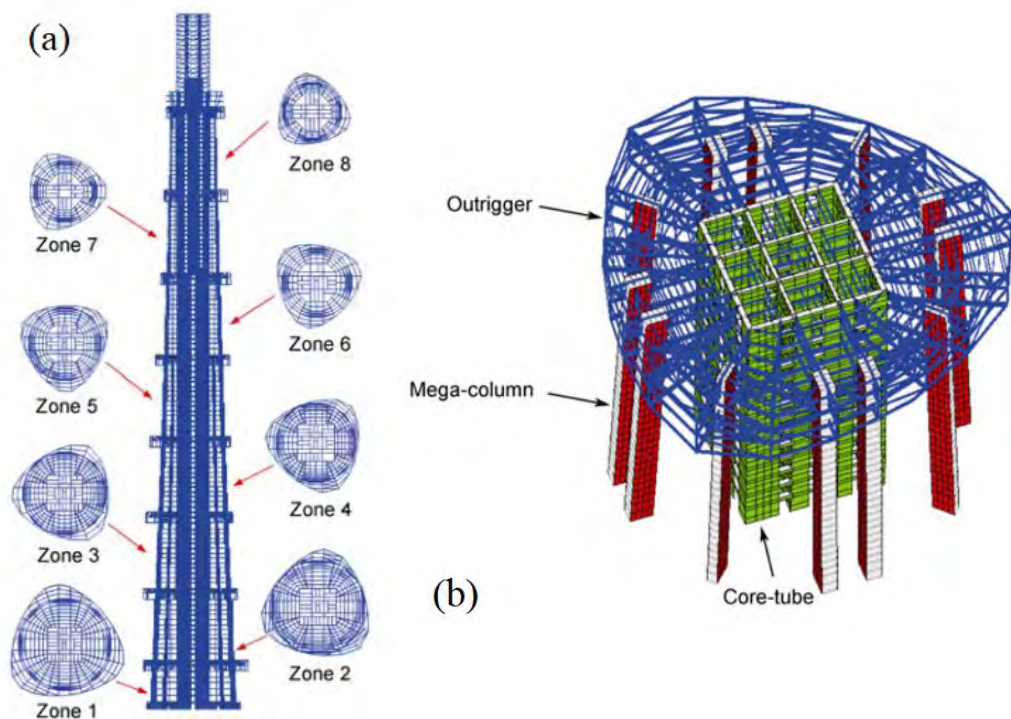
Figure 7: (a) The whole FE model of Shanghai Tower [20]; (b) Sketch of the lateral-force-resisting system of Shanghai Tower.

The multi-layer shell element prototype, shown in **Figure 8** (a), was adopted to model the core-tube RC walls, which is based on the principles of mechanics of composite materials. It is made up of layers with different thicknesses and material properties, allowing it to simulate coupled in-plane/out-of-plane bending. This is typically accompanied by in-plane direct shear and coupled bending-shear behavior of RC shear walls. The internal forces of the shell element can then be calculated, following the constitutive material laws, by integrating the stresses of different concrete and steel layers, as explained in **Figure 8** (b). This model accurately represents nonlinear behavior in RC shear walls through well-defined constitutive laws of concrete and steel. In OpenSees, a new high-performance flat shell element NLDKGQ is developed [21]. It consists of a planar membrane element GQ12 and a plate-bending element DKQ. The GQ12 element has two translational (along x- and y-axes) and one rotational (around the z-axis) DOFs per node, while the DKQ element has one translational (along the z-axis) and two rotational (around x- and y-axes) DOFs per node. The combination of these two elements results in 6 DOFs per node in an NLDKGQ element, as explained in **Figure 8** (c). Consequently, the NLDKGQ elements can be readily connected to the beam elements without resorting to the extra embedded beam elements, significantly reducing the modeling workload.
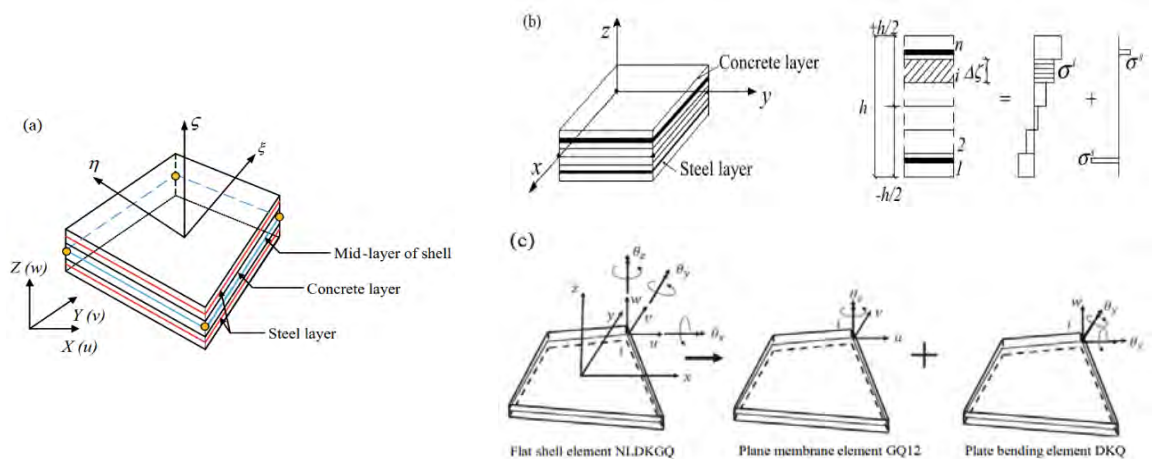
Figure 8: NLDKGQ element developed by [21]: (a) A 4-node shell element with multi-layer section; (b) Stress variations in concrete and steel layers in the multi-layer shell element; (c) Degree of freedoms of the NLDKGQ element in the local coordinate system.

The external frame and outriggers are simulated using a fiber-beam element model, which is capable of simulating the axial-flexural coupling behavior of RC

frames. Each fiber has its uniaxial constitutive law, and all the fibers in the same section follow the "plane section" assumption. Each cross-section segment (i.e., the flange and web) is divided into nine fibers to ensure computational accuracy. Conversely, this model cannot be accurate for mega-columns because their dimensions are so large that they go far beyond the general conception of columns. As shown in **Figure 9** (a), the designed section for mega-columns is nearly 20 m^2 with a steel ratio of 6.22% and a reinforcement ratio of 1.16%, which significantly confines the mechanical behavior of the concrete. The concrete, shaped steel, and rebar were modeled for a detailed FE model using hexahedral solid elements, quadrilateral shell elements, and truss elements. Despite the high fidelity of the detailed FE model, its computational workload is very time-consuming for implementing solid elements. Another approach, a simplified model with much fewer DOFs, is adopting multi-layer shell elements combined with truss elements. The concrete, the rebar distributed along the Y-direction, and the web of the shaped steel were modeled using multi-layer shell elements. However, the shaped-steel flange and the rebar distributed along the X-direction were modeled using truss elements. The accuracy of the simplified model approach was validated through various numerical simulations study of the mega-columns under pure compression, pure bending, bending with compression in one direction, biaxial direction, *etc.* Subsequently, this study proposed using the simplified model of the mega-columns in the global structural seismic response analysis.
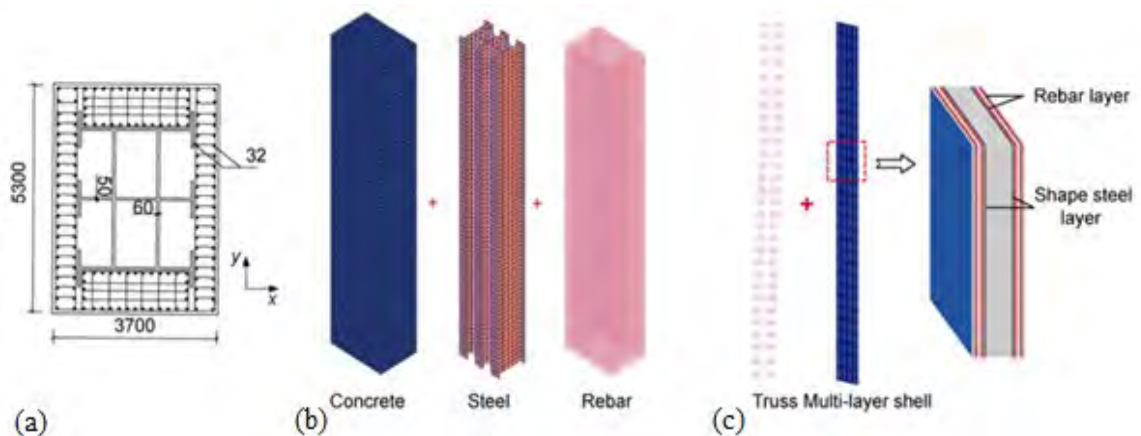
Figure 9: Typical cross-section of mega-column with detailed and simplified FE models: (a) Typical cross-section of mega-column (unit: mm); (b) Detailed FE model of mega-column; (c) Simplified FE model of the mega-column.

2.4 Simplified Models for Earthquake Disaster Simulation of Multiple Scales Buildings

The high-fidelity FE model integrates the fiber-beam elements for beams/columns and multi-layer shell elements for shear walls/core tubes. Furthermore, it enables an accurate simulation of the entire collapse process of tall and supertall buildings with sufficient adaptability. It requires a considerable workload and computational recourses, causing practical constraints in its usability. To address this issue, simplified models have great potential to facilitate academic research and practical applications. Such models can represent buildings' critical nonlinear and dynamic characteristics whilst being computationally effective. Selecting the simplified model is unequivocally based on the lateral drift mode of the original model. Usually, the shear deformation is common for moderate multistory buildings, while tall buildings are subjected to flexural-shear deformation mode.

In the case of shear mode lateral drift, the MCS model is a multi-degree-of-freedom model that can accurately calculate the local damage to different stories. Lu-Qu's model is used as a hysteretic model to represent inter-story behavior [19]. The calibration process (explained in **Figure 10**) is mainly about setting hysteric model parameters to achieve a matching nonlinear cyclic pushover with the typical FE model. As a practical procedure within an urban area, buildings can be divided into different classes according to their structural types and building properties. Then, one MCS model can be identified for each class. Furthermore, a 6-story RC frame building was a benchmark for investigating the accuracy of the MCS model. THA was performed using the widely known El Centro record with a 600 cm/s^2 PGA for refined FE and calibrated MCS models. Results showed an excellent agreement respecting the displacements of each story subjected to base shear or time history (**Figure 11**). The method explained in **Figure 11** requires an undefined number of trials to adjust the hysteric parameters, which could be highly time-consuming for an urban area study of thousands of buildings. Thus, an approach was developed to estimate the hysteric parameters from the basic building information (i.e., number of stories, height, year built, structural type, floor area, and occupancy) and the HAZUS database. It provided good accuracy and high computational efficiency in several studies such as;[14], [22].
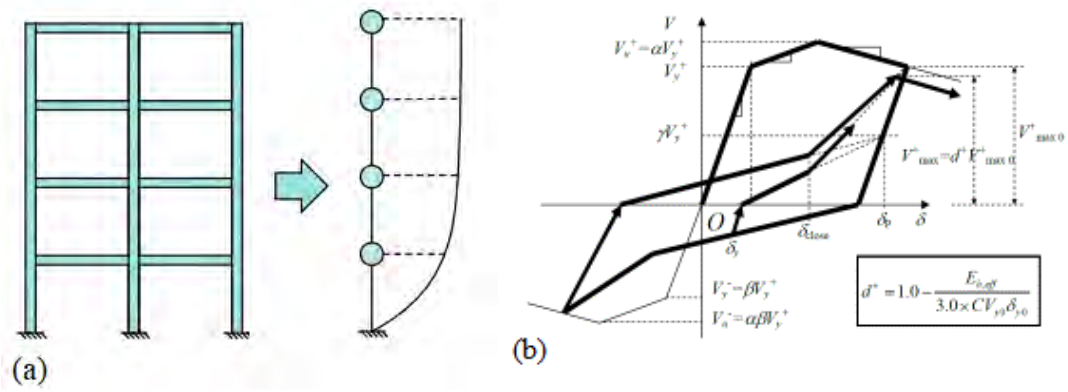
Figure 10: (a) The multistory concentrated-mass shear model for a building; (b) The inter-story hysteretic model [19]
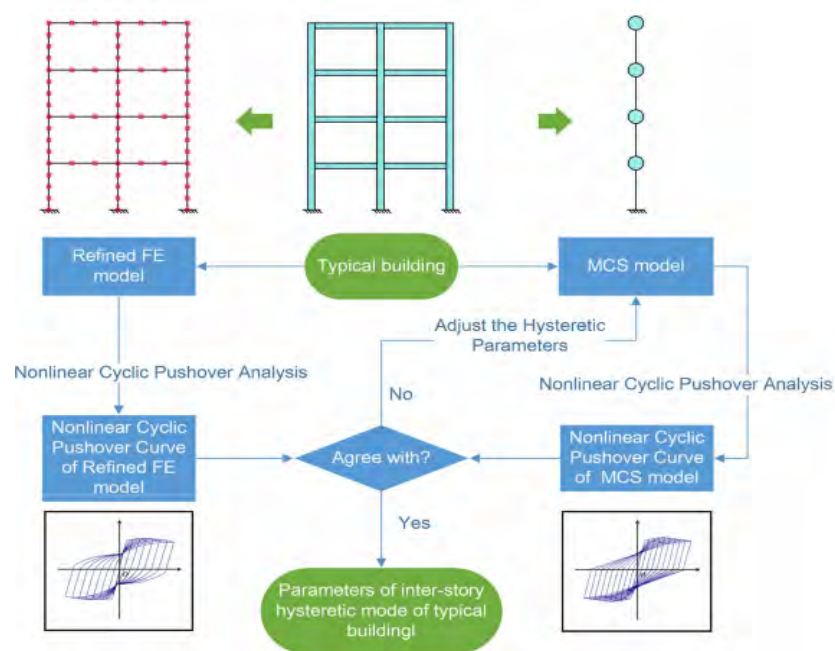
Figure 11: Method for determining the parameters of the hysteretic model in selected typical buildings [22].

Most super tall buildings depend on hybrid systems for lateral loads, resisting mega column-core, tube-outrigger systems, and mega-braced frame-core tube systems. The deformation modes of these structural systems are typically a combination of flexural deformation and shear deformation. The flexural-shear coupling elastic continuum model ("flexural-shear model" for short hereafter) was proposed to predict the seismic responses and dynamic characteristics with fewer computational resources [23]. As shown in **Figure 14**, the model consists of a flexural and a shear cantilever beam representing respectively flexural and shear components of structural

deformations. A finite number of axially rigid links are added, connecting both beams to ensure lateral deformation compatibility at the same story height. Also, partial differential equations were used to describe the dynamic response of this model under a ground motion acceleration.
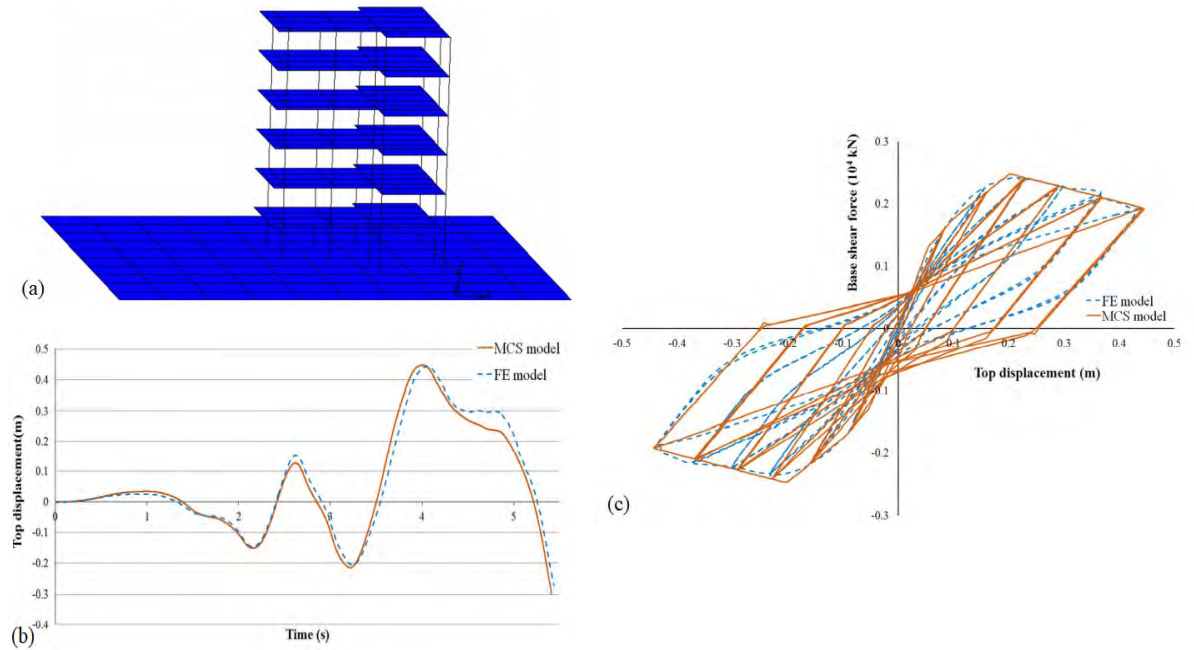
Figure 12: Validation of MCS model in comparison to refined FE model [22]: (a) Refined FE model of the 6-story RC frame building; (b) Top displacement versus time histories predicted by the FE and MCS models; (c) Lateral hysteretic behavior of the FE and MCS models in the bottom story.

The Shanghai Tower model is used to validate the accuracy of the flexural-shear model in predicting the elastic seismic responses. The cross-sections of the core tube and the mega columns reduce almost linearly from the bottom to the top. Linear varying mass distribution is assumed in the simplified model. Performing modal analysis on both models confirmed the reliability of the flexural-shear model in reporting the basic dynamic properties. **Figure 13** compares both models regarding the first vibration periods in the x-direction, where the error of the simplified model can be neglected.

The nonlinear MDOF flexural-shear (NMFS) model was proposed by [16] to simulate the nonlinear behavior and damage on different building stories. Instead of continuum flexural and shear beams in the flexural-shear model proposed by [23], each story was discretized into nonlinear shear and flexural springs explained in **Figure 14** (a). The NMFS model was originally developed to simplify RC frame-shear wall structures and standard hybrid lateral resistance systems and was widely used for

33

designing tall buildings. The shear spring represents the shear deformation mode resulting from RC frame behavior. Similarly, the flexural spring represents the flexural deformation mode resulting from shear walls. Following the elastic continuum model, rigid links are used at each story level for lateral deformation compatibility. They recommended adopting bi-linear and tri-linear backbone curves (**Figure 14** (b)) for flexural and shear springs.
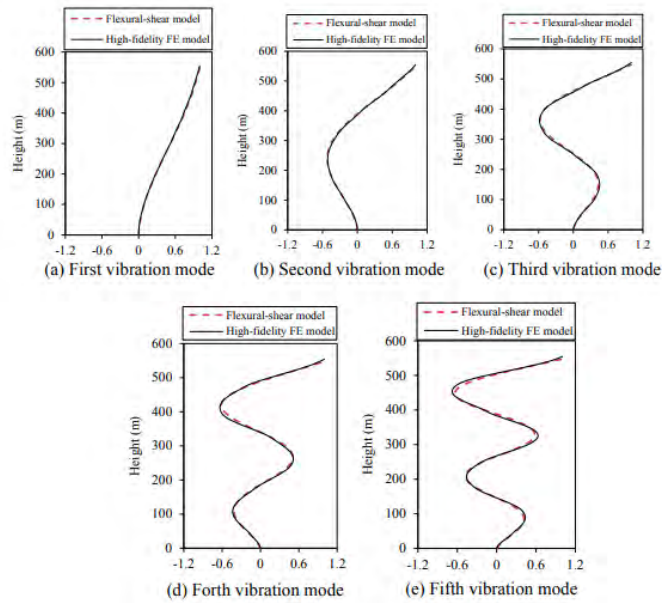
Figure 13: The first five vibration modes of the Shanghai Tower [23].
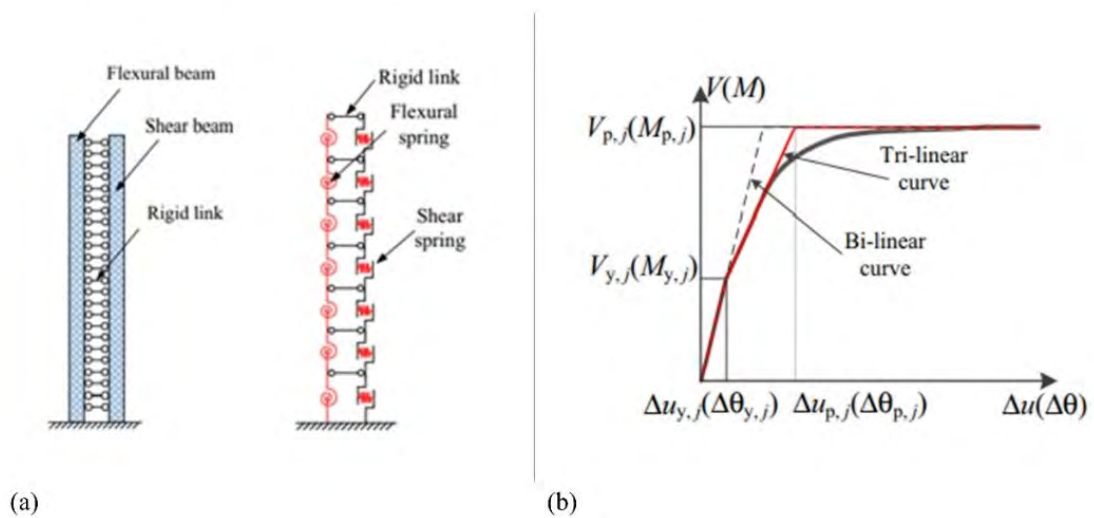
Figure 14: (a) Comparison of the elastic continuum [23] and nonlinear flexural-shear models [16]; (b) Bi-linear and trilinear backbone curves of HAZUS

The proposed calibration procedure for NMFS model parameters is illustrated in **Figure 15**, and it is divided into four steps: Calibration of the elastic parameters, calibration of the yield point, calibration of the peak point, and calibration of the hysteretic parameter.
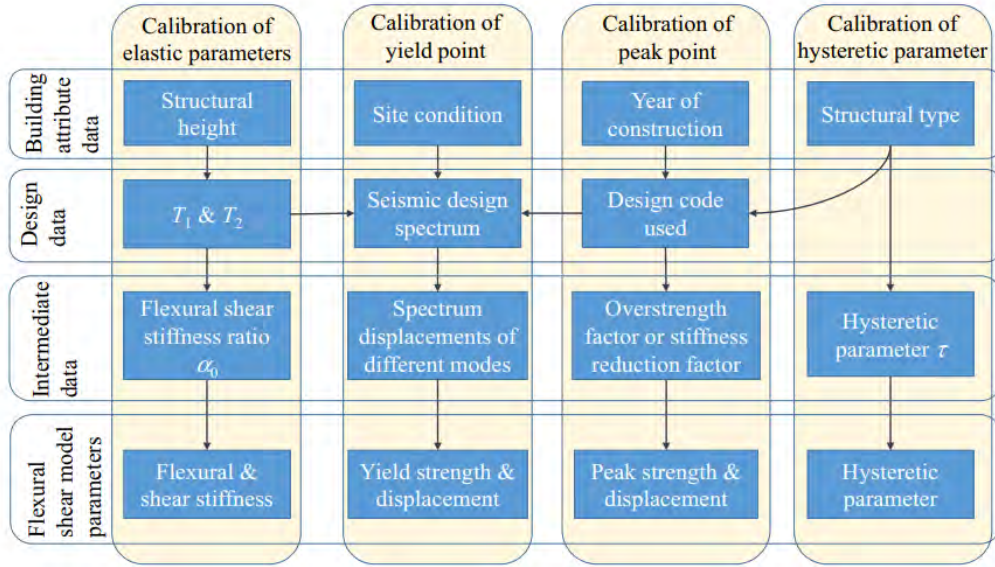
Figure 15: Calibration Process for NMFS model [15].

Two tall buildings are included to validate the calibration process. Three NMFS models are established and calibrated for both buildings. Then, their seismic responses are compared with those of the refined FE models. Buildings A and B are a 15-story RC frame-shear wall structure and a 42-story RC frame core-tube structure. The refined FE models of the two buildings (shown in **Figure 16**) are established using the general-purpose FE software MSC.MARC. The nonlinear analysis included 22 earthquake records (recommended by FEMA-P695). Bi-linear curves calibrate the NMFS-Bi model, and the NMFS-Tri-η model behavior is assumed with Trilinear curves, while the stiffness reduction method ($\eta = 0.7$) is used for peak point calibrations. In addition, the ductility factor method ($\mu = 4$) is adopted for the NMFS-Tri-μ model. The results of all these models compared to the detailed FE model are represented in **Figure 17**.
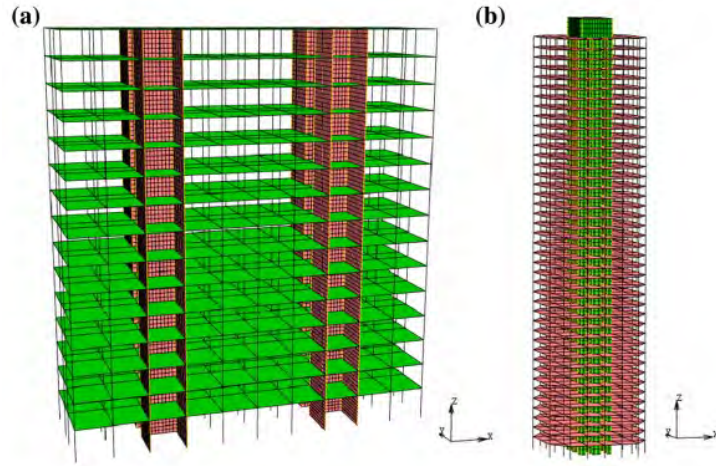
Figure 16: Benchmark models for simplified NMFS model calibration by [15]: (a) Building A (a 15-story RC frame-shear wall); (b) Building B (a 42-story RC frame core-tube structure).
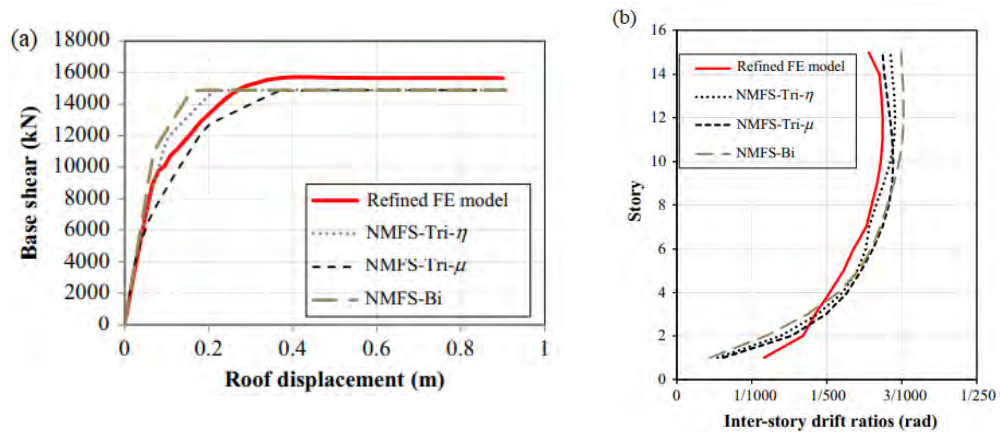
Figure 17: Nonlinear analysis results of Building A for Refined FE, NMFS-Bi, NMFS-Tri-η, and NMFS-Tri-μ models by [15]: (a) Base shear-roof displacement pushover curves of Models; (b) Inter-story drift ratios of Models.

2.5 Performance-Based Earthquake Engineering (PBEE)

After the consequences of the 1994 Northridge and 1995 Kobe earthquakes, structural designers started to adopt performance-based engineering concepts instead of the traditional deterministic specifications. The traditional philosophy is bounded by two primary variables: earthquake intensity and corresponding damage for structural and non-structural elements. The acceptance criteria are preventing low-intensity damage, only repairable damage in medium-intensity, and preventing a collapse in high-intensity earthquakes.

In 1995, The Structural Engineers Association of California (SEAOC) published its PBEE Vision 2000 report, which is considered the most remarkable document for the first-generation PBEE in the USA. It defines a framework for performance-based earthquake design (PBED) by selecting the desired system performance at various earthquake intensity levels, as shown in **Figure 18**. Seismic hazard intensity can be described as frequent, occasional, rare, or very rare events. Moreover, the system performance levels are classified as fully operational, operational, life safety, and near collapse. The design objective is determined based on the private property owners, e.g., residential or commercial buildings, or by the public resiliency requirements, e.g., hospital buildings. Additionally, other subsequent documents of first-generation PBEE, e.g., FEMA-356 [24], introduced a similar framework with different descriptions for hazard levels and system performance. Despite the conceptual progress, this framework has several shortcomings related to the system performance estimation; (1) The structure analysis procedure determines the engineering parameters, but the uncertainties in the numerical model are not considered. (2) The element performance is defined by a deterministic relationship with the engineering measures. These relationships can be calibrated from experimental tests or analytical models without a probability distribution. (3) The overall system performance is assumed to be equal to the worst performance of any component.
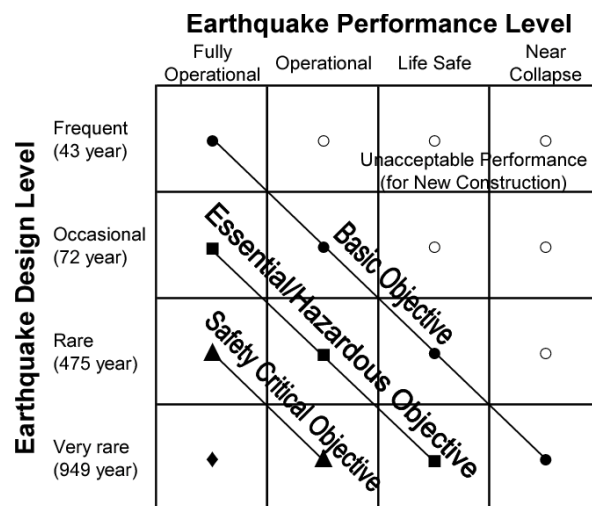
Figure 18: SEAOC Vision 2000 [25] recommended seismic performance objectives for buildings.

The Pacific Earthquake Engineering Research Center (PEER) developed a more robust methodology fitting the complex, multi-disciplinary nature of the problem and

overcoming the deficits of earlier PBEE methods. Unlike first-generation PBEE frameworks, estimating the system performance includes variables that reflect the direct interests of various stakeholders, such as monetary loss, repair duration, and casualties. System performance assessment is based on a rigorous probabilistic framework consisting of four logical, sequential components: hazard analysis, structural analysis, damage analysis, and loss analysis, as shown in **Figure 19**. Many publications have summarized and explained PEER methodology, such as [26]–[28].

The hazard analysis considers earthquake sources and facility characteristics to evaluate ground motion Intensity Measures (IM). It requires selecting nearby faults and collecting their descriptions, i.e., source-site distance, magnitude-recurrence frequencies, and fault mechanism. The facility data is defined in two terms: the location (O) and design characteristics (D), i.e., the fundamental period of vibration and foundation type. Engineering seismology relationships, such as ground motion prediction equations, are employed to quantify desired variables from these inputs, including issued uncertainties. The Intensity Measures variables might be Peak ground acceleration (PGA), peak ground velocity (PGV), spectral acceleration at the period of the first mode (Sa(T1)), spectral shape, and ground motion durations. The next generation will include a higher range of data variety, less dispersion, and more confidence in expecting shaking intensity. The hazard curve shows hazard analysis results by plotting the selected Intensity Measures versus their mean annual frequency (MAF) of exceedance [29]. These results can be transformed to IM versus POE (Probability of Exceedance) in "t" years by using Equation ((1) for the Poisson model, as shown in **Figure 19**.

$$p(IM) = 1 - e^{-\lambda(IM)t}$$
((1)

Where $\lambda(IM)$ is the annual frequency of exceedance of IM, and t can be considered as the duration of the facility life cycle.

After quantifying IM variables, the next step is to perform structural analysis to indicate structure responses for these ground motions. This process involves developing a computational model, performing nonlinear simulations, and calculating EDPs. This step's uncertainty is from the numerical model parameters such as mass, stiffness, strength, .etc. Generally, EDPs characterize the response in terms of deformations, accelerations, induced forces, or other appropriate quantities. Also, EDPs can be

determined for local structural components or overall building behavior. For a structural component, element forces (i.e., axial and shear forces) and plastic deformations (i.e., rotations and deflections) are examples of practical EDPs. The global building behavior can be described in EDPs such as inter-story drift, floor velocity, floor acceleration, roof drift, .etc. Global EDPs can indicate damages for different damageable components (both structural and non-structural elements). For example, inter-story drifts measure structural system damage [30], while floor acceleration is used for non-structural equipment, e.g., office or laboratory buildings [31]. PEER developed the incremental dynamic analysis (IDA) procedure to investigate the relationship between ground motions intensity and structural simulations. This procedure is based on repeating structural simulations with scaling input ground motions. The resulting series of values can establish statistical relations between IM and EDP or the POE of EDP at a certain given IM. The results of structural analysis can be summarized as the determination of probability distribution functions (PDFs) of EDP (e.g., EDPj) for a given IM (e.g., IM), as shown in **Figure 19**. The number of PDFs equals α multiplied by β, where α is the number of IM data points and β is the number of considered EDPs.

Damage Measures (DM) are the quantitative variables describing the physical damage to structural and non-structural elements and contents. These measures can be related to given EDPs through the damage analysis conditional probability relationships. Conditional relationships can be calibrated by experiment results or previous earthquake reconnaissance reports. PEER continuously develops conditional probability relationships for different components by collecting previous test data or performing other experiments. This procedure requires defining damageable groups, as each group includes facility parts that are similarly affected by certain EDP. For example, Bohl [32] proposed a methodology for damage analysis of a steel moment frame building. It considered 16 damageable groups; the structural system, exterior enclosure, drift-sensitive and acceleration-sensitive non-structural elements, and office content on each floor. Multiple DMs levels describing the type of required repair for a damageable group should be defined. For example, the three DMs levels of structural elements defined by [33] are light, moderate, and severe (or collapse). They respectively represent repair with epoxy injections, repair with jacketing, and element replacement. A single EDP value cannot be mapped deterministically into a certain DM level because this value can occur in different structural response scenarios and with

different behaviors. Instead, any DMs level can occur according to this value but with different probabilities. Fragility curves are established to show the variations in POE of all defined DMs in different EDP values, as shown in **Figure 19**.
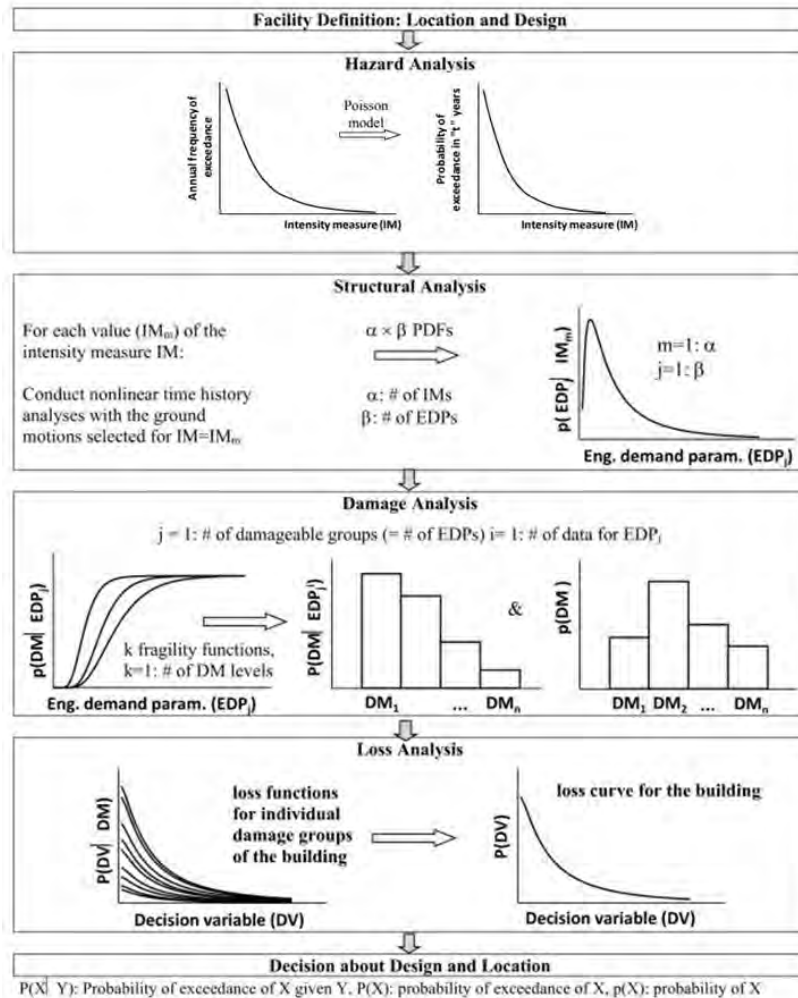
Figure 19: Analysis stages of PEER PBEE methodology [34].

The last step of the PEER PBEE methodology is the loss analysis to estimate Decision Variables (DVs). These variables reflect the direct interests of various stakeholders in the design. Some of the DVs are economic loss, repair duration, and the number of fatalities and injuries. A loss function is determined to calculate the POE of the losses for different damageable groups at different DMs. The total number of loss functions required for a facility is γ multiplied by λ, where γ and λ are the number of DMs and damageable groups, respectively. The accumulative loss curve can be calculated based on the total probability theorem. The probability of the nth value of the DV is according to Equation ((2) in the form of a triple summation.

$$p(DV^n)$$

$$= \sum_m \sum_i \sum_k p(DV^n|DM_k)\, p\big(DM_k|EDP_j^i\big) p\big(EDP_j^i|IM_m\big) p(IM_m)$$

((2)

The structural engineering community started to realize the impact of the PBEE methodology. It was included in several benchmark studies such as [30], [31], [35].

2.6 Open-Source Packages for Regional Earthquake Simulations

The Computational Modeling and Simulation Center (SimCenter)[36] develops many software tools specialized for natural hazard engineering (NHE) problems. The main goal is to provide an application framework for researchers to use, build, and extend scientific workflows for natural hazard simulations. This framework implements integrated relationships among three units; model, scientific workflow, and application. The model is a conceptual component with a particular role or analysis procedure. Practically, each model can be simulated by many software applications. However, a workflow is a collection of models integrated into a sequence to automate multi-step solutions. This approach requires developing pre- and post-processors for existing applications for data parsing. The end-user can customize the workflow by selecting the in-use application for each model depending on the nature of the problem, available input format, and the required specifications. Finally, the SimCenter application is defined by a workflow as a backend package connected with a wrapping frontend User Interface (UI). The purpose of UI components is to define workflow applications and their parameters, generate input file(s), and present output results. The architecture of the SimCenter application framework, shown in **Figure 20**, has an intelligent design because it considers the following principles: the architecture is designed as a modular framework to integrate with external applications or datasets. This feature can save the repeating work of an existing application and guarantee futural scalability and interoperability. For example, the SimCenter team developed pre-and post-processors to benefit from existing applications such as OpenSees [10], OpenFOAM [37], and PEER Strong Ground Motion Databases [38]. Moreover, they developed additional applications and linked them with the framework, such as Building Recognition using AI at Large-Scale (BRAIL) [39], to automate collecting building inventory data.

A scientific workflow was proposed to provide an open-source platform and a standard architecture for solving regional hazard simulations and loss estimation problems [14]. Conceptually, the workflow is divided into a sequence of modules, where each is determined to provide resulting data based on defined inputs. This design allows for future developments or enhancements in modules. It could also smoothly replace proposed applications with others, under the condition of preserving the format of inputs/outputs used in other models. The source code is published into the GitHub hosting platform. Some applications, programmed in C++ or Python, are provided for each module, while the data exchange through workflow modules is saved in JSON format.
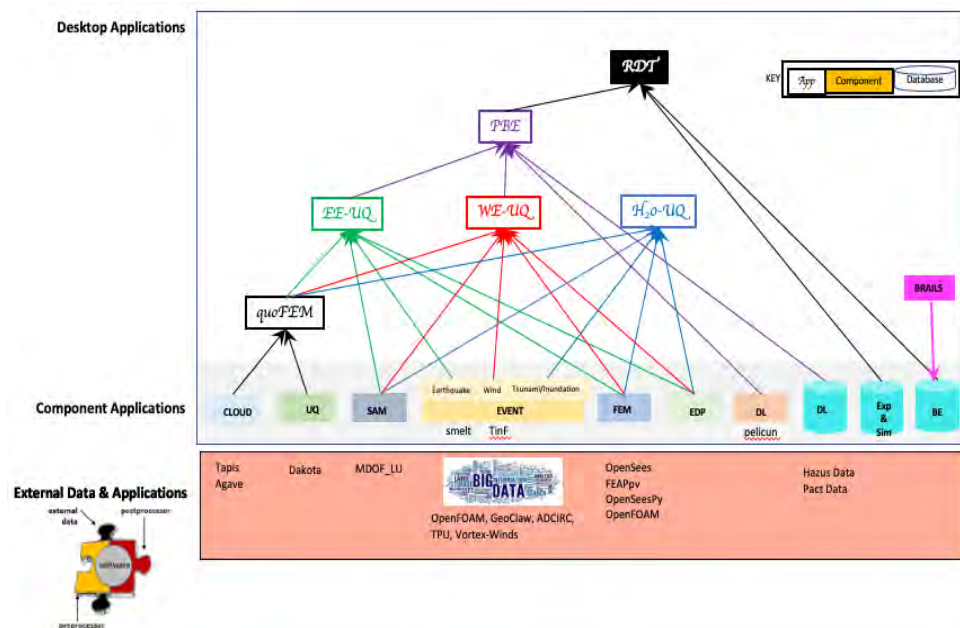
Figure 20: The architecture of the SimCenter application framework [36].

The definition of inputs, outputs, primary function, and available applications for each module, as well as the assumptions considered, are briefly plotted in **Figure 21** and explained as follows:

(1) Create Building Information Model (BIM): This module aims to create JSON files for each model that contains properties required in other modules. The definition of the BIM model requires the building's integer ID, name, floor area (in square feet), height (in feet), number of stories, location, replacement cost, replacement time, occupancy (residential, retail, office, .etc.), and structural type (W1, S1, C1, .etc.).

42

(2) Create Event: This module contains applications that can provide a separate input event file, such as ground motions records, concerning the location of the building. SHA-GM is a seismic hazard analysis application that depends on user-defined ground motion prediction equations and ground motion records databases. It provides ground motions over a grid of sites, in which each building is then assigned to ground motions at the nearest grid selected by the nearest neighbor algorithm.

(3) Create Structural Analysis Model (SAM): This module is meant to provide a structural model to perform THA analysis. MDOF_LU is a program developed to achieve this function. It maps buildings' properties to MCS models assuming the mass per unit area equals 1000 kg/m^2. The Tri-linear backbone curve is adopted to simulate inter-story behavior. The critical parameters of Trilinear curves are selected based on HAZUS technical manual recommendations (Table 5.7 and Table 5.5) for certain structural types and the number of stories.

(4) Create Engineering Demand Parameters (EDPs): EDPs include the maximum inter-story drifts, the floors' absolute accelerations, and residual displacements. These parameters can be determined by corresponding to node IDs defined in the SAM file.

(5) Perform Simulations: This means reading a SAM file, creating an OpenSees model, performing THA analysis, and setting the required EDP. For the previously mentioned procedure of the MCS model and earthquake events, the OpenSeesSimulation program can be used for processing this module.

(6) Create Damage Loss (DL): The primary function is determining the damage states (defined by HAZUS: slight, moderate, extensive, and complete) and the cost of replacement/repair of each building. FEMA_P58_LU is a damage and loss assessment tool that Prof. Xinzheng Lu's research group developed at Tsinghua University based on the FEMA-P58 methodology. As explained in **Figure 22**, this procedure assumes a conditional probability where the damage state corresponds to the determined EDP using fragility curves. Then, the repair cost is defined by a look-up table. This procedure is described in Chapters 3 and 7 of [40].
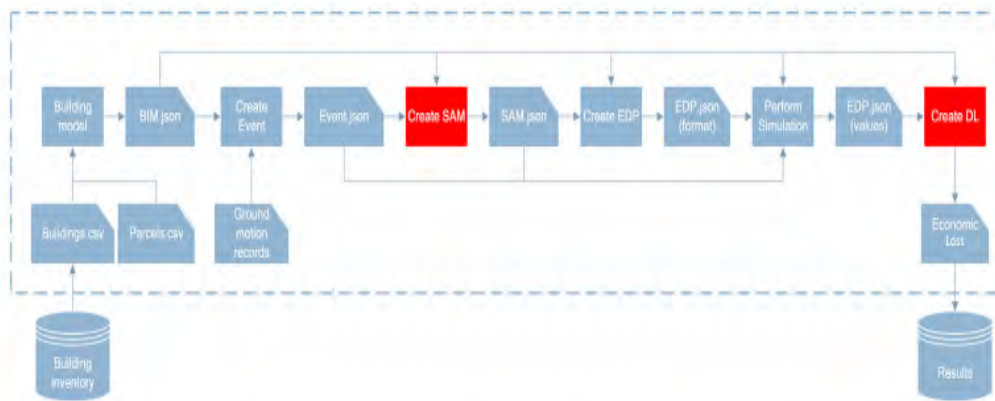
Figure 21: Scientific workflow for regional earthquake simulations [14].
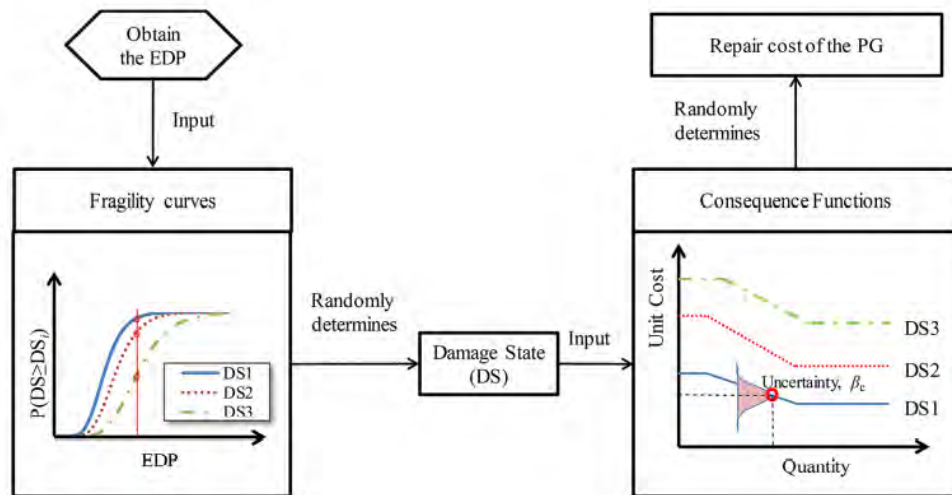
Figure 22: Estimating repair cost for a building component using the FEMA-P58 methodology [14].

On January 13, 2021, the SimCenter team released the first version of the Regional Resilience Determination R2D tool [9], which is a graphical user interface for the SimCenter application framework. It facilitates the process of defining studied events, building databases, and visual representations of maps and resulting DL ratios through integration with ESRI-ArcGIS SDK libraries, shown in **Figure 23**. The application was designed with an architecture of two components: frontend UI and backend applications. The front end was developed using the cross-platform QT framework to generate user inputs in the local machine. However, the backend is an application workflow written in C++ or Python that processes the critical analysis on a remote server (HPC utilizing resources available through DesignSafe). This design utilizes cloud computing concepts, particularly for large sets of data that require specific

44

computational resources and cannot fit with available PC potentials. The user manual, downloading source configurations, and solved examples are available on their website [9], [36].
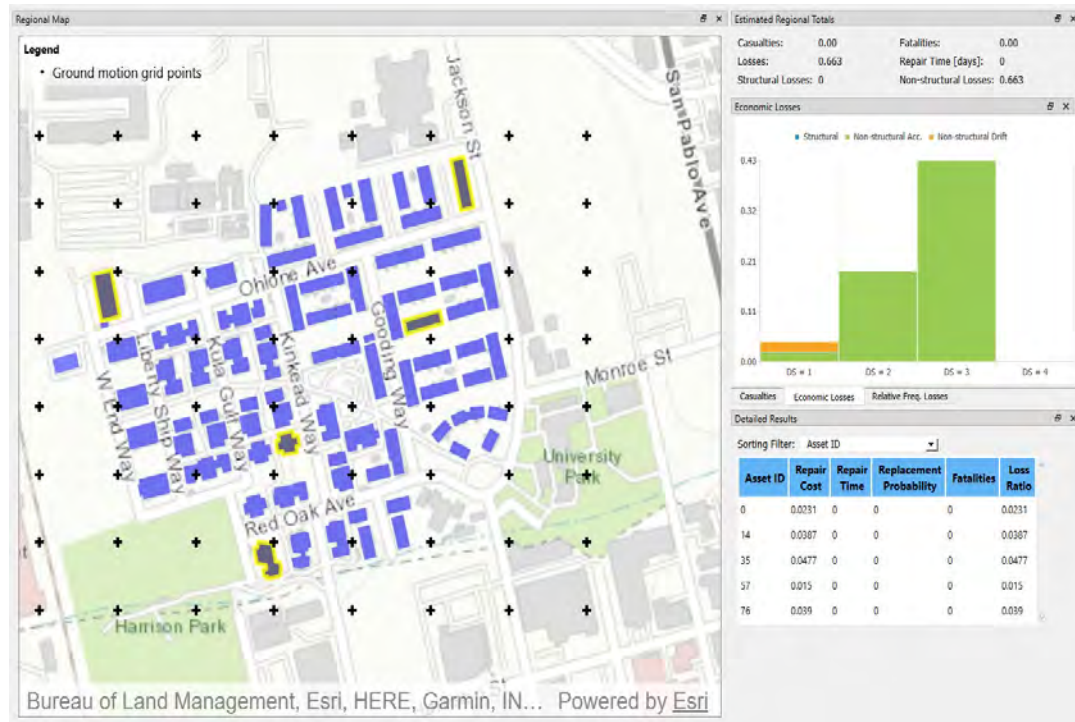
Figure 23: UI and results visualization of R2D tool [9] .

2.7 Examples of Applying Analysis to Urban Regions or Cities

A regional earthquake analysis was applied by to a medium-sized city in China called Shantou. The El Centro 1940 earthquake ground motion was implemented as a reference to perform THA on 7,449 buildings, and the MCS model was adopted for FE analysis. The results are represented in **Figure 24**, where the damage states are categorized into five sections (i.e., none, slight, moderate, extensive, and complete) as indicated in HAZUS [8]. Computationally, this required only 10 minutes in the processing environment of an i5 processor, 2.8 GHz, and 4-GB memory, which indicates the practical efficiency of the MCS model.
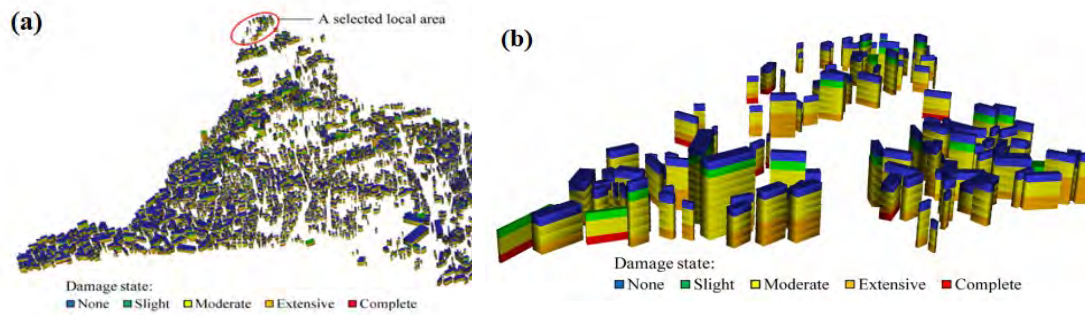
Figure 24: Regional earthquake analysis of Shantou city by [22]; (a) Buildings damage simulation (b) Seismic damage to buildings of a selected local area.

SimCenter workflow for regional seismic loss estimation [14] was applied on 1.8 million buildings (81% are single-story residential units and 17.3% are 2-story units) in the San Francisco Bay Area. The MCS was adopted for numerical modeling and for performing simulations for the M 7.0 Hayward Fault earthquake scenario. The map in **Figure 25** represents the distribution of estimated loss ratios for all buildings separated into five ranges. Results showed that 7.5% of the buildings are predicted to have a loss ratio greater than 60%. Single-story wood structures built before 1973 represent 62.6% of this sector. Based on this study, the computational efficiency can be considered acceptable since it consumed about three days using three moderate computers (with Inter(R) Xeon(R) CPU E5-2630 v3 @2.40 GHz).
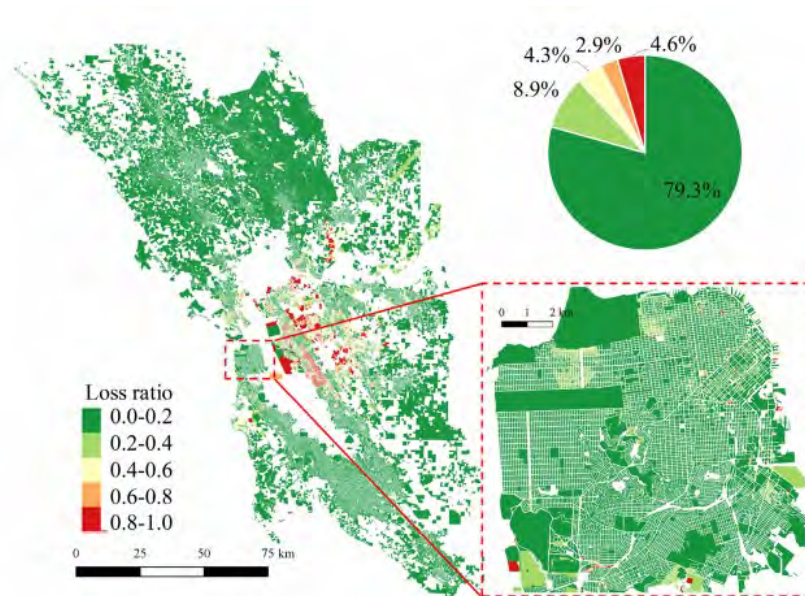
Figure 25: Buildings loss ratios distribution in the Bay Area of San Francisco [14].

Nine tall buildings and two medium-rise RC frame buildings (details in **Table 4** and **Figure 26**) were selected to perform a regional simulation using the proposed NMFS model [41]. Also, El-Centro EW ground motion with PGA = 400 gals is adopted as a reference event for performing THA. Using a desktop computer with resources of 2.67-GHz Intel Xeon X5650 CPU and 48 GB of 1333-MHz DDR3 and RAM, the analysis process took only 261 CPU seconds to prove the importance of the NMFS model.
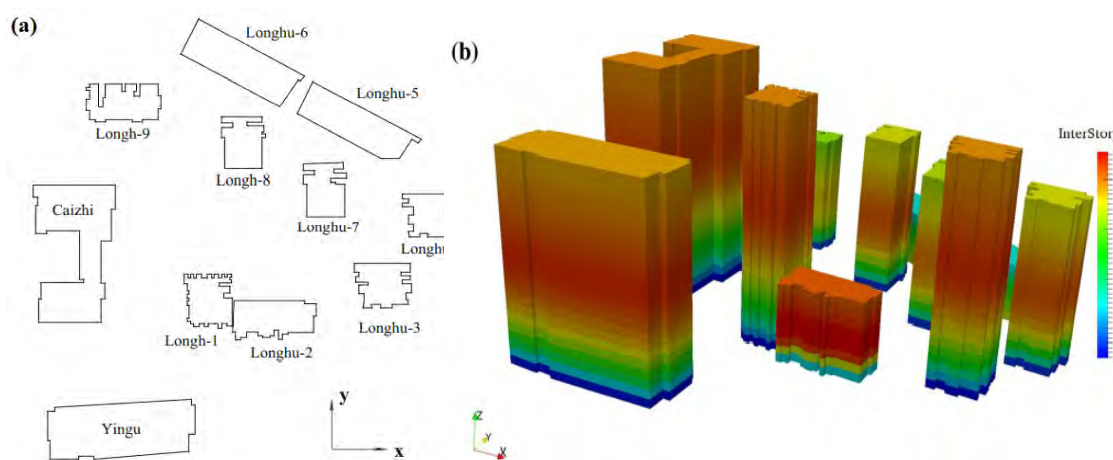
Figure 26: Regional earthquake study [16] : (a) 2D-GIS plan of buildings; (b) inter-story drift ratios at t =10 s.

Table 4: Inventory of buildings included in the regional study [16].

Label	Name of building	Number of stories	Height (m)	Site condition	Year of construction	Structural type
1	Yingu	23ss	92	Class II	2000	RC frame-shear wall
2	Caizhi	28	112	Class II	1998	RC frame-shear wall
3	Longhu-1	27	108	Class II	2010	RC frame-shear wall
4	Longhu-2	9	36	Class II	2010	RC frame-shear wall
5	Longhu-3	25	100	Class II	2010	RC frame-shear wall
6	Longhu-4	19	76	Class II	2010	RC frame-shear wall
7	Longhu-5	7	28	Class II	2010	RC frame
8	Longhu-6	7	28	Class II	2010	RC frame
9	Longhu-7	18	72	Class II	2010	RC frame-shear wall
10	Longhu-8	19	76	Class II	2010	RC frame-shear wall
11	Longhu-9	15	60	Class II	2010	RC frame-shear wall

These are just a few examples of the latest research in regional earthquake risk assessment. The field is constantly evolving, and new methods and tools are being developed all the time. As a result, it is important to stay up-to-date on the latest research to make informed decisions about earthquake risk mitigation. here are some of the latest journal papers on regional earthquake risk assessment in the last three years:

- In 2023, Sianko et al. [42] presented a framework for probabilistic seismic risk assessment (PRSA) for the city of Adapazari, Turkey. The framework is based on a Monte Carlo simulation approach, and it incorporates seismic hazard, vulnerability, and exposure models. The framework is used to assess the risk of earthquake damage for different return periods. The study also found that the risk of earthquake damage is not evenly distributed across the city. The most vulnerable areas are those that are located near active faults and those that have older, less seismically resistant buildings. The results of this study can be used to inform decision-making about earthquake risk mitigation in Adapazari. The study suggests that there is a need to focus on reducing the risk of earthquake damage in the most vulnerable areas of the city.

- In 2022, M.J. Smith et al. [43] published research describing a comprehensive earthquake hazard and risk assessment study program for the Canterbury region of New Zealand. The study includes the identification and characterization of earthquake sources, probabilistic hazard assessment, and formulation of earthquake scenarios.

- In 2022, a multidimensional urban earthquake impact simulation (MDUES) platform was developed by C. Hsu et al. [44]to simulate the dynamic seismic response of buildings and the damage they may incur due to earthquakes in urban areas. The platform was used to simulate an earthquake scenario in Taipei City, Taiwan. The results of the simulation showed that the earthquake-induced dynamic seismic response of buildings varied depending on their location and structural characteristics. The risk of building damage was also calculated, and the results showed that some buildings were more vulnerable to damage than others.

- In 2021, R. Adhikari et al. [45] presents a seismic risk assessment for Nepal that integrates seismic hazards with social vulnerability. The study uses OpenQuake

to compute the risk analysis and then integrates the results with socio-economic parameters.

- In 2019, G. Deiana et al. [46] reviewed the state of the art in regional earthquake risk assessment in Italy. The paper discusses the different approaches to risk assessment and the challenges that need to be addressed.

2.8 UAE Seismicity Uncertainties

The previous UAE seismic hazard investigations studies reported a high variation from no seismic hazard to very high seismicity, as shown in **Table 5**. For examples:

- In 1999, the Global Seismic Hazard Map Project (GSHAP) provided the PGA values for Europe, Africa, and the Middle East that consider 475-year return periods. The estimated Dubai and Abu Dhabi values were 0.32g and 0.24g [47], respectively, reflecting a very high-risk probability. No local seismicity activities were included in this research.

- In 2004, Abdalla and Al Homoud [48] disagreed with the GSHAP outcomes and considered it very conservative through a robust scientific investigation. Their research was based on Zagros thrust attenuation equations and assuming a bedrock. The estimated PGA values for Dubai are 0.14g, adopting 475 years as a return period and 10 % POE.

- In 2006, Sigbjornsson and Elnashai [49] provided a focused study on Dubai and the west coast fault as the primary source of seismic activities. It included the significant impact of dual earthquake situations from both distant and local sources. They estimated PGA values for Dubai were 0.16g and 0.22g corresponding to 10% and 2% POE, respectively.

- In 2008, Abdalla et al. [50] studied the effect of the earthquake that occurred on Qeshm island, Iran, in 2005 on Dubai's tall buildings. The recorded earthquake had a 6.2 body wave magnitude, 10 km focal depth, and 185 km epicentral distance to Dubai. They recommended increasing the seismic hazard level for high-rise buildings according to the distant resources' risks, especially the Makran subduction zone and Zagros thrust fault. Also, they suggested installing earthquake monitoring devices on important skyscrapers.

- In 2006, Dubai Seismic Network (DSN) [51] was established to record earthquakes from local and distant resources through four stations. From 2006

to 2014, a large number of regional seismic activities were recorded from faults surrounding the UAE, as shown in **Figure 27** (a). Additionally, local seismic activities are noticed from three main sources; (1) Masafi-Bani Hamid, (2) Northern Huwaylat, and (3) Wadi-Nazwa, as shown in **Figure 27** (b).

Table 5: Comparison of results for Dubai seismic hazard studies [52].

Study	PGA (return period = 475 years) (g)
Al-Haddad et al. [53]	< 0.05
Grunthel et al. [47]	0.32
Abdalla and Al Homoud [48]	0.14
Sigbjornsson and Elnashai [49]	0.16
Peiris et al. [54]	0.06
Musson et al. [55]	0.05
Aldama-Bustos et al. [56]	< 0.05
Shama [57]	0.17

The uncertainties in estimating the seismicity level in UAE regions caused ambiguity for designers regarding defining analytical loads and the best practices of the statical systems and material properties. Several studies have been conducted in this area, like:

- In 2011, the seismic design factors had been investigated by [58]; (the Response Modification Factor (R), Deflection Amplification Factor (C_d), and the System Over-strength Factor (Ω_0)) for three reference buildings designed in Dubai of four, sixteen, and thirty-two stories. The chosen structure system was RC special moment resisting frames, and two different sets of ground motions were applied corresponding to 475 and 2475 return periods. The conclusion was that the seismic design level significantly impacts the building R factor, and they recommended period-dependent R and C_d Tables.
- Also, in 2011, a similar study was conducted by [59] for five shear wall buildings from 20 to 60 stories. Incremental Dynamic Analysis (IDA) results showed that R and C_d's code values were very conservative. Also, higher values for Ω_0 were recommended.
- In 2012, the effect of the structural system on lateral behavior was studied by [60] depending on analyzing and designing four 20 stories buildings with

different systems. The chosen systems were Special Moment Resisting Frames (SMRF) and a dual system of SMRF with Special Shear Walls adopted for both RC and Steel buildings. It concluded that stiffer systems would be subjected to higher forces and accelerations while softer systems are expected to suffer higher drift and inelastic damage.

- In 2020, an investigation was produced by [61] that referenced twelve archetypes of buildings that include a variation in building height (6, 9, and 12 stories), design seismicity level (low, intermediate, and high), and type of shear wall (ordinary or special). They recommended being conservative in designing seismic intensity and utilizing the special RC shear walls for optimizing lateral behavior based on the probability of collapse and economic loss results.

- In 2022, three companion studies [62]–[64] compared the lateral performance of RC tall buildings with two layers of ductile coupled shear walls according to building heights (20, 40, and 60 stories), shear wall alignments, and concrete properties among normal concrete strengths and different Ultra-High-Performance Concrete (UHPC) materials. The results showed a significant impact for UHPC on structure performance and total cost aspects.

According to a large collected dataset from satellite images and site visits, a GIS-based risk assessment study for Dubai was conducted by [65]. They divided Dubai into 221 areas, and each area is classified by occupancy as residential, commercial, or industrial, as shown in **Figure 28** on a GIS map. The distribution of total buildings is weighted as 49%, 38%, 12%, and 1% for residential, commercial, industrial, and unidentified usage, respectively. Five reference archetypes were chosen for simulating all assets, with a variety in building height and structural system. The adopted seismic parameters were; $S_s = 0.71g$, $S_1 = 0.59g$, and $T_L = 8s$. The authors used a set of 44 strong earthquake records recommended by FEMA-P695 [66] in the performed nonlinear analyses. An Incremental Dynamic Analysis (IDA) of 25 increments was conducted to determine the collapse probability at three performance levels (by ASCE 41-17, [67]) Immediate Occupancy (IO), Life Safety (LS), and Collapse Prevention (CP). The results obtain that at the design and MCE levels, the probabilities of exceeding the CP limit state are low for all buildings, particularly below 10% for Buildings C1 and C4 and

slightly less than 20% for Building C5. Building C5 exhibited the least favorable performance regarding exceedance probabilities and maximum drifts.

(a)   (b)
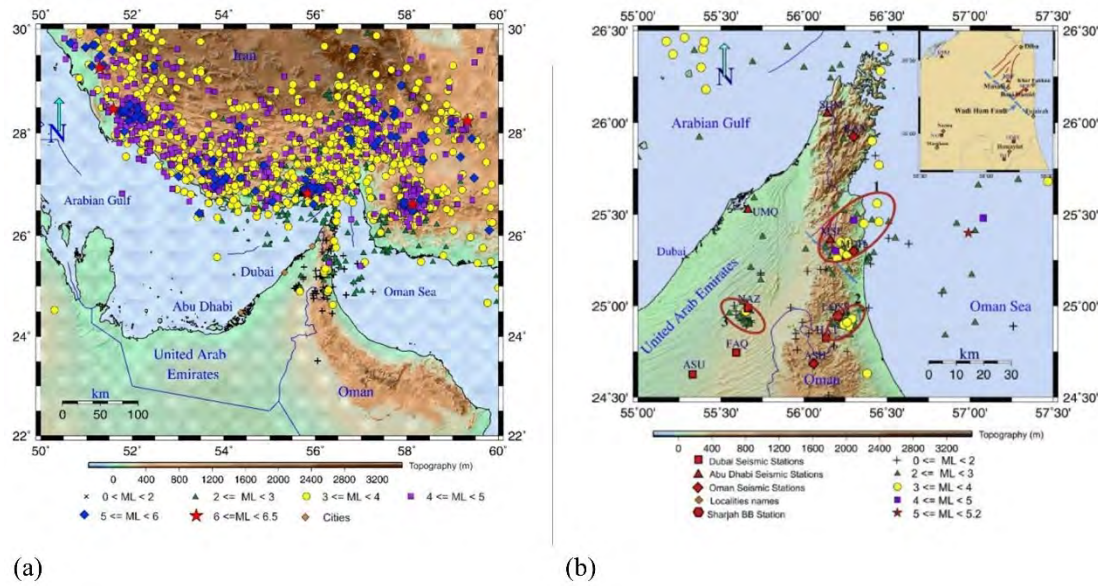
Figure 27: Regional earthquakes recorded by DSN [51] (a) Regional earthquakes; (b) Local seismic sources.
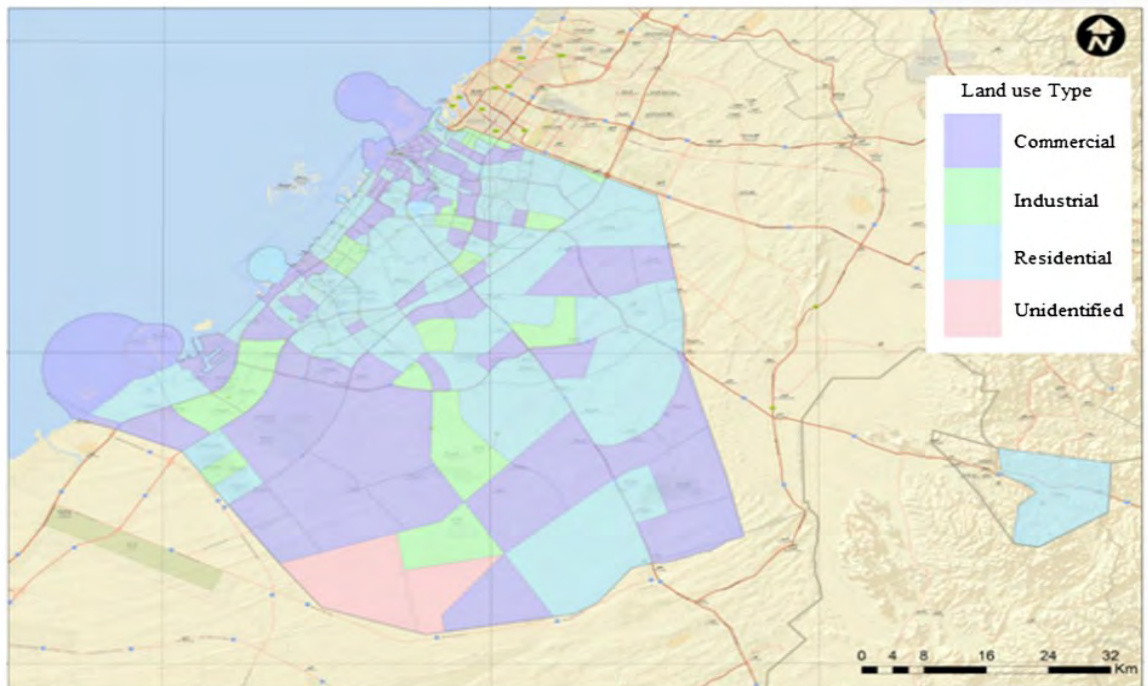
Figure 28: The distribution of building occupancy GIS Map [7], [65].

Table 6: Details of the representative buildings utilized by the GIS risk assessment study [7], [65].

Building/HAZUS designation	LFRS	Number of stories	Material properties		Sector usage
			Fc' (MPa)	Fy (MPa)	
C1: low-rise RC frame	Ordinary moment-resisting frame	2	35	420	Residential
C2: low-rise RC shear wall	Ordinary RC shear wall	2	35	420	Residential
C3: midrise RC shear wall	Ordinary RC shear wall	6	40	420	Commercial
C4: high-rise RC shear wall	Special RC shear wall	12	40	420	Commercial
C5: high-rise RC frame	Special MRF	16	40	420	Commercial

Chapter 3: Design of Tall Buildings Archetypes

3.1 Description of Archetypes

The material properties and the number of floors of the selected high-rise buildings are shown in **Table 3,** while the unified floor layout and structural system are presented in **Figure 29**. The assumed layout is a double symmetric plan view for an office building that consists of five 20-foot-bays (6.0 m) in both North-South and East-West directions. The lateral resisting system consists of two shear wall layers (single shear walls in the edge perimeter and double shear walls connected with coupling beams in interior axes). For slabs, the fc' is assumed to 4.0 ksi (28 MPa). Additionally, the associated loads are defined as per ASCE7-16 [24]; 42.5 psf (2.036 kPa) for Super Imposed Load (SDL), 7.5 psf (0.359 kPa) for the curtain wall (cladding) on the perimeter of each floor, 50 psf (2.394 kPa) for typical floors live load, 20 psf (0.958 kPa) for roof live loads, and the self-weight of the concrete slabs. The soil classification for the site will be taken as "D" as the code recommends when there is no specific soil exploration information available.

ASCE7-16 [24] specifies the response modification coefficient (R) and the deflection amplification factor (C_d) for specially reinforced shear walls as 6, and 5, respectively. While the applied elastic design response spectrum considered a high seismicity condition with (S_s = 1.65 g) and (S_l = 0.65g). A software package was developed to automate analysis and design processes for all reference models, where its source code is available through a GitHub repository [68]. It contains pre/post mediators for Opensees [10] to perform modal analysis and a nonlinear pushover. Additionally, this package contains functionalities to define vertical and horizontal loads as specified in ASCE7-16 [24]. The cross-section design checks are following ACI318-11 for structural concrete requirements [69] including the minimum reinforcement specifications for both column and shear walls. The designed sections were grouped in every 5 stories to simplify the layout. In Opensees, the columns and shear walls were represented by dispBeamColumn object [70] to reflect the reinforcement precisely using a fiber section [70]. The following two subsections outline the detailed design process and results of the gravity system and lateral force-resisting system of the nine buildings.
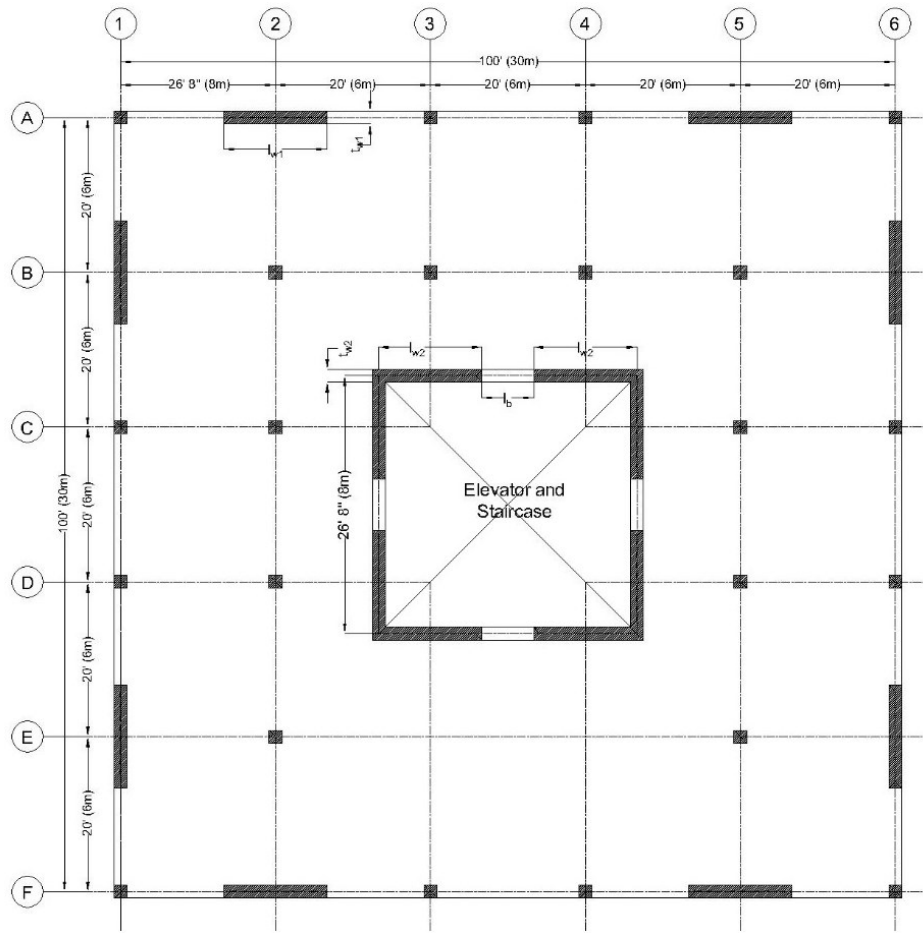
Figure 29: Typical floor plan view for tall buildings archetypes

3.2 Gravity System Design

The gravity system is designed to resist all vertical loads in addition to the deformation compatibility requirements. The columns are designed for bending moments and shear forces that are expected from earthquake excitation deformations to ensure structural stability. According to the IBC'12 [69], the maximum allowable inter-story drift is 2%. Equation (3) define how to calculate column stiffness (K) corresponding to the modulus of elasticity, the moment of inertia (I), and the floor height (L) assuming a rigid diaphragm behavior. Then the applied Bending-Moment (M) and shear force (V) can be estimated as functions of the deformed displacement (d). The vertical reinforcement ratio (ρ) should be from 0.01 to 0.08 according to ACI318-11 [69].

$$K = 12\,EI/L^3 \tag{3}$$

$$V = K \times d \tag{4}$$

$$M = L \times V / 2 \tag{5}$$

All designed column sections with reinforcement details are listed in **Table 17** (Appendix A), while **Table 7** presents the reinforcement of the slab section.

Table 7: Typical Floors Slab Reinforcement Schedule.

Thickness	Top Reinforcement	Bottom Reinforcement	Remarks
20 cm	Φ 10 @ 14.00 cm	Φ 10 @ 14.00 cm	Additional Φ 10 @ 17.00 cm 2.5 m long provided over columns in both directions

3.3 Lateral Force Resisting System Design

According to ASCE-16 [24], the minimum number of modes required to determine lateral forces should guarantee modal mass participation of at least 90% of the actual mass in each orthogonal horizontal direction of response considered in the model. Opensees [10] was utilized to perform the modal analysis through the Eigen command [70], where the mass was lumped at one mode in the center of each story. As an alternative to performing an analysis to determine the fundamental period, The approximate fundamental period T_a, can be estimated according to equation (**6**) (C_t = 0.03, x = 0.9, and H refers to the total Height). The computed fundamental period should not exceed (CuT_a). For every mode shape (*j*), the participating horizontal force for the ith floor can be estimated according to the equation (7)

$$\boldsymbol{T_a} = \boldsymbol{C_t H^x} \tag{6}$$

$$\boldsymbol{F_{ij}} = \boldsymbol{\gamma_j \phi_{ij} Sa_j W_i} \tag{7}$$

where $\boldsymbol{\gamma}$ is the mode participation factor, $\boldsymbol{\phi}$ is the modal deformation, $\boldsymbol{Sa}$ is the elastic response and $\boldsymbol{W}$ is the floor weight. This force should be multiplied by (R/C_d). Then, the combination of mode shapes forces should be estimated using the square root of the sum of the squares (SRSS). The design lateral for the diaphragm at level x ($\boldsymbol{F_{px}}$) can be determined as defined in the equation (8), ASCE-16 [24].

Table 8: Modal Analysis results

Ref.Building	Approximate Period		Computed mode shapes by Opensees [6]	
	T_a	CuT_a	T_1	
M1_10F_50RC	0.83	1.16	1.11	$T_a < T_1 < CuT_a$
M2_15F_50RC	1.20	1.67	1.94	$T_1 > CuT_a$
M3_20F_50RC	1.55	2.17	2.57	$T_1 > CuT_a$
M4_25F_60RC	1.89	2.65	3.49	$T_1 > CuT_a$
M5_30F_60RC	2.23	3.12	3.75	$T_1 > CuT_a$
M6_35F_60RC	2.56	3.59	4.53	$T_1 > CuT_a$
M7_40F_70RC	2.89	4.05	3.87	$T_1 > CuT_a$
M8_45F_70RC	3.21	4.50	5.65	$T_1 > CuT_a$
M9_50F_70RC	3.53	4.95	6.66	$T_1 > CuT_a$

$$F_{px} = \frac{\sum_{i=x}^{n} F_i}{\sum_{i=x}^{n} W_i} W_{px} \tag{8}$$

where the w_{px} is the tributary weight at level x. However, (F_{px}) should be not less than (0.2 S_{DS} I_e w_{px}) or more than (0.4 S_{DS} I_e w_{px}). ACI318-11 [69] determines two conditions for the cases of special boundary in reinforcement, refer to equations (9), and (10).

$$h_w/l_w < 2 \tag{9}$$

$$\frac{1.5 \, \delta_u}{h_w} \geq \frac{l_w}{600 \, c} \tag{10}$$

where the (*c*) refers to the compression zone in the shear wall section, and the drift ratio (δ_u/h_w) should not be less than 0.005. The length of special boundary reinforcements should not be less than the greater of (*C – 0.1 lw*) and (*C/2*). According to these specifications, multiple trials were conducted for modal analysis and shear section checks until reaching a safe design for each model. The shear wall length (in-plan view) is kept constant throughout the building height. To avoid excessive out-of-plane slenderness complications in walls, the cross-sectional aspect ratio (l_w/t_w) is kept in the range (~6-12).
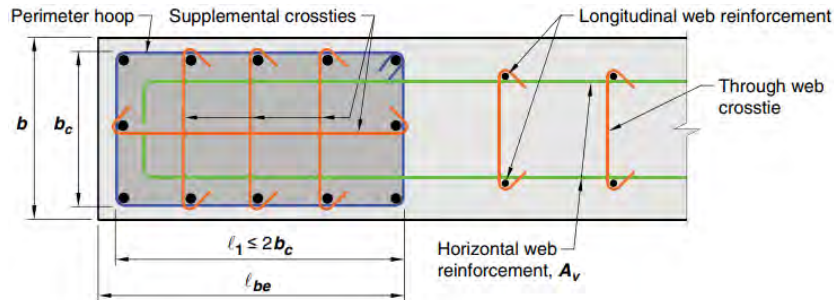
Figure 30: The details of special boundary reinforcement in the shear wall.

3.4 Cost Estimation for Structural Elements' Materials

The bill of quantities, reported in **Table 9**, shows the accumulative of concrete and steel materials required for designed superstructures. Slabs are the most demanding elements, they required from 72.44% to 52.26% of concrete volumes and from 72.61% to of steel weights. Slabs Quantities ratios are decreasing respecting to increasing the number of floors, unlike columns and walls. Columns require from 6.76 % to 12.01 % of concrete quantities and from 6.76 % to 12.01 % of steel quantities. While, Shear walls consume a range of 20.80 % to 35.73 % and 37.77 % to 52.02 % for concrete and steel, respectively. The estimated concrete and steel quantities per floor are 230.8 m^3 and 22.28 tons for the "M1_10F_50RC" model. They gradually increase respecting the number of floors 319.924 m^3 and 54.26 tons for the "M9_50F_70RC" model.

Table 9: Bill of Quantities of structural elements.

Ref. Building	Concrete Volume (m3)				Steel Quantity (ton)			
	Columns	Slabs	Walls	Total	Columns	Slabs	Walls	Total
M1_10F_50RC	156	1672	480	2308	23.24	161.76	37.77	222.77
	(6.76%)	(72.44%)	(20.80%)		(10.43%)	(72.61%)	(16.95%)	
M2_15F_50RC	214.8	2508	720	3442.8	35.84	242.64	56.66	335.14
	(6.24%)	(72.85%)	(20.91%)		(10.69%)	(72.40%)	(16.91%)	
M3_20F_50RC	273.6	3344	914.5	4532.1	65.42	324.27	211.34	601.03
	(6.04%)	(73.78%)	(20.18%)		(10.88%)	(53.95%)	(35.16%)	
M4_25F_60RC	332.4	4180	1157	5669.4	94.81	405.34	267.11	767.26
	(5.86%)	(73.73%)	(20.41%)		(12.36%)	(52.83%)	(34.81%)	
M5_30F_60RC	411.6	5016	1581	7008.6	117.87	487.55	378.55	983.97
	(5.87%)	(71.57%)	(22.56%)		(11.98%)	(49.55%)	(38.47%)	
M6_35F_60RC	1367.4	5852	2688	9907.4	295.3	570.13	610.57	1476
	(13.80%)	(59.07%)	(27.13%)		(20.01%)	(38.63%)	(41.37%)	
M7_40F_70RC	1456.8	6688	3601	11745.8	307.83	651.58	839.51	1798.92
	(12.40%)	(56.94%)	(30.66%)		(17.11%)	(36.22%)	(46.67%)	
M8_45F_70RC	1546.2	7524	4212	13282.2	347.62	736.44	1140.14	2224.2
	(11.64%)	(56.65%)	(31.71%)		(15.63%)	(33.11%)	(51.26%)	
M9_50F_70RC	1921.2	8360	5715	15996.2	479.7	822.05	1411.23	2712.98
	(12.01%)	(52.26%)	(35.73%)		(17.68%)	(30.30%)	(52.02%)	

According to these quantities, and assuming the cost of a cubic meter of concrete and a ton of reinforcement steel was assumed 235 and 2,200 AED, the cost estimations, in **Table 10**, are found. The total material cost of the designed archetypes are varying from 1.00 to 7.99 million. In other words, The cost of materials per floor is from 0.1 for ten floors archetype to 0.19 respecting 50 floors archetype million AED. Finally, the cost of the square meter for structural elements (without counting the wasted quantity) is in a range from 120 to 235 AED.

Table 10: Structural cost estimation.

Ref. Building	Structural Material Cost (million AED)				Avg. Cost per m2 (AED)
	Concrete	Steel	Total	Avg. Per Floor	
M1_10F_50RC	0.51	0.49	1.00	0.10	119.36
M2_15F_50RC	0.76	0.74	1.49	0.10	119.2
M3_20F_50RC	1.00	1.32	2.32	0.12	138.72
M4_25F_60RC	1.27	1.69	2.96	0.12	141.51
M5_30F_60RC	1.57	2.16	3.74	0.12	148.98
M6_35F_60RC	2.24	3.25	5.49	0.16	187.55
M7_40F_70RC	2.74	3.96	6.69	0.17	200.16
M8_45F_70RC	3.09	4.89	7.99	0.18	212.34
M9_50F_70RC	3.75	5.97	9.72	0.19	232.46

Chapter 4: Calibrating NMFS Models for Tall Buildings Archetypes

4.1 Introduction and Background

Instead of depending on multiple trials to adjust the hysteric parameters for the MCS models, a simplified and more effective calibration process has been developed to estimate these parameters from the basic building information and the HAZUS database [19]. The process can be explained as follows; the initial stiffness (K) and mass (M) are assumed to be uniform along with the height for regular structures. They are given according to equations (11) and (12), respectively.

$$[K] = k_0 \begin{bmatrix} 2 & -1 & 0 & \cdots & 0 \\ -1 & 2 & -1 & \ddots & \vdots \\ 0 & -1 & \ddots & \ddots & 0 \\ \vdots & \ddots & \ddots & 2 & -1 \\ 0 & \cdots & 0 & -1 & 2 \end{bmatrix} \tag{11}$$

$$[M] = m \ [I] \tag{12}$$

Eq.(13) demonstrates estimating the first vibration period of the building (T_1) from the number of stories in the building (N)

$$T_1 = \frac{N}{N_0} \cdot T_0 \tag{13}$$

N_0 and T_0 are the numbers of stories and fundamental periods, respectively, of the typical buildings presented in Tables 5.5 and 5.7 of the HAZUS dataset [8]. The below equations from (14) to (15) explain in detail how to determine the backbone curve, shown in **Figure 10**, for an inter-story (i), according to HAZUS dataset [8] values for the yield capacity point (SD_y, SA_y), the ultimate capacity point (SD_u, SA_u), and the mode factor (α_1).

$$\lambda = \left(\frac{[\phi_1]^T \ [I] \ [\phi_1]}{[\phi_1]^T \ [A] \ [\phi_1]} \right) \tag{14}$$

$$k_0 = \lambda \ \frac{4 \, \pi^2 \, m}{T_1^{\,2}} \tag{15}$$

$$V_{y,i} = SA_y \cdot \alpha_1 \cdot m \cdot g \cdot \Gamma_i \tag{16}$$

$$\eta_i = \frac{SA_u - SA_y}{SD_u - SD_y} \cdot \frac{SD_y}{SA_y} \tag{17}$$

$$\beta_i = \frac{SA_u}{SA_y} \tag{18}$$

$$\Delta_{c,i} = \delta_{co} \cdot h \tag{19}$$

where g is the acceleration of gravity and δ_{co} is the inter-story drift ratio at the threshold of the complete damage state. As shown in Eq. (20), Γ_i refers to the ratio between the inter-story shear strength of the ith story ($V_{y,i}$) and the first story ($V_{y,1}$).

$$\Gamma_i = \frac{V_{y,i}}{V_{y,1}} \tag{20}$$

Additionally, the coefficient for the severity of degradation (τ) is required to determine the hysteric behavior. As shown in Eq. (21), it is defined as the ratio between areas of the pinching envelope (A_p) and full bilinear envelope (A_b) and it is values are given in Table 5.18 of HAZUS [8], [71].

$$\tau = \frac{A_p}{A_b} \tag{21}$$

The flexural-shear coupling elastic continuum model was proposed by [23] to simulate the seismic responses and dynamic characteristics of tall buildings. The deformation modes of these structural systems are typically a combination of flexural deformation and shear deformation. Partial differential equations were used to describe the dynamic response of this model under a ground motion acceleration as follows:

$$\frac{\rho(x)}{EI_0} \frac{\partial^2 u(x,t)}{\partial t^2} + \frac{c(x)}{EI_0} \frac{\partial u(x,t)}{\partial t} + \frac{1}{H^4} \frac{\partial^2}{\partial x^2} \left(s(x) \frac{\partial^2 u(x,t)}{\partial x^2} \right)$$
$$- \frac{\alpha_0^2}{H^4} \frac{\partial}{\partial x} \left(s(x) \frac{\partial u(x,t)}{\partial x} \right) = -\frac{\rho(x)}{EI_0} \frac{\partial^2 u_g(x,t)}{\partial t^2} \tag{22}$$

$$\alpha_0 = H \, (GA_0/EI_0)^{1/2} \tag{23}$$

$$EI(x) = EI_0 \, s(x), \quad GA(x) = GA_0 \, s(x) \tag{24}$$

where: $\rho(x)$ is the mass per unit length in the model; $c(x)$ is damping per length coefficient; x is a non-dimensional height (varies from 0 at the base to 1 at the top level); t is time; $u(x,t)$ is lateral displacement respecting discrete values of x and t. EI_0 and GA_0 refer to the flexural and shear stiffnesses at the model's base. H is the total height of the building. EI(x) and GA(x) are the flexural stiffness of the flexural beam and the shear stiffness of the shear beam along with the structural height, respectively. $s(x)$ is the dimensionless function that defines the stiffness variation along with the model's height, assuming that the variations of the flexural and shear stiffnesses

along the height are identical. Where, α_0 is a dimensionless parameter controlling the proportions of the flexural and shear deformations in the model. Assuming, $u_g(x,t)$ is the acceleration history of the ground motion. Furthermore, they investigated the relationship between α_0 values and different types of structures. **Table 11** identifies these recommended values, where the shear deformation dominates the deformation mode if α_0 is greater than 30.

Table 11: Approximate ranges of α_0 for different types of structures [23].

Type of structures	α_0
Shear wall structure	0-1.5
Combined moment-resisting frame and shear wall structure	1.5-5.0
Combined moment-resisting frame and braced frame structure	1.5-5.0
Frame structure	5.0-20

The nonlinear MDOF flexural-shear (NMFS) model was proposed by [16] to include nonlinear where the calibration process is summarized in **Figure 15** and it is divided into four steps:

(1) Calibration of the elastic parameters:

In this stage, the initial flexural and shear stiffness (*EI*, *GA*) values are estimated based on the modal analysis parameter: the period T_i, eigenvalue parameter γ_i, and the omega parameter ω_i for each I mode; as shown in Eqs. (25) and (26).

$$\omega_1{}^2 = \frac{EI}{\rho\,H^4}\gamma_1{}^2(\gamma_1{}^2 + \alpha_0{}^2) \tag{25}$$

$$\alpha_0 = H\sqrt{\frac{GA}{EI}} \tag{26}$$

where α_0 is the flexural-shear stiffness ratio and can be calculated as follows

$$\frac{T_i}{T_1} = \frac{\gamma_1}{\gamma_i}\sqrt{\frac{\gamma_1{}^2 + \alpha_0{}^2}{\gamma_i{}^2 + \alpha_0{}^2}} \tag{27}$$

(2) Calibration of the yield point:

For the jth story and n^{th} mode shapes, the total displacement/inter-story displacement $(u_{j,n}/\Delta u_{j,n})$ and the total rotation/inter-story rotation $(\theta_{j,n}/\Delta\theta_{j,n})$ are derived from the modal shapes $(\phi_{j,n})$ and the spectrum displacement (D_n)

$$u_{j,n} = \Gamma_n\phi_{j,n}D_n \tag{28}$$

$$\Delta u_{j,n} = u_{j,n} - u_{j-1,n} \tag{29}$$

$$\theta_{j,n} = \partial u_{j,n}/\partial z \tag{30}$$

$$\Delta\theta_{j,n} = \theta_{j,n} - \theta_{j-1,n} \tag{31}$$

The inter-story shear force $(V_{j,n})$ and the bending moment $(M_{j,n})$ for each mode shape are calculated based on Eqs. (32) and (33). Then they are combined using the square root of the sum of the squares (SRSS) to obtain the shear force $(V_{a,j})$ and bending moment $(M_{a,j})$ demands on each story (Eqs. (34) and (35)).

$$V_{j,n} = \Delta u_{j,n}\ GA/h_j \tag{32}$$

$$M_{j,n} = \Delta\theta_{j,n}\ EI/h_j \tag{33}$$

$$V_{a,j} = \sqrt{\sum V_{j,n}^2} \tag{34}$$

$$M_{a,j} = \sqrt{\sum M_{j,n}^2} \tag{35}$$

The values of $(V_{j,n})$ and $(M_{j,n})$ are adjusted to follow design specifications. The value of design inter-story shear force $(V_{d,j})$ is estimated according to Eq. (36), where (V_{base}) is the total shear force. The design inter-story moment $(M_{d,j})$ can be obtained according to (JGJ 3-2010) manual [72], where (h_w) is a critical height from Eq. (37).

$$V_{d,j} = \max[V_{a,j},\ 0.2\ V_{base}] \tag{36}$$

$$h_w = \max[2h_{story},\ 0.1h_{wall}] \tag{37}$$

The yield overstrength parameter (Ω_y) is adopted to determine the yield strength for shear forces and bending moments as follows:

$$V_{y,j} = V_{d,j}\ \Omega_y \tag{38}$$

$$M_{y,j} = M_{d,j}\ \Omega_y \tag{39}$$

Finally, the calibrated yield displacement, $(\Delta u_{y,j})$ and rotation, $(\Delta\theta_{y,j})$ can be determined according to the equations below.

$$\Delta u_{y,j} = V_{y,j}\cdot h_j/GA \tag{40}$$

$$\Delta\theta_{y,j} = M_{y,j}\cdot h_j/EI \tag{41}$$

(3) Calibration of the peak point:

The plastic strength for each story shear spring ($V_{p,j}$) and flexural spring ($M_{p,j}$) can be derived directly by multiplying the corresponding yield value by the plastic overstrength factor (Ω_p).

$$V_{p,j} = V_{y,j}\, \Omega_p \tag{42}$$

$$M_{p,j} = M_{y,j}\, \Omega_p \tag{43}$$

For the bi-linear backbone curve, the peak displacement ($\Delta u_{p,j}$) and the peak rotation ($\Delta \theta_{p,j}$) are determined directly from plastic strengths and elastic stiffnesses as follows:

$$\Delta u_{p,j} = V_{p,j} \cdot h_j / GA \tag{44}$$

$$\Delta \theta_{p,j} = M_{p,j} \cdot h_j / EI \tag{45}$$

For the tri-linear backbone curve, peak values can be determined using two different methods:

- Stiffness reduction method:

The elastic stiffnesses for shear and bending are reduced by a reduction factor (η) according to ACI specifications [73].

$$G_r A = \eta GA \tag{46}$$

$$E_r I = \eta EI \tag{47}$$

Then, the peak displacement ($\Delta u_{p,j}$) and the peak rotation ($\Delta \theta_{p,j}$) are estimated using the reduced elastic stiffnesses (G_r, E_r).

$$\Delta u_{p,j} = V_{p,j} \cdot h_j / G_r A \tag{48}$$

$$\Delta \theta_{p,j} = M_{p,j} \cdot h_j / E_r I \tag{49}$$

- Ductility factor method:

In this method, the peak displacement and rotation on each story are determined based on the ductility factor (μ), determined as explained in Eq. (50).

$$\mu\, \Omega_p = D_p / D_y \tag{50}$$

$$\Delta u_{p,j} = \mu\, \Omega_p\, \Delta u_{y,j} \tag{51}$$

$$\Delta \theta_{p,j} = \mu\, \Omega_p\, \Delta \theta_{y,j} \tag{52}$$

(4) Calibration of the hysteretic parameter:

The degradation behavior through several hystereses is adjusted using the (τ) coefficient defined using Eq. (21).

4.2 Pushover Analysis

Non-linear pushover analyses were performed using Opensees [6], to be the reference for calibrating refined FE models to simplified NMFS models. For each archetype model, three pushover analyses with different loading profiles (typically; linear, fundamental mode shape, and quadratic profiles) were conducted to define the most critical loading profile. **Table 12** shows the maximum estimated base shear within each profile which identifies that the quadratic is the most critical case $(where: F_{story} \: \alpha \: \left(\frac{h_{story}}{H}\right)^2)$.

Table 12: Estimated base shear for different pushover profiles.

Archetype	Maximum base shear for pushover profiles (KN)		
	Quadratic	Fundamental mode shape	Linear
M1_10F_50RC	4644.147	4961.205	5256.298
M2_15F_50RC	3089.289	3323.500	3493.262
M3_20F_50RC	5598.494	5913.735	6324.472
M4_25F_60RC	5112.531	5403.890	5779.516
M5_30F_60RC	5247.347	5467.470	5923.897
M6_35F_60RC	7249.382	7539.039	8208.556
M7_40F_70RC	8540.247	8812.850	9695.039
M8_45F_70RC	9190.481	9398.635	10533.141
M9_50F_70RC	9328.643	9546.907	10713.458

4.3 Calibration Resulting Model

A trial heuristic algorithm was implemented to determine the best values for NMFS model parameters that achieve the closest pushover curve to the detailed FE models. The main optimization criteria were reducing the mean squared error between the two curves. The final values for: Ω_y, Ω_p and μ are reported in **Table 13**.

The final pushover curves compared to the FE model curves are plotted in Appendix B figures. The figures show how similar both models are in lateral behavior. Numerically, the relative errors for peak strength and total curve area are in 0.02, 0.08 worst cases, and less than 1.0E-05, and 0.04 average. While the MSE estimations were below 0.006 and in with an average value of 0.004. The efficiency of using NMFS is clarified by the difference in the time required for both models. As represented in **Table 21** the time required for the simplified models represents only 4/1000 of the

computational time required for the detailed models on average. Specifically, this is the ratio in arrange between 3/1000 to 6/1000.

Table 13: Estimated parameters for NMFS models

Archetype	NMFS models parameters				
	Ω_y	Ω_p	μ	EI (KN.m^4)	GA (KN.m^2)
M1_10F_50RC	2.65	1.20	5.28	1.7E+08	1.2E+06
M2_15F_50RC	1.25	1.25	6.11	1.4E+08	5.9E+05
M3_20F_50RC	1.62	1.24	2.36	2.9E+08	4.7E+05
M4_25F_60RC	1.22	1.23	2.41	3.8E+08	3.8E+05
M5_30F_60RC	1.06	1.24	2.28	1.1E+09	3.1E+05
M6_35F_60RC	1.25	1.26	1.83	4.5E+09	3.4E+05
M7_40F_70RC	1.30	1.26	2.01	7.3E+09	3.5E+05
M8_45F_70RC	1.24	1.27	1.40	4.3E+09	2.7E+05
M9_50F_70RC	1.13	1.27	1.40	6.2E+09	2.4E+05
Average	1.41	1.25	2.80	2.7E+09	4.6E+05

Chapter 5: GIS Databases for Buildings, Ground Motions, and Risk Assessment Results

5.1 Input Ground Motions

As shown in **Table 1** and **Figure 27**, UAE is surrounded by regional and local seismic geological resources. The "Earthquake Scenario Simulation" component in R2D [9] was utilized to generate input ground motions. Multiple-point-earthquake sources were defined as listed in **Table 14**, which were collected from different resources to represent the surrounding seismic resources ([74]–[76]). An input ground motion was estimated at each neighbor's representative location (longitude and latitude) corresponding to every seismic source using Chiou & Youngs' prediction equation [77].

Table 14: Properties of earthquakes included in an earthquake simulation scenario.

Location	Date	Longitude	Latitude	M_w	Focal Depth (Km)
Chaldoran	24/11/1976	39.07	44.38	7.0	15
Tabas	16/09/1978	33.60	56.93	7.4	11
KuliBonyabad	27/11/1979	30.67	51.60	7.0	25
Sirch	28/07/1981	30.20	57.54	7.2	15.5
ArdekulGhaen	10/05/1997	34.61	49.85	7.2	10
Manjil	06/11/1990	28.25	55.46	7.4	11
Hormozgan, North-West of Dehbarez	??/??/2000	27.56	56.84	4.2	41
Hormozgan, North-West of Dehbarez	??/??/2002	27.64	56.74	5.3	12
Hormozgan, North-East of Bandar-e Abbas	??/??/2002	27.49	56.62	4.4	33
Masafi-Bani Hamid	13/09/2007	25.46	56.2	4.0	20

5.2 Buildings Database

This study included 17 archetypes that represent different occupancy classes, the number of stories, and design seismicity levels. Dubai has been segmented into 221 Neighbours by [65] and for each, the number of buildings was estimated approximately according to the population density. In addition, every area was classified according to its major occupancy into residential, commercial, industrial, and unidentified. In order to estimate the number of archetype buildings in a certain area, the archetypes have been grouped according to the occupancy class and a close number of stories, as defined

in **Table 15**. Then, hypothetical distribution ratios were defined to represent each group out of the total buildings in each neighborhood, as shown in **Table 16**.

Table 15: Definition and description of archetypes groups.

Archetypes Group	Description	Stories	Year Built	Archetypes
RES (1-5)	Low and Medium rise residential buildings	1-5	1981-2002	LR_RES_F1, LR_RES_F2, LR_RES_F3, LR_RES_F5
IND	Light industrial buildings	1	2003	LR_IND_F1
COM (3-7)	Low and Medium rise commercial buildings	3-7	1990 - 2010	LR_COM_F3, MR_COM_F6, MR_COM_F7
COM (10-20)	High-rise commercial buildings	10-20	2000	HR_COM_F10, HR_COM_F15, HR_COM_F20
COM (25-35)	High-rise commercial buildings	25-35	2005	HR_COM_F25, HR_COM_F30, HR_COM_F35
COM (40-50)	High-rise commercial buildings	40-50	2010	HR_COM_F40, HR_COM_F45, HR_COM_F50

Table 16: Hypothetically distribution ratios for archetypes in different neighbor classes.

Archetypes Group	Neighbour Class			
	Residential	**Commercial**	**Industrial**	**unidentified**
RES (1-5)	0.50	0.00	0.30	0.40
IND	0.00	0.00	0.70	0.10
COM (3-7)	0.25	0.25	0.15	0.15
COM (10-20)	0.15	0.25	0.00	0.15
COM (25-35)	0.05	0.25	0.00	0.10
COM (40-50)	0.05	0.25	0.00	0.10

5.3 Risk Assessment Results

The simulation process included three forms of inputs assigned two spatial attributes; ground motions, buildings database, and FE scripts for MCS, and NMFS models. While the results contain the expected collapse probability and losses for each building. The results were encapsulated in different scales: (1) overall studied city; (2)

neighbors; (3) neighbors classes; (4) archetypes group; and (5) archetypes. A detailed report is provided in the tables of Appendix C, while a summary representation is given as follows;

R2D [9] utilizes utilizes the PELICUN [78] package for the FEMA-P58 methodology to determine decision variables. FEMA developed a method to determine collapse probability by developing fragility curves. Fragility functions are calibrated using a variety a combination of analytical, experimental, and simulation methods. Analytical methods use mathematical equations to calculate the collapse probability of a building from the Engineering demanding parameters (EDPs) in addition to material properties, and asset classification. FEMA fragility functions are calibrated using a variety of methods, including:

- Expert judgment: FEMA uses the judgment of experts to develop fragility functions. Experts are typically engineers, architects, and seismologists who have experience in the design and construction of buildings.

- Data analysis: FEMA uses data from past earthquakes and other hazard events to develop fragility functions. This data includes information on the damage that was caused to buildings, the intensity of the hazard event, and the characteristics of the buildings.

- Simulation modeling: FEMA uses simulation models to develop fragility functions. Simulation models are computer programs that can be used to simulate the behavior of buildings under different loading conditions.

FEMA uses data from a variety of sources to calibrate its fragility functions, including:

- Earthquake damage surveys: FEMA conducts earthquake damage surveys to collect data on the damage that was caused to buildings in past earthquakes.

- Building codes: FEMA uses building codes to collect data on the design and construction of buildings.

- Engineering studies: FEMA uses engineering studies to collect data on the performance of buildings under different loading conditions.

FEMA uses the estimates of repair cost, repair time, and injuries to develop plans for responding to and recovering from disasters. These plans include disaster assistance and recovery planning. Disaster assistance provides financial assistance, grants, loans, and other forms of aid to individuals and businesses that have been affected by a

disaster. Recovery planning helps communities to identify the needs of the community and the steps that need to be taken to recover from a disaster. Here are some of the specific methods that FEMA uses to calculate repair cost, repair time, and injuries:

- Repair cost: FEMA calculates repair cost by considering the following factors: the type of damage that was caused to the building, the cost of materials and labor, the cost of demolition and removal, the cost of temporary housing

- Repair time: FEMA calculates repair time by considering the following factors: the type of damage that was caused to the building, the availability of materials and labor, The complexity of the repairs, the availability of funding

- Injuries: FEMA calculates injuries by considering the following factors: the type of damage that was caused to the building, the location of the building, the number of people in the building, and the severity of the damage.

Here are some examples of previous earthquake data used by FEMA to calibrate fragility functions:

1. San Francisco Earthquake, 1906: The San Francisco earthquake of 1906 was a magnitude 7.9 earthquake that caused widespread damage in San Francisco and the surrounding area. FEMA used data from this earthquake to develop fragility functions for buildings of different types and ages.

2. Northridge Earthquake, 1994: The Northridge earthquake of 1994 was a magnitude 6.7 earthquake that caused widespread damage in the Los Angeles area. FEMA used data from this earthquake to improve the accuracy of its fragility functions.

3. Kobe Earthquake, 1995: The Kobe earthquake of 1995 was a magnitude 7.2 earthquake that caused widespread damage in Kobe, Japan. FEMA used data from this earthquake to develop fragility functions for buildings in areas with high seismic risk.

4. Haiti Earthquake, 2010: The Haiti earthquake of 2010 was a magnitude 7.0 earthquake that caused widespread damage in Haiti. FEMA used data from this earthquake to improve the accuracy of its fragility functions for buildings in developing countries.

5.3.1 Collapse Probability:

The obtained results can be summarized as follows:

- The collapse probability for the modeled buildings can differ from 0.00 % to 60% with a mean value of almost 4%. The "LR_RES_F1" archetype represents the highest collapse probability ratio is slightly less than 8%, while the lowest ratio is 0.00 % expected for the "LR_IND_F1" archetype, shown in **Figure 31** (c).

- For concrete structures, the expected collapse ratios are in a range from 3% to 8%, from 1.2% to 3.5%, and from 0.2% to 2.3% for low-rise, medium-rise, and high-rise archetypes respectively.

- In other words, "RES (1-5)" is the highest archetypes group with an expected collapse probability of 5.5%. The collapse probability for commercial concrete structures decreases respecting the height from 3% for "COM (3-7)" to 0.2% for "COM (40-50)", shown in Figure 31 (b).

- As expected residential neighbors have the highest mean collapse probability of almost 4%, and commercial neighbors have the lowest ratio of 0.8%, while the ratios for industrial and unidentified neighbors are 1.8% and 3.1% as represented in Figure 31 (a), respectively.

- Projecting these results on a GIS scale leads to the choropleth map shown in Figure 36 (a), which determines the mean collapse probability for Dubai's neighbors.

5.3.2 Repair Cost to Replacement Cost Ratio:

The monetary losses due to replacement or repair are a factual parameter in the assessment of earthquake disasters, which is depending on the collapse probability, construction material (Steel, Concrete,… etc.), and the structure system. These factors are reflected in the estimations as follows:

- The highest archetype for the repair-to-replacement ratio is the single-story masonry building "LR_RES_F1" with 28%, then the light steel industrial structure "LR_IND_F1" with 26%, as shown in **Figure 32** (c).

- The average ratio for residential archetypes is 21 % and for commercial archetypes groups in a range from for "COM (3-7)" group 12 % to 2% for the "COM (40-50)" group, as represented in **Figure 32** (b).

- For the GIS scale, the average losses for neighbors' classes can be ordered in descending as industrial (23%), residential (15%), unidentified (11.5%), and commercial (4.5%), see **Figure 32** (a).

- Additionally, the expected losses per individual neighbor were represented in **Figure 36** (b). which vary from 0% to 35%. Finally, the average cost for the cumulative city is expected to be 14% accompanied by a 0.25 standard deviation.

5.3.3 Repair Time:

Similar to the repair cost, the required time for repairs is related to construction materials, and the structural system. The key values are listed below:

- **Figure 33** (d) clarifies that the "LR_IND_F1" archetype requires the most number of days for repairs (223 days for mean value) with a significant difference from other archetypes.

- "LR_RES_F1" is the 2nd highest archetype in repair time with 29 days associated with a 49 standard deviation.

- The average repair days required for concrete archetypes are 25 for low-rise, 16 for medium-rise buildings, and in a range from 25 to 4 for high-rise buildings.

- As represented in **Figure 33** (c), the average required repair days for residential archetypes is 25 days, and for commercial archetypes groups in a range from 18 for the "COM (3-7)" group to 6 days for the "COM (40-50)" group.

- **Figure 33** (b) shows the repair time probabilities for different neighbors' classes. The mean values can be ordered in descending as industrial (148 days), unidentified (48 days), residential (20 days), and commercial (11 days).

- The overall estimated probability is 22 days associated with a 52 standard deviation, as referred to in **Figure 33** (a).

- Finally, **Figure 36** (c) includes the choropleth map for the expected repair time for the studied neighbors in the form of a colored scale from 0 to 220 days.

5.3.4 Injuries:

The expected injuries of the total occupancy population are classified in an ascending severity order from one to four. The estimated injuries are summarized as follows:

- The mean total injuries for the studied region are estimated to be approximately 1.5% of the population, 62% of them represent the lowest severity while 10% for the highest severity, See **Figure 34.**

- As a result of the collapse probabilities and expected damage variables, the expected average injuries are from 1.7% to 6.5% for low-rise archetypes, from 0.2% to 5.3%, for medium-rise archetypes, and from 0.04% to zero for high-rise archetypes, as shown **Figure 35**.

- The "LR_RES_F1" archetype has the highest total injuries with 6.5% distributed as 83%, 16.5 % for 1st and 2nd severity, and 0.02% for 3rd and 4th. Then, the "LR_IND_F1" archetype with 5%. and the ratios of the injuries' severity are 60%, 24%, 5%, and 10% from lowest to highest. While for concrete models the total injuries are 2 % in the worst case 61% for the lowest severity and 10% for the highest.

- The mean values for neighbors classes can be ordered in descending as industrial (4.1%), residential (1.6%), unidentified (1.1%), and commercial (0.1%), see Figure 34 (c).

- Finally, the representative map for injuries distributed per studied neighbors can be found in **Figure 34** (b).
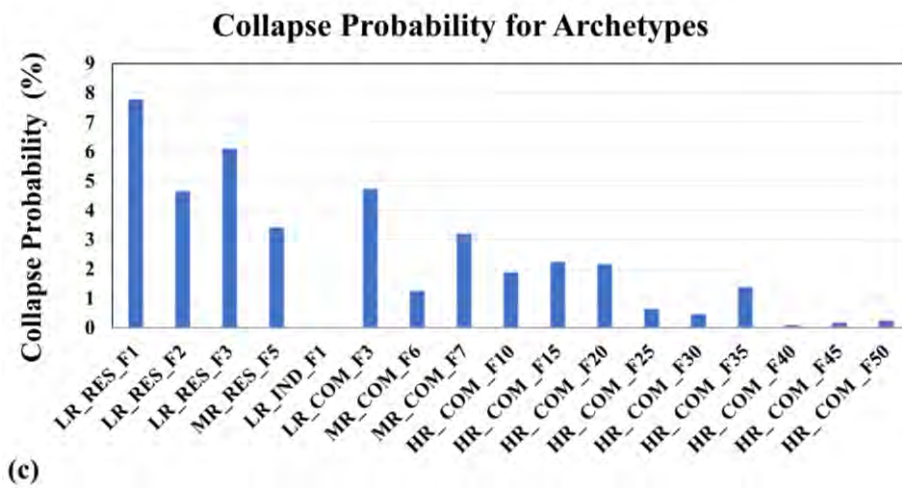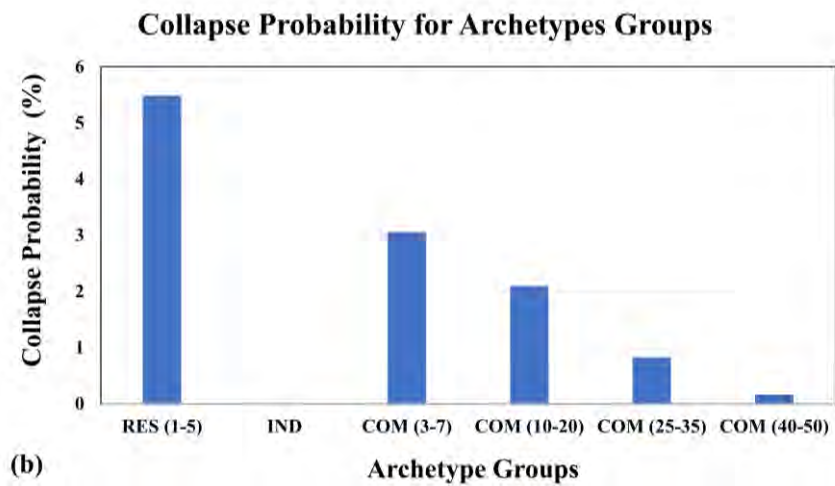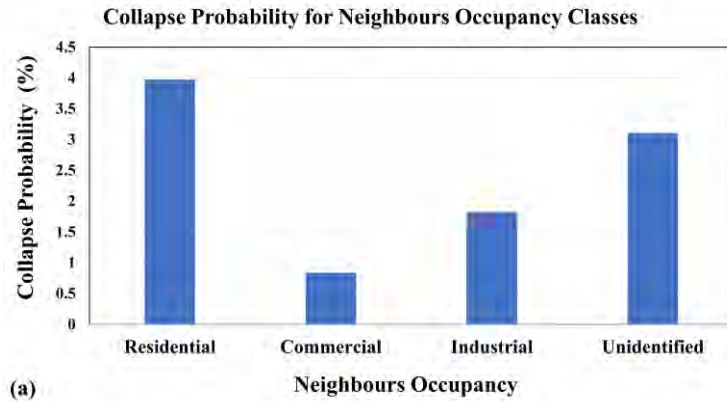
Figure 31: Mean values of the estimated collapse probability: (a) Neighbors classes;

(b) Archetypes groups; and (c) Archetypes.
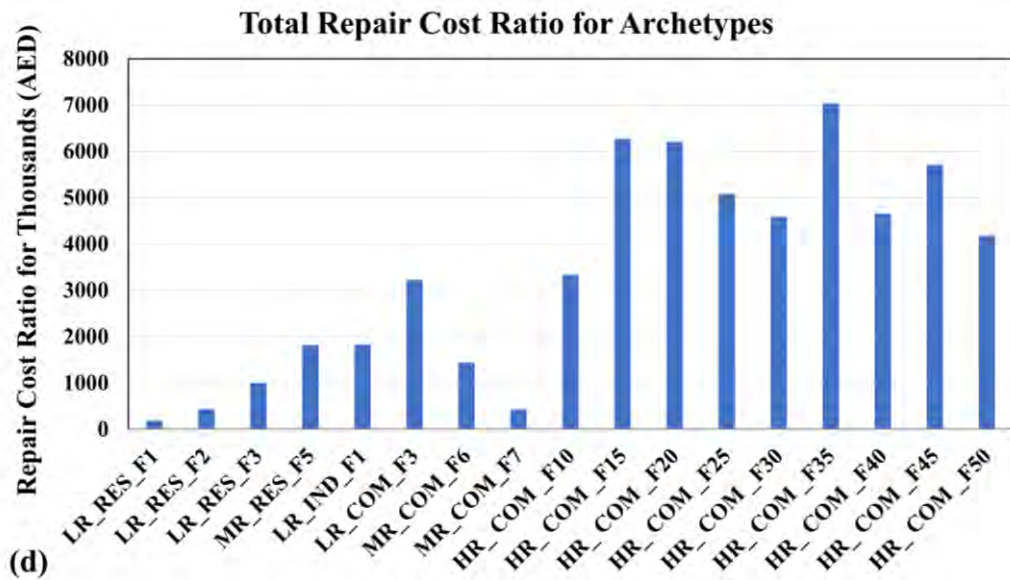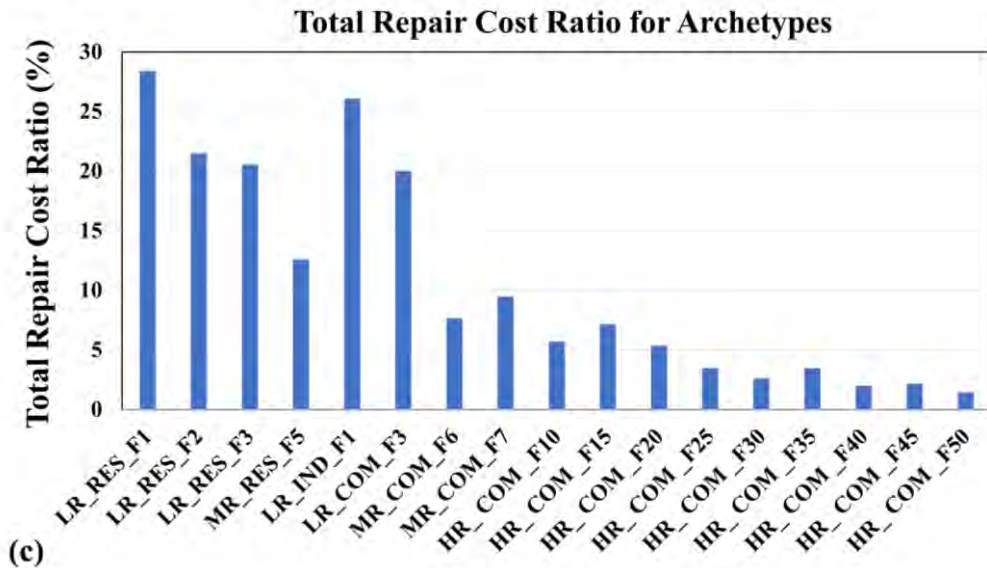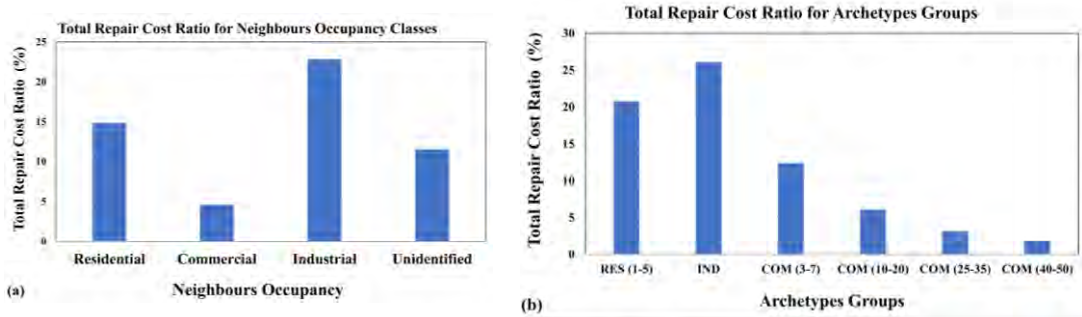
Figure 32: Mean values of estimated repair cost-to-replacement cost ratio: (a)

Neighbors classes; (b) Archetypes groups; and (c) Archetypes (d) Archetypes repair

cost in thousands AED
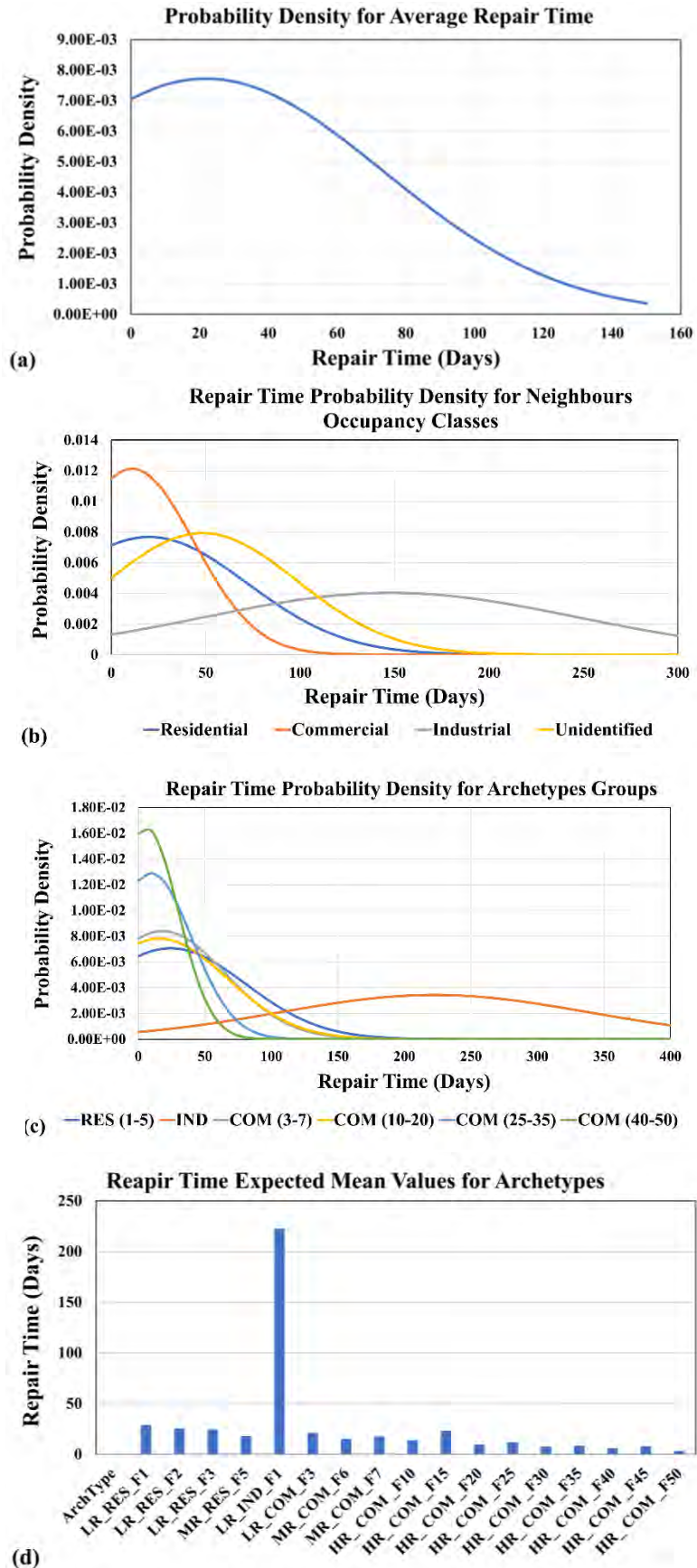
Figure 33: Estimated repair time, as a probability density: (a) Overall assets; (c) Neighbors classes; (c) Archetypes groups; and (d) Mean values of archetypes.
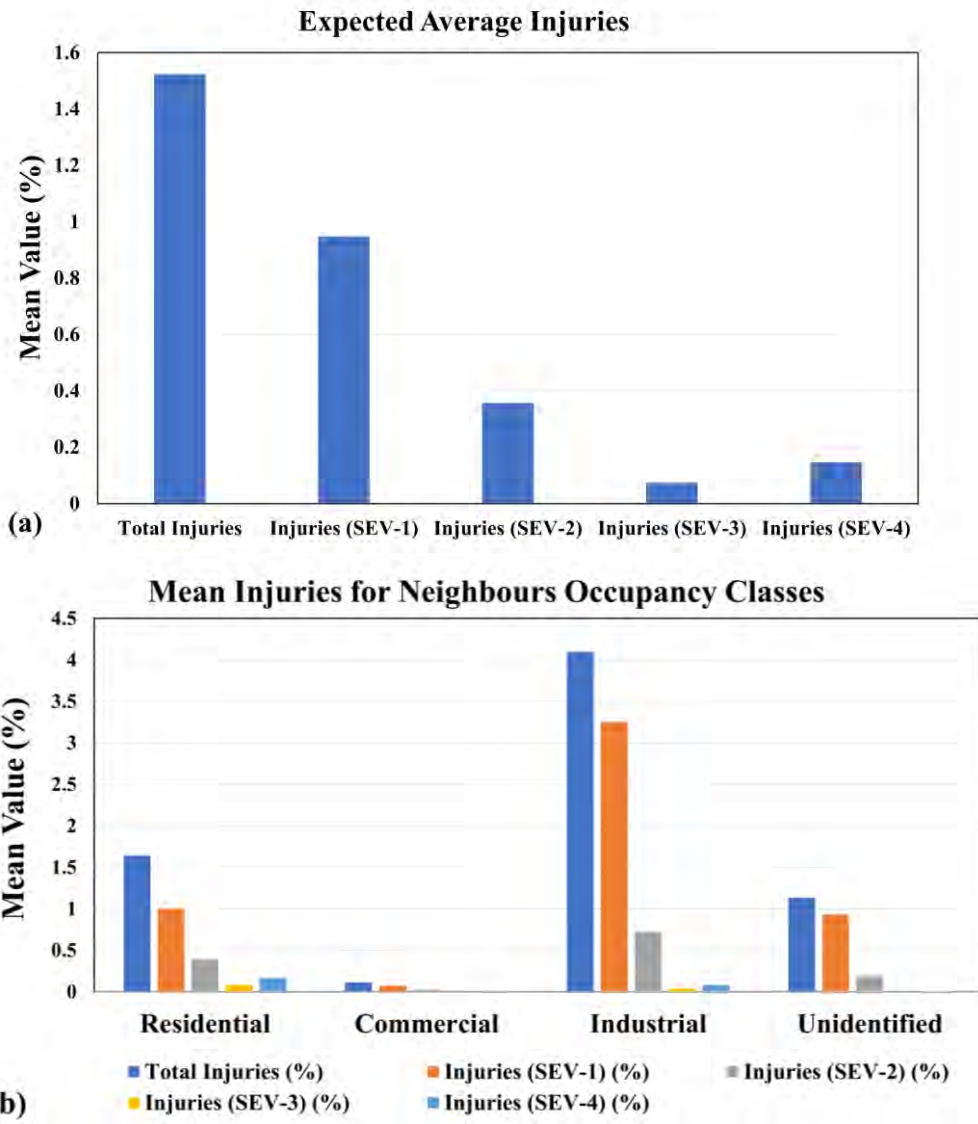
Figure 34: Mean values of estimated injuries: (a) Overall averages; and (b) Neighbors

classes.
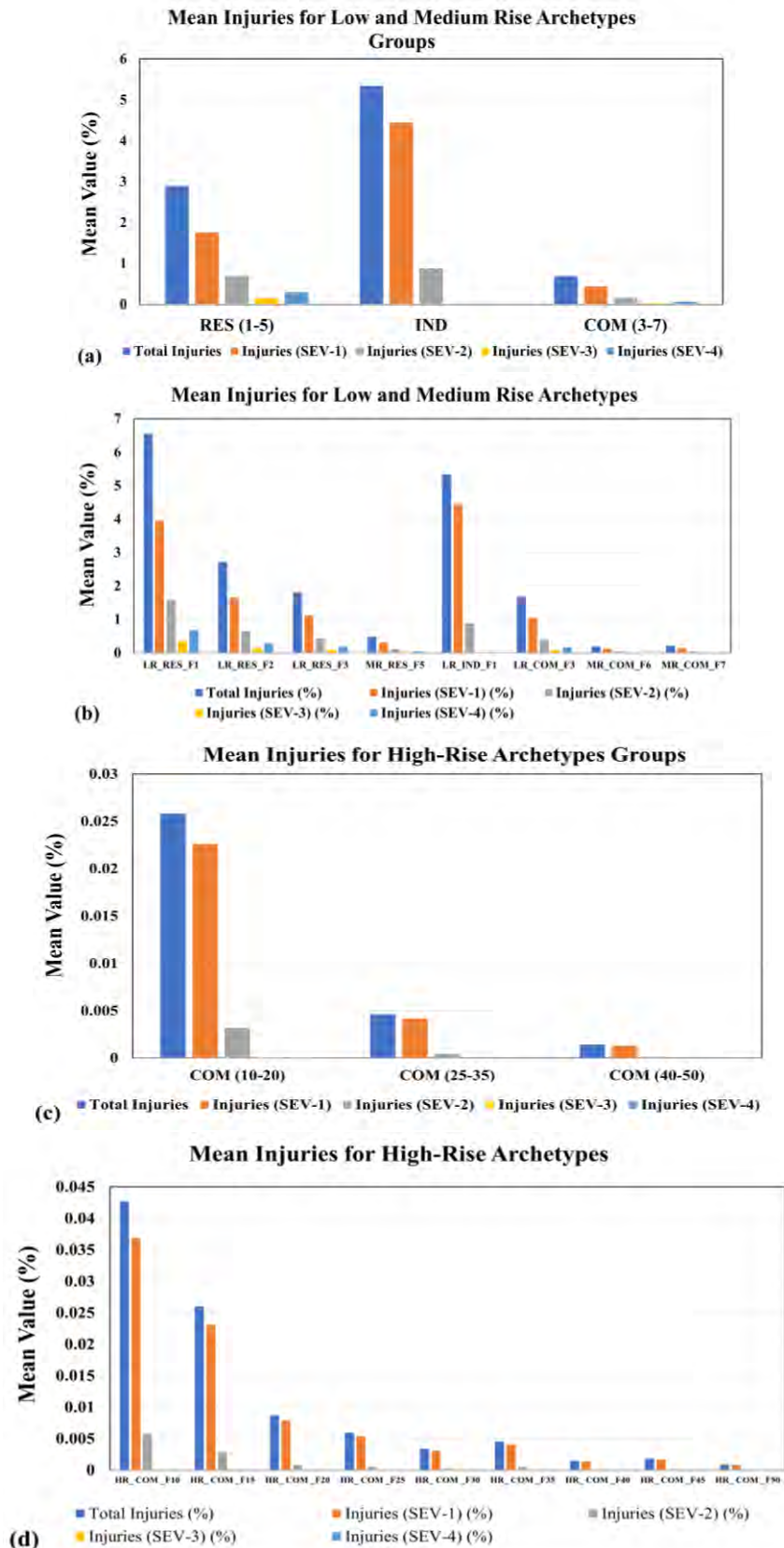
Figure 35: Mean values of estimated injuries: (a) Low and medium-rise archetypes groups; (b) Low and medium-rise archetypes; (c) High-rise archetypes groups; and (d) High-rise archetypes.

78
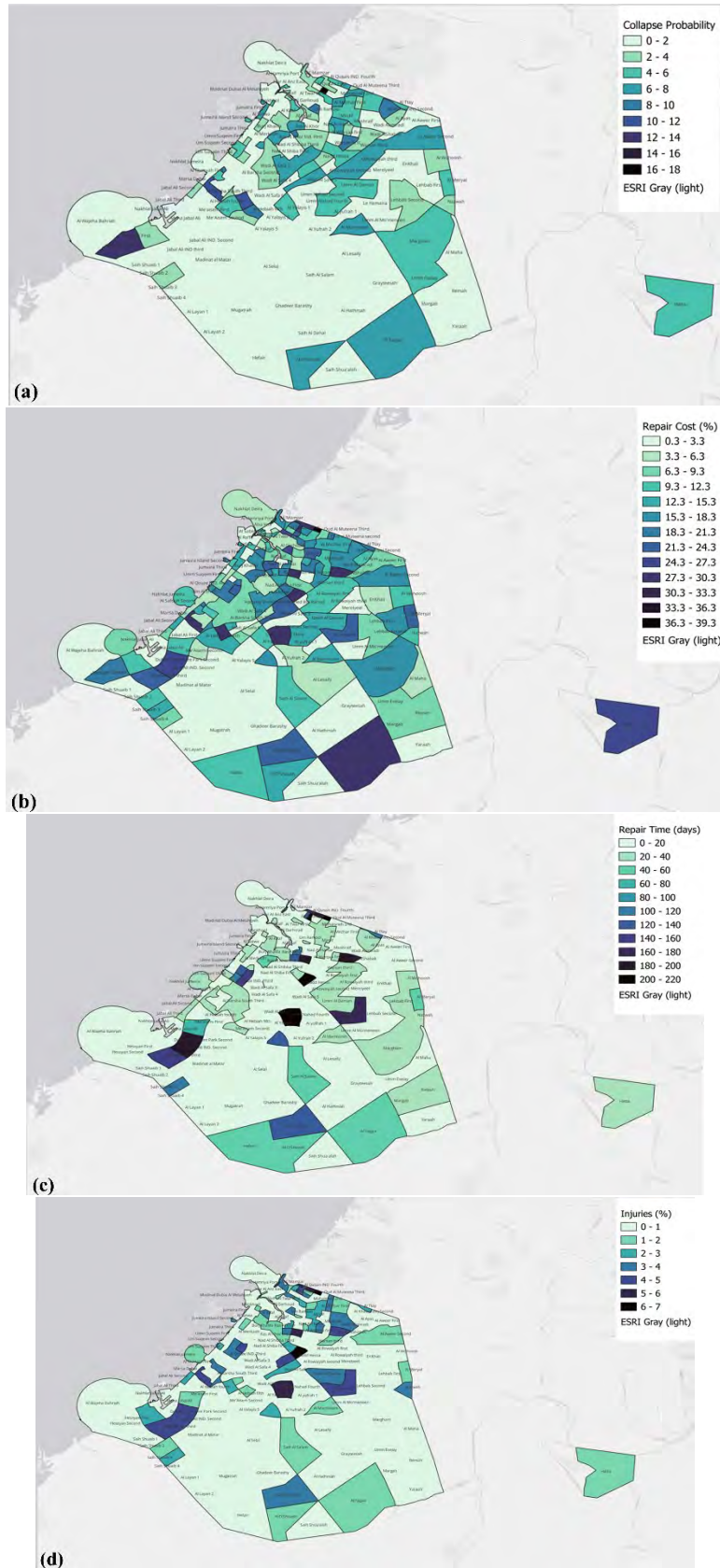
Figure 36: GIS choropleth maps representative for loss variables: (a) Collapse

probability; (b) Repair cost; (c) Repair time; (d) Injuries.

Chapter 6: Conclusions and Recommendations.

6.1 Summary

The location of UAE is surrounded by multiple earthquake sources both regionally (like; the Zagros Fold and Thrust Belt, and the Makran Subduction Zone), and locally (like; Oman Mountains, and the Dibba Line), as obtained in **Table 1**, **Figure 1**, and **Figure 27**. Based on observations and several studies from 2000-2006, three seismic events per year are expected in this region. The UAE construction sector expenditure occurred in an era when this region suffered from a lack of data related to seismic events and design response parameters. The diversity among studies was from no seismic hazard to very high seismicity, as shown in **Table 5,** so a regional earthquakes simulation is required to estimate the expected losses. This simulation process requires constructing databases for all buildings with their structural and spatial attributes as existed in reality. It is a challenging process that requires excessive data collection work, in addition to computational demands, and results uncertainties. For reducing the computational effort required for structure analysis, many methodologies were developed to calibrate refined FE models to simplified models that can present a similar lateral resistance behavior with few DOFs. On the other hand, the PEER PBEE methodology was established to estimate losses in a probabilistic manner that incorporates UQ with all loss estimation analyses. This study provided a prototype regional earthquake simulation for Dubai, with few assumptions to fill the unavailable data. The study depended on 17 archetypes that vary in occupancy, building height, structure type, and design seismic intensity, as shown in **Table 2**, and **Table 3**. The collected data for neighbors (like; locations, occupancy class, and the total number of buildings) were implemented to define the GIS databases, while distributing archetypes to GIS locations following arbitrary assumptions. For structure responses, the MCS model, proposed by [19], was implemented for low-rise, and medium-rise models, while the NMFS models were used for high-rise models. Calibrating NMFS models followed the process identified by [23], and showed the simplified models demand only 0.003 to 0.0006 of the time required time for refined FE models. The earthquake scenario component at R2D [9] was utilized to generate input ground motions per neighbor location, where the input earthquake source points were collected from different studies and summarized in **Table 14**. The simulation outputs included the collapse probability, repair cost, repair time, and expected injuries for every building in

the assumed database. Finally, the results had been filtered and grouped in scales of neighbors, neighbor classes, archetypes, and archetypes groups to analyze the impact of different input parameters.

6.2 Conclusion

The conclusion of configured outputs for studied archetypes is as follows:

- The "LR_RES_F1" and "LR_IND_F1" archetypes have different results patterns than other archetypes. "LR_RES_F1" is a bearing masonry wall residential house for a single family that was built more than 40 years ago. "LR_IND_F1" is a steel moment-framing structure for a light industrial purpose constructed almost 20 years ago, while other archetypes represent concrete structures for residential or commercial assets. "LR_RES_F1" produces the highest collapse probability of 8%, repair cost of 28%, and total injuries of 6.5%. Despite the "LR_IND_F1" being the lowest archetype in collapse probability (equals zero), it produces 2nd highest repair cost and total injury losses (26%, and 5% respectively). Moreover, it represents the longest repair time by 223 days with a significant difference from other models (2nd longest repair time equals 29 days).

- The seismic design spectrum is the key factor in scaling all loss parameters. The archetypes were designed assuming low seismic intensity had a collapse probability range from 4.6% to 8%, repair cost from 20% to 28.5%, and total injuries from 1.7% to 6.6%. For medium-rise archetypes, these results decrease: from 1.3% to 3.4% for collapse probability, and from 9.5% to 12.6% for the repair cost. and from 0.2% to 5.3%, for injuries. While archetypes designed for a high seismic intensity achieved the lowest loss values: from 0.2% to 2.3%, from 1.4% to 7%, and from 0.04% to zero for collapse probability, repair cost, and injuries, respectively.

The obtained results for neighbors' occupancy according to the estimated number of assets and assumed archetypes distributions weights are:

- The residential neighbors possess the highest collapse probability estimation. They have an expected collapse probability of 4%, a repair cost-to-replacement cost ratio of 15%, an average expected 20 days for repairs, and total injuries of 1.6% (1%, 0.4%, 0.08%, and 0.2% for different severity levels, ascendingly).

- The average expected collapse probability in a commercial is 0.8%. Their estimated repair costs and time are 4.6% and 11 days. The expected total injuries are only 0.1%, 65% of them for the lowest severity and only 9% represent the hardest cases.

- The industrial areas possess the highest values for loss variables except for the collapse probability which is 2%. Their estimated repair costs and time are 23% and 148 days. The expected total injuries are 4%, 79% of them for the lowest severity and only 2% represent the hardest cases.

- For neighbors with undefined classifications, the estimated loss variables are; a collapse probability of 3%, a repair cost-to-replacement cost ratio of 11.6%, an average expected 48 days for repairs, and total injuries of 1.1% (0.9%, 0.2%, 0.00%, and 0.01% for different severity levels, ascendingly).

Finally, the overall expected losses as average values are; a collapse probability of 3.6%, a repair cost is 14% of the total replacement cost, a repair time of 22 days for each asset, and total injuries of almost 1.5% of the total population. The injuries differ from lowest to highest severity as; 1%, 0.4%, 0.07%, and 0.15% respectively.

6.3 Recommendations

According to the estimated results, two major recommendations outcome from this study. The first recommendation is to design buildings in Dubai's region considering a conservative seismic hazard estimate (high or moderate), which will contribute to decreasing all loss variables. This recommendation was already introduced by a previous seismic hazard study [15]. Additionally, it is recommended to give a higher priority to evaluating structures that are designed assuming low seismic intensity as the built status, to be renovated or replaced. A higher priority should be given to assets with more populations and older construction time.

In 2004, J.P. Moehle and M.E. Jackson published a book [79] that provides a comprehensive overview of the principles and practices of earthquake retrofitting of existing buildings. The book begins by discussing the importance of earthquake retrofitting and the different types of retrofitting techniques. It then goes on to discuss the specific retrofitting methods that are used for different types of buildings, such as concrete buildings, steel buildings, and wood buildings. This book provides a comprehensive overview of the principles and practices of earthquake retrofitting of

existing buildings. The book begins by discussing the importance of earthquake retrofitting and the different types of retrofitting techniques. It then goes on to discuss the specific retrofitting methods that are used for different types of buildings, such as concrete buildings, steel buildings, and wood buildings. Here are some of the specific methods that can be used to check the earthquake resistance of already-built assets:

- Visual inspection: This involves inspecting the asset for any signs of damage or deterioration that could compromise its earthquake resistance.

- Non-destructive testing: This involves using non-destructive testing methods, such as ultrasonic testing or ground-penetrating radar, to assess the condition of the asset's structural elements.

- Destructive testing: This involves removing samples of the asset's structural elements to assess their strength and ductility.

The specific methods that are used will depend on the type of asset and the level of detail required. However, all of the methods mentioned above can be used to provide valuable information about the earthquake resistance of an asset.

6.4 Future Work and Possible Extensions

The proposed study achieved some enhancements to the previous Dubai regional seismic evaluation [65], like; considering more archetypes models, implementing earthquake scenario simulation, and adopting the HAZUS dataset [8] in estimating losses. But it still represents only a prototypal example that is limited to a few assumed models, and all high-rise archetypes follow the same plan layout and the LFRS. For extensions, adding more archetypes that contain different structural systems and a variation in material properties could be an accountable expenditure for the research significance. The long-term is to produce a regional simulation that reflects reality. This kind of accuracy required a long effort in data collection and the development of multiple programs to generate required building attributes and non-linear models from commercial documents/formats like 2D drawings or 3D models.

The research was based on FEMA-P58 methodology to determine decision variables. These methods depend on an analytical procedure for data North-America earthquakes where the community response, Cultural behavior with such disasters, and governmental and decision-making or preparedness, and financial conditions are

different from the UAE community. So Working on calibration Fragility curves for UAE simulation is a key path to improve the accuracy and reality of similar research. Over the past few years, the advancement of seismic risk assessment systems have been significant. However, this progress has created a need for further development in incremental dynamic analyses. Despite this, these systems have the potential to make significant contributions to various areas of structural engineering applications, such as structural assessment [80]–[85] and the application of soft computing techniques in civil engineering [86]–[95]. Additionally, they can aid in the evaluation of structures under various lateral loads (e.g., seismic [96]–[128] and wind [129]–[133] loads), as well as many other applications [134]–[199].

References

[1]   R. Sigbjornsson and A. S. Elnashai, "Hazard assessment of dubai, united arab emirates, for close and distant earthquakes," *Journal of Earthquake Engineering*, vol. 10, no. 5, pp. 748–773, 2006, doi: 10.1080/13632460609350617.

[2]   D. Al-Dogom, K. Schuckma, and R. Al-Ruzouq, "Geostatistical seismic analysis and hazard assessment; United Arab Emirates," *International Archives of the Photogrammetry, Remote Sensing and Spatial Information Sciences - ISPRS Archives*, vol. 42, no. 3W4, pp. 29–36, 2018, doi: 10.5194/isprs-archives-XLII-3-W4-29-2018.

[3]   Incorporated Research Institutions for Seismology, "IRIS Earthquake Browser." Accessed: May 12, 2022. [Online]. Available: http://www.iris.edu/servlet/eventserver/map.do

[4]   "International Seismological Centre," *Disaster Prevention and Management: An International Journal*, vol. 8, no. 1, p. 452, 1999, doi: 10.1108/dpm.1999.07308aag.015.

[5]   "National Geoscience Database of IRAN." 2011. Accessed: May 22, 2021. [Online]. Available: http://www.ngdir.ir/Earthquake/Earthquake.asp

[6]   D. Andes, "GIS Lounge." 2006. Accessed: May 12, 2023. [Online]. Available: https://www.gislounge.com

[7]   M. AlHamaydeh, G. Al-Shamsi, N. Aly, and T. Ali, "Geographic Information System-Based Seismic Risk Assessment for Dubai, UAE: A Step toward Resilience and Preparedness," *Practice Periodical on*

Structural Design and Construction, vol. 27, no. 1, 2022, doi: 10.1061/(asce)sc.1943-5576.0000637.

[8] Hazus, "Hazus–MH 2.1: Technical Manual," *Federal Emergency Management Agency*, p. 718, 2012, [Online]. Available: www.fema.gov/plan/prevent/hazus

[9] Frank McKenna *et al.*, "The Regional Resilience Determnation (R2D)." 2021. Accessed: May 22, 2021. [Online]. Available: https://nheri-simcenter.github.io/R2D-Documentation/index.html

[10] F. McKenna, M. H. Scott, and G. L. Fenves, "Nonlinear Finite-Element Analysis Software Architecture Using Object Composition," *Journal of Computing in Civil Engineering*, vol. 24, no. 1. University of California, Berkeley, pp. 95–107, 2010. doi: 10.1061/(asce)cp.1943-5487.0000002.

[11] B. M. Adams *et al.*, "DAKOTA , A Multilevel Parallel Object-Oriented Framework for Design Optimization , Parameter Estimation , Sensitivity Analysis , and Uncertainty Quantification Acknowledgment," no. May, p. 354, 2021.

[12] N. A. Abrahamson, W. J. Silva, and R. Kamai, "Update of the AS08 Ground-Motion Prediction equations based on the NGA-west2 data set," *Pacific Engineering Research Center Report*, no. May, p. 174, 2013.

[13] "UAE Construction Cost Insight Report UAE projects snapshot." jll-mena, 2021. Accessed: Mar. 23, 2022. [Online]. Available: https://www.jll-mena.com/en/trends-and-insights/research/the-uae-construction-market-report

[14] X. Lu, F. McKenna, Q. Cheng, Z. Xu, X. Zeng, and S. A. Mahin, "An open-source framework for regional earthquake loss estimation using the

city-scale nonlinear time history analysis," *Earthquake Spectra*, vol. 36, no. 2, pp. 806–831, 2020, doi: 10.1177/8755293019891724.

[15] M. AlHamaydeh, N. Aly, and K. Galal, "Effect of Diverse Seismic Hazard Estimates on Design and Performance of RC Shear Wall Buildings in Dubai, UAE," *The 2015 World Congress on Advances in Structural Engineering and Mechanics (ASEM15), August 25-29*, 2015.

[16] C. Xiong, X. Lu, H. Guan, and Z. Xu, "A nonlinear computational model for regional seismic simulation of tall buildings," *Bulletin of Earthquake Engineering*, vol. 14, no. 4, pp. 1047–1069, 2016, doi: 10.1007/s10518-016-9880-0.

[17] "Wikipedia." Accessed: May 12, 2023. [Online]. Available: https://en.wikipedia.org/wiki/CUDA

[18] "Cusp." Accessed: May 12, 2023. [Online]. Available: https://cusplibrary.github.io

[19] B. Han, X. Lu, Z. Xu, and Y. Li, "Seismic damage simulation of urban buildings based on high performance GPU computing," *Journal of Natural Disasters*, vol. 21, no. 5, pp. 16–22, 2012.

[20] L. Xiao, L. Xinzheng, Z. Wankai, and Y. Lieping, "Collapse simulation of a super high-rise building subjected to extremely strong earthquakes," *Sci China Technol Sci*, vol. 54, no. 10, pp. 2549–2560, 2011, doi: 10.1007/s11431-011-4548-0.

[21] X. Lu, Y. Tian, S. Cen, H. Guan, L. Xie, and L. Wang, "A High-Performance Quadrilateral Flat Shell Element for Seismic Collapse Simulation of Tall Buildings and Its Implementation in OpenSees,"

Journal of Earthquake Engineering. 2018. Accessed: Apr. 15, 2021. [Online]. Available: https://doi.org/10.1080/13632469.2017.1297269

[22]   Z. Xu, X. Lu, H. Guan, B. Han, and A. Ren, "Seismic damage simulation in urban areas based on a high-fidelity structural model and a physics engine," *Natural Hazards*, vol. 71, no. 3, pp. 1679–1693, 2014, doi: 10.1007/s11069-013-0972-8.

[23]   S. Taghavi and E. Miranda, "Approximate Floor Acceleration Demands in Multistory Buildings. II: Applications," *Journal of Structural Engineering*, vol. 131, no. 2, pp. 212–220, 2005, doi: 10.1061/(asce)0733-9445(2005)131:2(212).

[24]   American Society of Civil Engineers (ASCE), *Prestandard and Commentary for the Seismic Rehabilitation of Buildings*, FEMA-356., no. 1. Washington, D.C., 2000.

[25]   SEAOC, *Performance-based seismic engineering*. Sacramento, CA: SEAOC Vision 2000 Committee, 1995.

[26]   M. S. Günay and K. M. Mosalam, "PEER Performance Based Earthquake Engineering Methodology , Revisited," no. Moehle, 2003.

[27]   K. A. Porter, "An Overview of PEER's Performance-Based Earthquake Engineering Methodology," *9th International Conference on Applications of Statistics and Probability in Civil Engineering*, vol. 273, no. 1995, pp. 973–980, 2003.

[28]   J. Moehle and G. G. Deierlein, "a Framework Methodology for Performance-Based Earthquake Engineering," *13th World Conference on Earthquake Engineering*, no. 679, 2004.

[29] J. J. Bommer and N. A. Abrahamson, "Why do modern probabilistic seismic-hazard analyses often lead to increased hazard estimates?," *Bulletin of the Seismological Society of America*, vol. 96, no. 6, pp. 1967–1977, 2006, doi: 10.1785/0120060043.

[30] H. Krawinkler, "Van Nuys Hotel Building Testbed Report: Exercising Seismic Performance Assessment," *PEER Report 2005/11*. Pacific Earthquake Engineering Research Center College of Engineering University of California, Berkeley, 2005. Accessed: Jul. 01, 2022. [Online]. Available: https://peer.berkeley.edu/sites/default/files/peer_511_krawinkler_testbed.pdf

[31] M. C. Comerio, "PEER testbed study on a laboratory building: exercising seismic performance assessment," no. November. 2005. Accessed: Jan. 07, 2022. [Online]. Available: http://peer.berkeley.edu/publications/peer_reports/reports_2005/PEER_512_COMERIO_testbed.pdf

[32] A. Bohl, "[THESIS] Comparison of Performance Based Engineering Approaches," Master of Applied Science, The University of British Columbia, 2009.

[33] C. A. Goulet *et al.*, "Evaluation of the seismic performance of a code-conforming reinforced-concrete frame building - From seismic hazard to collapse safety and economic losses," *Earthq Eng Struct Dyn*, vol. 36, no. 13, pp. 1973–1997, 2007, doi: 10.1002/eqe.694.

[34] S. Günay and K. M. Mosalam, "PEER performance-based earthquake engineering methodology, revisited," *Journal of Earthquake Engineering*, vol. 17, no. 6, pp. 829–858, 2013, doi: 10.1080/13632469.2013.787377.

[35] J. Mitrani-Reiser, C. Haselton, C. Goulet, K. Porter, J. Beck, and G. Deierlein, "Evaluation of the seismic performance of a code-conforming reinforced-concrete frame building - Part II: Loss estimation," in *8th US National Conference on Earthquake Engineering 2006*, San Francisco, California, 2006.

[36] SimCenter, "SimCenter." Accessed: Oct. 01, 2022. [Online]. Available: https://simcenter.designsafe-ci.org/

[37] H. Jasak, "OpenFOAM: Open source CFD in research and industry," *International Journal of Naval Architecture and Ocean Engineering*, vol. 1, no. 2, pp. 89–94, 2009, doi: 10.2478/ijnaoe-2013-0011.

[38] PEER, "PEER Strong Motion Database," *University of California at Berkeley*. Pacific Earthquake Engineering Research Center, 2010. Accessed: Jan. 10, 2022. [Online]. Available: http://peer.berkeley.edu/peer_ground_motion_database

[39] C. Wang *et al.*, "Building Recognition using Artificial Intelligence at Large Scale (BRAILS)." NHERI-SimCenter/BRAILS, 2021. doi: http://doi.org/10.5281/zenodo.4570554.

[40] FEMA, "Seismic performance assessment of buildings, volume 1 - methodology," *Fema P-58-1*, vol. 1, no. December 2018. p. 340, 2018. Accessed: Jan. 12, 2022. [Online]. Available: https://femap58.atcouncil.org/%0Ahttps://www.fema.gov/media-library/assets/documents/90380

[41] Z. Xu, X. Lu, and K. H. Law, "A computational framework for regional seismic simulation of buildings with multiple fidelity models," *Advances in Engineering Software*, vol. 99, pp. 100–110, 2016, doi: 10.1016/j.advengsoft.2016.05.014.

[42] I. Sianko, Z. Ozdemir, I. Hajirasouliha, and K. Pilakoutas, "Probabilistic seismic risk assessment framework: case study Adapazari, Turkey," *Bulletin of Earthquake Engineering*, 2023, doi: 10.1007/s10518-023-01674-2.

[43] P. A. Kingsbury, J. R. Pettinga, and R. J. Van Dissen, "Earthquake hazard and risk assessment study for the Canterbury Region, South Island, New Zealand: Outline of programme development," *Bulletin of the New Zealand Society for Earthquake Engineering*, vol. 34, no. 4, pp. 276–281, 2001, doi: 10.5459/bnzsee.34.4.276-281.

[44] C. H. Hsu, S. S. Ke, and T. H. Wu, "Development and Application of a Platform for Multidimensional Urban Earthquake Impact Simulation," *Front Built Environ*, vol. 8, 2022, doi: 10.3389/fbuil.2022.938747.

[45] S. Bhochhibhoya and R. Maharjan, "Integrated seismic risk assessment in Nepal," *Natural Hazards and Earth System Sciences*, vol. 22, no. 10, pp. 3211–3230, 2022, doi: 10.5194/nhess-22-3211-2022.

[46] M. Dolce *et al.*, "Seismic risk assessment of residential buildings in Italy," *Bulletin of Earthquake Engineering*, vol. 19, no. 8, pp. 2999–3032, 2021, doi: 10.1007/s10518-020-01009-5.

[47] G. Grünthal, C. Bosse, S. Sellami, D. Mayer-Rosa, and D. Giardini, "Compilation of the GSHAP regional seismic hazard for Europe, Africa

and the Middle East," *Annals of Geophysics*, vol. 42, no. 6, 2021, doi: 10.4401/ag-3782.

[48] J. A. Abdalla and A. S. Al-Homoud, "Seismic hazard assessment of United Arab emirates and its surroundings," *Journal of Earthquake Engineering*, vol. 8, no. 6, pp. 817–837, 2004, doi: 10.1080/13632460409350510.

[49] R. Sigbjornsson and A. S. Elnashai, "Hazard assessment of dubai, united arab emirates, for close and distant earthquakes," *Journal of Earthquake Engineering*, vol. 10, no. 5, pp. 748–773, 2006, doi: 10.1080/13632460609350617.

[50] J. A. Abdalla, J. T. Petrovski, and Y. E. Mohamedzein, "Vibration characteristics of a far field earthquake and its shaking effects on Dubai emerging skyscrapers," in *The 14 th World Conference on Earthquake Engineering*, Beijing, China, 2008.

[51] E. Al Khatibi and A. Elenean, "Dubai seismic network." Dubai Municipality, p. 2460, 2012. Accessed: Apr. 10, 2021. [Online]. Available: https://www.seismo.geodesy.ae/dsn.aspx

[52] Z. Khan, M. El-Emam, M. Irfan, and J. Abdalla, "Probabilistic seismic hazard analysis and spectral accelerations for United Arab Emirates," *Natural Hazards*, vol. 67, no. 2, pp. 569–589, 2013, doi: 10.1007/s11069-013-0586-1.

[53] M. Al-Haddad, G. H. Siddiqi, R. Al-Zaid, A. Arafah, A. Necioglu, and N. Turkelli, "A Basis for Evaluation of Seismic Hazard and Design Criteria for Saudi Arabia," *Earthquake Spectra*, vol. 10, no. 2, pp. 231–258, 1994, doi: 10.1193/1.1585773.

[54] N. Peiris, M. Free, Z. Lubkowski, and a. T. Hussein, "Seismic hazard and seismic design requirements for the Arabian Gulf region," *First European Conference on Earthquake Engineering and Seismology*, no. 2006, p. 10, 2006.

[55] R. M. W. Musson *et al.*, "The Geology and Geophysics of the United Arab Emirates Volume 4 : Geological Hazards The Geology and Geophysics of the United Arab Emirates Volume 4 : Geological Hazards," vol. 4, p. 251, 2006.

[56] G. Aldama-Bustos, J. J. Bommer, C. H. Fenton, and P. J. Stafford, "Probabilistic seismic hazard analysis for rock sites in the cities of Abu Dhabi, Dubai and Ra's Al Khaymah, United Arab Emirates," *Georisk*, vol. 3, no. 1, pp. 1–29, 2009, doi: 10.1080/17499510802331363.

[57] A. A. Shama, "Site specific probabilistic seismic hazard analysis at Dubai Creek on the west coast of UAE," *Earthquake Engineering and Engineering Vibration*, vol. 10, no. 1, pp. 143–152, 2011, doi: 10.1007/s11803-011-0053-5.

[58] M. AlHamaydeh, S. Abdullah, A. Hamid, and A. Mustapha, "Seismic design factors for RC special moment resisting frames in Dubai, UAE," *Earthquake Engineering and Engineering Vibration*, vol. 10, no. 4, pp. 495–506, 2011, doi: 10.1007/s11803-011-0084-y.

[59] A. Mwafy, "Assessment of seismic design response factors of concrete wall buildings," *Earthquake Engineering and Engineering Vibration*, vol. 10, no. 1, pp. 115–127, 2011, doi: 10.1007/s11803-011-0051-7.

[60] M. AlHamaydeh, S. Yehia, N. Aly, A. Douba, and L. Hamzeh, "Design Alternatives for Lateral Force-Resisting Systems of Tall Buildings in

Dubai, UAE," *International Journal of Civil and Environmental Engineering*, vol. 6, pp. 185–188, 2012.

[61]   N. Aly, M. AlHamaydeh, and K. Galal, "Quantification of the Impact of Detailing on the Performance and Cost of RC Shear Wall Buildings in Regions with High Uncertainty in Seismicity Hazards," *Journal of Earthquake Engineering*, vol. 24, no. 3, pp. 421–446, 2020, doi: 10.1080/13632469.2018.1453406.

[62]   M. AlHamaydeh, M. E. Elkafrawy, N. G. Aswad, R. Talo, and S. Banu, "Evaluation of UHPC Tall Buildings in UAE with Ductile Coupled Shear Walls under Seismic Loading," pp. 1–6, 2022, doi: 10.1109/aset53988.2022.9734863.

[63]   M. AlHamaydeh, M. E. Elkafrawy, F. M. Amin, A. M. Maky, and F. Mahmoudi, "Analysis and Design of UHPC Tall Buildings in UAE with Ductile Coupled Shear Walls Lateral Load Resisting System," pp. 1–6, 2022, doi: 10.1109/aset53988.2022.9735104.

[64]   M. AlHamaydeh, M. Elkafrawy, and S. Banu, "Seismic Performance and Cost Analysis of UHPC Tall Buildings in UAE with Ductile Coupled Shear Walls," *Materials*, vol. 15, no. 8, p. 2888, 2022, doi: 10.3390/ma15082888.

[65]   M. AlHamaydeh, G. Al-Shamsi, N. Aly, and T. Ali, "Seismic risk quantification and GIS-based seismic risk maps for Dubai-UAE_Dataset," *Data Brief*, vol. 39, 2021, doi: 10.1016/j.dib.2021.107566.

[66]   FEMA P695, "Quantification of Building Seismic Performance Factors," *Fema P695*, no. June, p. 421, 2009.

[67] ASCE/SEI, "Asce/Sei 41-17," *Seismic Evaluation and Retrofit of Existing Buildings*. American Society of Civil Engineers, pp. 1–576, 2017. Accessed: Mar. 12, 2022. [Online]. Available: http://ascelibrary.org/doi/book/10.1061/9780784414859

[68] "Github Repository for Pre/Post packaging for design archetypes and calibrating tall buildings models." Accessed: May 10, 2023. [Online]. Available: https://github.com/AhmedMaky93/DUBAIseismicData

[69] ACI 318, "Building Code Requirements for Structural Concrete and Commentary," *ACI Struct J*, vol. 552, no. d, p. 503, 1994.

[70] "OpenSeesWiki." Accessed: Jun. 25, 2022. [Online]. Available: https://opensees.berkeley.edu/wiki/index.php

[71] J. S. Steelman and J. F. Hajjar, "Influence of inelastic seismic response modeling on regional loss estimation," *Eng Struct*, vol. 31, no. 12, pp. 2976–2987, 2009, doi: 10.1016/j.engstruct.2009.07.026.

[72] JGJ 3, "Technical Specification for Concrete Structures of Tall Building - JGJ 3-2010," p. 177, 2010.

[73] American Concrete Institute, "ACI Committee 318: Building Code Requirements for Structural Concrete," *MI:Farmington Hills*, 2011.

[74] M. Zaré and H. Memarian, "the Iranian Earthquake Intensity Database: 1975-2000," no. January, 2002.

[75] Y. Al Marzooqi, K. M. Abou Elenean, A. S. Megahed, I. El-Hussain, A. J. Rodgers, and E. Al Khatibi, "Source parameters of March 10 and September 13, 2007, United Arab Emirates earthquakes," *Tectonophysics*, vol. 460, no. 1–4, pp. 237–247, 2008, doi: 10.1016/j.tecto.2008.08.017.

[76] K. Hessami, H. A. Koyi, and C. J. Talbot, "The significance of strike-slip faulting in the basement of the Zagros fold and thrust belt," *Journal of Petroleum Geology*, vol. 24, no. 1, pp. 5–28, 2001, doi: 10.1111/j.1747-5457.2001.tb00659.x.

[77] B. S.-J. Chiou and R. R. Youngs, "Chiou and Youngs PEER-NGA Empirical Ground Motion Model for the Average Horizontal Component of Peak Acceleration and Pseudo-Spectral Acceleration for Spectral Periods of Interim Report for USGS Review," *PEER Report Draft, Pacific Earthquake Engineering ...*. p. 219, 2006. Accessed: Apr. 18, 2023. [Online]. Available: http://peer.berkeley.edu/lifelines/nga_docs/jul_10_06/Chiou_Youngs_NGA_2006.pdf

[78] A. Zsarnóczay and G. G. Deierlein, "PELICUN - A Computational Framework for Estimating Damage , Loss and Community Resilience," *17th World Conference on Earthquake Engineering*, pp. 1–12, 2020.

[79] M. D'amato, R. Laguardia, and R. Gigliotti, "Seismic retrofit of an existing RC building with isolation devices applied at base," *Front Built Environ*, vol. 6, pp. 1–16, 2020, doi: 10.3389/fbuil.2020.00082.

[80] M. AlHamaydeh, M. A. Jaradat, M. Serry, L. Sawaqed, and K. S. Hatamleh, "Structural control of MR-dampers with genetic algorithm-optimized Quasi-Bang-Bang controller," in *2017 7th International Conference on Modeling, Simulation, and Applied Optimization (ICMSAO)*, IEEE, Apr. 2017, pp. 1–6. doi: 10.1109/ICMSAO.2017.7934887.

[81] A. H. El-Sinawi, M. H. AlHamaydeh, and A. a. Jhemi, "Optimal Control of Magneto-Rheological Fluid Dampers for Seismic Isolation of Structures," *Math Probl Eng*, vol. 2013, pp. 1–7, 2013, doi: 10.1155/2013/251935.

[82] S. Hussain, P. Van Benschoten, M. Al Satari, and S. Lin, "Use of Viscous Fluid Dampers to Retrofit Steel Moment Frame Structures," in *The 10th World Conference on Seismic Isolation, Energy Dissipation and Active Vibrations Control of Structures*, 2007.

[83] S. Hussain and M. Al Satari, "Viscous-Damped Seismic Isolation System for a Near-Fault Essential Services Facility," in *The 10th World Conference on Seismic Isolation, Energy Dissipation and Active Vibrations Control of Structures*, 2007.

[84] S. Yehia, M. Al Satari, A. Abdelfatah, and S. Tabsh, "Civil Engineering Curriculum Development Based on Track Approach," in *ICERI2009 Proceedings*, 2009, pp. 5442–5448.

[85] M. AlHamaydeh, A. M. Maky, and M. Elkafrawy, "INSPECT-SPSW: INelastic Seismic Performance Evaluation Computational Tool for Steel Plate Shear Wall Modeling in OpenSees," *Buildings*, vol. 13, no. 4, p. 1078, Apr. 2023, doi: 10.3390/buildings13041078.

[86] M. I. Awad, M. AlHamaydeh, and A. Faris, "Fault detection via nonlinear profile monitoring using artificial neural networks," *Qual Reliab Eng Int*, vol. 34, no. 6, pp. 1195–1210, Oct. 2018, doi: 10.1002/qre.2318.

[87] M. AlHamaydeh, I. Choudhary, and K. Assaleh, "Virtual Testing of Buckling-Restrained Braces via Nonlinear AutoRegressive eXogenous

Neural Networks," *Journal of Computing in Civil Engineering, ASCE*, vol. 27, no. 6, pp. 755–768, 2013.

[88] I. Choudhary, K. Assaleh, and M. AlHamaydeh, "Nonlinear AutoRegressive eXogenous Artificial Neural Networks for predicting Buckling Restrained Braces Force," in *The 2012 International Symposium on Mechatronics and its Applications (ISMA 2012)*, 2012.

[89] S. Barakat and M. AlHamaydeh, "Preliminary Design of Seismic Isolation Systems Using Artificial Neural Networks," in *The 2014 International Conference on Neural Networks - Fuzzy Systems (NN-FS 2014)*, 2014, pp. 91–95.

[90] M. Awad, M. AlHamaydeh, and A. F. Mohamed, "Structural damage fault detection using Artificial Neural network profile monitoring," in *2017 7th International Conference on Modeling, Simulation, and Applied Optimization (ICMSAO)*, 2017, pp. 1–6.

[91] S. A. Barakat and M. H. AlHamaydeh, "Preliminary Design of Seismic Isolation Systems Using Artificial Neural Networks," *International Journal of Neural Networks and Advanced Applications*, vol. 9, pp. 12–17, 2022.

[92] K. Assaleh, M. AlHamaydeh, and I. Choudhary, "Modeling nonlinear behavior of Buckling-Restrained Braces via different artificial intelligence methods," *Appl Soft Comput*, vol. 37, pp. 923–938, 2015.

[93] M. AlHamaydeh, G. Markou, N. Bakas, and M. Papadrakakis, "AI-based shear capacity of FRP-reinforced concrete deep beams without stirrups," *Eng Struct*, vol. 264, p. 114441, 2022.

[94] M. Al Satari and J. Abdalla, "Optimization of A Base-Isolation System Consisting of Natural Rubber Bearings and Fluid Viscous Dampers," in *The 11th World Conference on Seismic Isolation, Energy Dissipation and Active Vibration Control of Structures*, 2009.

[95] M. H. AlHamaydeh, A. F. Mohamed, and M. I. Awad, "Development of Fault-Detection ANNs for Structural Damage Prediction," in *ACI SP-350: The Concrete Industry in the Era of Artificial Intelligence*, American Concrete Institute (ACI), 2021, pp. 45–53.

[96] M. AlHamaydeh, M. Elkafrawy, and S. Banu, "Seismic Performance and Cost Analysis of UHPC Tall Buildings in UAE with Ductile Coupled Shear Walls," *Materials*, vol. 15, no. 8, pp. 1–23, 2022, doi: 10.3390/ma15082888.

[97] M. AlHamaydeh, M. E. Elkafrawy, M. Kyaure, M. Elyas, and F. Uwais, "Cost Effectiveness of UHPC Ductile Coupled Shear Walls for High-Rise Buildings in UAE Subjected to Seismic Loading," in *2022 Advances in Science and Engineering Technology International Conferences (ASET)*, IEEE, Feb. 2022, pp. 1–6. doi: 10.1109/ASET53988.2022.9734843.

[98] M. AlHamaydeh, M. E. Elkafrawy, N. G. Aswad, R. Talo, and S. Banu, "Evaluation of UHPC Tall Buildings in UAE with Ductile Coupled Shear Walls under Seismic Loading," in *2022 Advances in Science and Engineering Technology International Conferences (ASET)*, IEEE, Feb. 2022, pp. 1–6. doi: 10.1109/ASET53988.2022.9734863.

[99] M. AlHamaydeh, G. Al-Shamsi, N. Aly, and T. Ali, "Seismic Risk Quantification and GIS-based Seismic Risk Maps for Dubai-

UAE_Dataset," *Data Brief*, vol. 37, no. December, pp. 107565–107566, 2021.

[100] M. AlHamaydeh, G. Al-Shamsi, N. Aly, and T. Ali, "Geographic Information System-Based Seismic Risk Assessment for Dubai, UAE: a Step towards Resilience and Preparedness," *Practice Periodical on Structural Design and Construction, ASCE*, vol. 27, no. 1, p. DOI--10, 2022.

[101] M. AlHamaydeh, G. Al-Shamsi, N. Aly, and T. Ali, "Data for Seismic Risk Quantification and GIS-Based Seismic Risk Maps for Dubai-UAE," *Mendeley Data, V5, http://doi.org/10.17632/shpfp7bdx7.5*. 2021.

[102] R. Sawires, J. Peláez, M. AlHamaydeh, and J. Henares, "Up-to-date earthquake and focal mechanism solutions datasets for the assessment of seismic hazard in the vicinity of the United Arab Emirates," *Mendeley Data, v3, http://dx.doi.org/10.17632/t4ck8gp3jh.3*. 2019.

[103] R. Sawires, J. A. Peláez, M. AlHamaydeh, and J. Henares, "Up-to-date Earthquake and Focal Mechanism Solutions Datasets for the Assessment of Seismic Hazard in the Vicinity of the United Arab Emirates," *Data Brief*, vol. 28, no. February, p. p--104844, 2020.

[104] M. AlHamaydeh and M. Siddiqi, "OpenSEES GUI for Elastomeric Seismic Isolation Systems," *First Eurasian Conference on OpenSEES (OpenSEES Days Eurasia), Hong Kong*, 2019.

[105] R. Sawires, J. A. Peláez, M. AlHamaydeh, and J. Henares, "A State-Of-The-Art Seismic Source Model for the United Arab Emirates," *J Asian Earth Sci*, vol. 186, no. December, pp. 104063--DOI, 2019.

[106] M. AlHamaydeh and L. Elayyan, "Impact of diverse seismic hazard estimates on design and performance of Steel Plate Shear Walls buildings in Dubai, UAE," in *2017 7th International Conference on Modeling, Simulation, and Applied Optimization (ICMSAO)*, IEEE, Apr. 2017, pp. 1–4. doi: 10.1109/ICMSAO.2017.7934869.

[107] M. AlHamaydeh, L. Elayyan, and M. Najib, "Impact of Eliminating Web Plate Buckling on the Design, Cost and Seismic Performance of Steel Plate Shear Walls," *The 2015 International Conference on Steel and Composite Structures(ICSCS15)*, 2015.

[108] M. AlHamaydeh, S. Barakat, and O. Nassif, "Optimization of Quatropod Jacket Support Structures for Offshore Wind Turbines Subject to Seismic Loads Using Genetic Algorithms," in *The 5th International Conference on Computational Methods in Structural Dynamics and Earthquake Engineering (COMPDYN2015), Crete Island, Greece*, 2015, pp. 3505–3513.

[109] S. Barakat, M. AlHamaydeh, and O. Nassif, "Optimization of Seismic Isolation Systems with Viscous Fluid Dampers Using Genetic Algorithms," in *The 5th International Conference on Computational Methods in Structural Dynamics and Earthquake Engineering (COMPDYN2015), Crete Island, Greece*, 2015, pp. 4086–4095.

[110] M. AlHamaydeh and N. Aly, "Optimum Seismic Isolation System Design for Retrofitting and Upgrading Existing Concrete Bridges," in *The 2014 International Conference on Mechanics, Fluid Mechanics, Heat and Mass Transfer (MFMHMT 2014)*, 2014, pp. 135–139.

[111] M. Al Satari, *Estimation of Seismic Response Demands for R/C Framed Structures: An Insight Into The Nonlinear Seismic Behavior*. VDM Verlag, Saarbrücken, Germany, 2008.

[112] S. Hussain and M. Al Satari, "Design of a Seismic Isolation System with Supplemental Viscous Damping for a Near-Fault Essential Facility," in *The 14th World Conference on Earthquake Engineering*, 2008.

[113] M. Al Satari and J. Anderson, "Nonlinearity Effects on the Seismic Behavior of RC Framed Structures," in *The 76th SEAOC Annual Convention, September 26-29*, Squaw Creek, California, USA, 2007.

[114] J. Anderson, V. Bertero, and M. Al Satari, "Inelastic Seismic Response of a Tilt-up Wall Building and Design Implications," in *The 74th SEAOC Annual Convention*, 2005.

[115] M. H. Al Satari, "Estimation of Seismic Response Demands for RC Framed Structures," University of Southern California, 2005.

[116] S. Hussain and M. Al Satari, "Design of a Seismic Isolation System with Supplemental Viscous Damping for a Near-Fault Essential Services Facility," in *The 76th SEAOC Annual Convention*, 2007.

[117] J. C. Anderson, V. V. Bertero, M. Kargahi, and M. Al Satari, "Seismic Performance of an Instrumented Tilt-up Wall Building." Pacific Earthquake Engineering Research Center, 2004.

[118] A. H. ElSinawi, A. Jhemi, and M. AlHamaydeh, "Adaptive seismic isolation of structures using MR-fluid dampers," in *2013 5th International Conference on Modeling, Simulation and Applied Optimization (ICMSAO)*, IEEE, Apr. 2013, pp. 1–6. doi: 10.1109/ICMSAO.2013.6552603.

[119] M. AlHamaydeh, K. Galal, and S. Yehia, "Impact of Lateral Force-Resisting System and Design/Construction Practices on Seismic Performance and Cost of Tall Buildings in Dubai, UAE," *Earthquake Engineering and Engineering Vibration Journal*, vol. 12, no. 3, pp. 385–397, 2013.

[120] M. AlHamaydeh, J. Abdalla, S. Abdalla, A. Al-Rahmani, and A. Mostafa, "Inelastic Seismic Demands For Reinforced Concrete Frames In Dubai," *The 14th European Earthquake Engineering Conference (14EEEC), Aug. 30-Sept. 3*, 2010.

[121] S. Hussain, M. AlHamaydeh, and N. Aly, "Jakarta's First Seismic-Isolated Building - A 25 Story Tower," *The 15th World Conference on Earthquake Engineering (15WCEE), September 24-28*, 2012.

[122] N. Aly, M. AlHamaydeh, and K. Galal, "Quantification of the Impact of Detailing on the Performance and Cost of RC Shear Wall Buildings in Regions with High Uncertainty in Seismicity Hazards," *Journal of Earthquake Engineering*, vol. 24, no. 3, pp. 421--446DOI, 2020.

[123] M. AlHamaydeh, N. Aly, and K. Galal, "Effect of Diverse Seismic Hazard Estimates on Design and Performance of RC Shear Wall Buildings in Dubai, UAE," *The 2015 World Congress on Advances in Structural Engineering and Mechanics (ASEM15), August 25-29*, 2015.

[124] M. AlHamaydeh, N. Aly, and K. Galal, "Impact of Seismicity on Performance and Cost of RC Shear Wall Buildings in Dubai, United Arab Emirates," *Journal of Performance of Constructed Facilities*, vol. 31, no. 5, 2017, doi: 10.1061/(ASCE)CF.1943-5509.0001079.

[125] M. AlHamaydeh, S. Abdullah, A. Hamid, and A. Mustapha, "Seismic design factors for RC special moment resisting frames in Dubai, UAE," *Earthquake Engineering and Engineering Vibration*, vol. 10, no. 4, pp. 495–506, Dec. 2011, doi: 10.1007/s11803-011-0084-y.

[126] M. AlHamaydeh, N. Aly, and K. Galal, "Seismic Response and Life-Cycle Cost of Reinforced Concrete Special Structural Wall Buildings in Dubai, UAE," *Structural Concrete*, pp. 1–12, 2017, doi: 10.1002/suco.201600177.

[127] M. AlHamaydeh and S. Hussain, "Innovative Design of a Seismically-Isolated Building with Supplemental Damping," *The 14th European Earthquake Engineering Conference (14EEEC), Aug. 30-Sept. 3*, 2010.

[128] M. AlHamaydeh, M. E. Elkafrawy, F. M. Amin, A. M. Maky, and F. Mahmoudi, "Analysis and Design of UHPC Tall Buildings in UAE with Ductile Coupled Shear Walls Lateral Load Resisting System," in *2022 Advances in Science and Engineering Technology International Conferences (ASET)*, IEEE, Feb. 2022, pp. 1–6. doi: 10.1109/ASET53988.2022.9735104.

[129] M. Al Satari and S. Hussain, "Vibration-Based Wind Turbine Tower Foundation Design Utilizing Soil-Foundation-Structure Interaction," in *The 3rd International Conference on Modeling, Simulation and Applied Optimization (ICMSAO'09)*, 2009.

[130] S. Hussain and M. Al Satari, "Vibration-Based Wind Tower Foundation Design." 2009.

[131] M. AlHamaydeh and S. Hussain, "Optimized frequency-based foundation design for wind turbine towers utilizing soil--structure interaction," *J Franklin Inst*, vol. 348, no. 7, pp. 1470–1487, 2011.

[132] M. AlHamaydeh, S. Barakat, and O. Nasif, "Optimization of Support Structures for Offshore Wind Turbines Using Genetic Algorithm with Domain-Trimming," *Math Probl Eng*, vol. 2017, no. 5978375. DOI:10.1155/2017/5978375, pp. 1–14, 2017.

[133] M. Al Satari and S. Hussain, "Vibration Based Wind Turbine Tower Foundation Design Utilizing Soil-Foundation-Structure Interaction," in *The 14th World Conference on Earthquake Engineering*, 2008.

[134] Y. Abdel-Jawad and M. Al Satari, "Freeze-Thaw Resistance of Concrete Incorporating Recycled Tire Rubbers as Fine Aggregate," in *The Fifth International Conference on Concrete Technology for Developing Countries: Proceedings*, 1999.

[135] S. Hussain, P. Van Benschoten, M. Al Satari, and S. Lin, "Buckling Restrained Braced Frame (BRBF) Structures: Analysis, Design and Approvals Issues," in *The 75th SEAOC Annual Convention*, 2006.

[136] S. Hussain, P. Van Benschoten, A. Nerurkar, M. Al Satari, and T. Guttema, "Viscous Fluid Damper Retrofit of Pre-Northridge Steel Moment Frame Structures," in *The 75th SEAOC Annual Convention, Long Beach, California, USA, September 13-16, 2006*, 2006.

[137] S. Hussain, P. Van Benschoten, M. Al Satari, and S. Lin, "Viscous-Fluid-Spring Damper Retrofit of a Steel Moment Frame Structure," in *The 2008 Seismic Engineering International Conference commemorating the 1908*

Messina and Reggio Calabria Earthquake (MERCEA'08), 2008, pp. 1381–1389.

[138] S. Yehia, M. AlHamaydeh, Y. Al-Khanchi, and O. Ghonima, "Investigation of Utilizing Lightweight Fine Aggregate on the Development of SCC Matrix," *The 7th International Conference on Material Sciences (CSM7), May 20-22*, 2010.

[139] M. AlHamaydeh, S. Hussain, and F. Tasbihgoo, "Design of a High-Rise Building Utilizing Supplemental Damping," *The 14th European Earthquake Engineering Conference (14EEEC), Aug. 30-Sept. 3*, 2010.

[140] S. Yehia, M. AlHamaydeh, H. Al Ali, M. Al Jarwan, and Y. Al-Khanchi, "Effect of Aggregate Source on the Development of High Strength Lightweight SCC Matrix," *The 7th International Conference on Material Sciences (CSM7), May 20-22*, 2010.

[141] S. Yehia, M. Al Satari, H. Al Ali, M. Al-Jarwan, and F. Al-Omari, "High Strength Light Weight Self-Consolidating Concrete Mixture: Development and Evaluation," in *The 4th International Conference on the Applications of Traditional and High Performance Materials in Harsh Environment (IMS/4)*, 2010, pp. 83–90.

[142] S. Tabsh, A. Abdelfatah, M. AlHamaydeh, and S. Yehia, "Comparison of civil engineering curricula in the Arab Middle-East countries," in *The 5th International Forum on Engineering Education (IFEE2010)*, 2010, pp. 403–412.

[143] S. Yehia, M. AlHamaydeh, R. Alhajri, A. Abdelsalam, and A. Farid, "Steel Fiber SCC High Strength Lightweight Concrete with Local Available

Materials," *The Central European Congress on Concrete Engineering (CCC 2011), September 22-23*, pp. 1–4, 2011.

[144] S. Yehia, M. AlHamaydeh, S. El Kalie, and Y. Ibrahim, "Recommended Concrete Properties for High Strength Steel Reinforcement – Overview," *The Central European Congress on Concrete Engineering (CCC 2011), September 22-23*, pp. 1–4, 2011.

[145] M. AlHamaydeh, S. Yehia, N. Aly, A. Douba, and L. Hamzeh, "Design Alternatives for Lateral Force-Resisting Systems of Tall Buildings in Dubai, UAE," *International Journal of Civil and Environmental Engineering*, vol. 6, pp. 185–188, 2012.

[146] S. Yehia, M. AlHamaydeh, A. Abdelfatah, and S. Tabsh, "ABET-accredited civil engineering programmes following track system: Part II-implementation of the proposed framework," *Global Journal of Engineering Education*, vol. 14, no. 1, pp. 69–76, 2012.

[147] S. Yehia, M. AlHamaydeh, A. Abdelfatah, and S. Tabsh, "ABET-accredited civil engineering programmes following track system: Part I-survey and framework development," *Global Journal of Engineering Education*, vol. 14, no. 1, pp. 57–68, 2012.

[148] S. W. Tabsh, A. Abdelfatah, M. Alhamaydeh, and S. Yehia, "Comparison of Civil Engineering Curricula in the Arab World," *International Journal of Engineering Education*, vol. 28, no. 5, pp. 1213–1220, 2012.

[149] S. Yehia, M. Alhamaydeh, R. Alhajri, and A. Abdelsalam, "Development and Evaluation of Self-Consolidated High Strength Lightweight Steel Fiber Concrete in UAE," *IABSE Symposium Report, May 6-8*, vol. 99, no. 16, pp. 1068–1074, 2013.

[150] S. Yehia *et al.*, "Evaluation of Concrete Properties for High Strength Steel Applications," *IABSE Symposium Report, May 6-8*, vol. 99, no. 16, pp. 1083–1090, May 2013, doi: 10.2749/222137813806501614.

[151] S. Abdalla, F. Abed, and M. AlHamaydeh, "Behavior of CFSTs and CCFSTs under Quasi-Static Axial Compression," *J Constr Steel Res*, vol. 90, pp. 235–244, Nov. 2013, doi: 10.1016/j.jcsr.2013.08.007.

[152] A. H. ElSinawi, A. Jhemi, and M. AlHamaydeh, "Linearized State-Space Model of the behavior of MR-Fluid Dampers," in *The 5th International Conference on Modeling, Simulation and Applied Optimization (ICMSAO'13)*, 2013.

[153] M. AlHamaydeh and G. Al-Shamsi, "Development of Analytical Fragility Curves for Representative Buildings in Dubai, United Arab Emirates," *The International Conference on Earthquake Engineering; Skopje Earthquake - 50 Years of European Earthquake Engineering (SE-50EEE), May 29-31*, 2013.

[154] S. Yehia, M. AlHamaydeh, and S. Farrag, "High Strength Lightweight SCC Matrix with Partial Normal Weight Coarse Aggregate Replacement : Strength and Durability Evaluations," *Journal of Materials in Civil Engineering, ASCE*, 2014, doi: 10.1061/(ASCE)MT.1943-5533.0000990.

[155] M. AlHamaydeh, N. Ibrahim, D. Kaloti, O. Alhasan, and A. Aisha, "Structural Design of Steel Plate Shear Wall Systems in Dubai, UAE," in *West-Meets-East: Exploring Sustainable Development, Innovation, and Entrepreneurship Opportunities*, 2014.

[156] M. AlHamaydeh, M. Najib, and L. Elayyan, "INSPECT-Lite: A GUI Pre-Processor Package for IDARC-2D Ver 7.0," in *The 2015 World Congress*

on Advances in Structural Engineering and Mechanics (ASEM15), Incheon, Korea, 2015.

[157] M. AlHamaydeh, F. Abed, and A. Mustapha, "Key parameters influencing performance and failure modes for BRBs using nonlinear FEA," *J Constr Steel Res*, vol. 116, pp. 1–18, Jan. 2016, doi: 10.1016/j.jcsr.2015.08.038.

[158] M. AlHamaydeh, M. Najib, and S. Alawnah, "INSPECT: A graphical user interface software package for IDARC-2D," *SoftwareX*, vol. 5, pp. 243–251, 2016, doi: 10.1016/j.softx.2016.10.004.

[159] G. Tiberti, I. Trabucchi, M. AlHamaydeh, F. Minelli, and G. Plizzari, "Crack Control in Concrete Members Reinforced by Conventional Rebars and Steel Fibers," *The 9th International Conference on Fibre Reinforced Concretes (FRC), Textile Reinforced Concretes (TRC) and Ultra-High Performance Concretes (UHPC) (FIBRE CONCRETE 2017), September 13-16*, p. 012008, 2017, doi: 10.1088/1757-899X/246/1/012008.

[160] M. AlHamaydeh and A. Sagher, "Key parameters influencing the behavior of Steel Plate Shear Walls (SPSW)," in *2017 7th International Conference on Modeling, Simulation, and Applied Optimization (ICMSAO)*, IEEE, Apr. 2017, pp. 1–6. doi: 10.1109/ICMSAO.2017.7934868.

[161] G. Markou, M. AlHamaydeh, and D. Saadi, "Effects of the Soil-Structure-Interaction Phenomenon on RC Structures with Pile Foundations," *the 9th GRACM International Congress on Computational Mechanics, June 4-6*, 2018.

[162] G. Tiberti, I. Trabucchi, M. AlHamaydeh, F. Minelli, and G. A. Plizzari, "Crack development in steel-fibre-reinforced concrete members with

conventional rebars," *Magazine of Concrete Research*, vol. 71, no. 11, pp. 599–610, Jun. 2019, doi: 10.1680/jmacr.17.00361.

[163] M. AlHamaydeh, N. Aly, M. Najib, and S. Alawnah, "INSPECT-PBEE: A performance-based earthquake engineering GUI for IDARC-2D," *SoftwareX*, vol. 9, pp. 132–144, Jan. 2019, doi: 10.1016/j.softx.2019.01.010.

[164] N. Kuehn, T. Kishida, M. AlHamaydeh, G. Lavrentiadis, and Y. Bozorgnia, "nikuehn/BayesTruncRegGMM: Pre-review," *Zenodo, v0.0.1, http://doi.org/10.5281/zenodo.3738494*. 2020.

[165] N. M. Kuehn, T. Kishida, M. AlHamaydeh, G. Lavrentiadis, and Y. Bozorgnia, "A Bayesian model for truncated regression for the estimation of empirical ground-motion models," *Bulletin of Earthquake Engineering*, vol. 18, no. 4, pp. 6149–6179, 2020.

[166] E. Saleh, A. Tarawneh, H. Dwairi, and M. AlHamaydeh, "Guide to non-destructive concrete strength assessment: Homogeneity tests and sampling plans," *Journal of Building Engineering*, vol. 49, no. May, pp. 104047--DOI, 2022.

[167] Z. A. Al-Sadoon, A. Saboor Karzad, A. Sagheer, and M. AlHamaydeh, "Replaceable fuse buckling-restrained brace (BRB): Experimental cyclic qualification testing and NLFEA modeling," *Structures*, vol. 39, pp. 997–1015, May 2022, doi: 10.1016/j.istruc.2022.03.081.

[168] A. Moghadam, M. AlHamaydeh, and R. Sarlo, "Bridge-weigh-in-motion approach for simultaneous multiple vehicles on concrete-box-girder bridges," *Autom Constr*, vol. 137, no. May, pp. 104179--DOI, 2022.

[169] A. Alashkar, M. Elkafrawy, R. Hawileh, and M. AlHamaydeh, "Buckling Analysis of Functionally Graded Materials (FGM) Thin Plates with Various Circular Cutout Arrangements," *Journal of Composites Science*, vol. 6, no. 9, p. 277, Sep. 2022, doi: 10.3390/jcs6090277.

[170] D. K. Nambiar, T. Kishida, T. F. Abdallatif, and M. H. AlHamaydeh, "VS30 Correlations from Shear Wave Velocity Profiles in the UAE," in *The 4th International Conference on Performance Based Design in Earthquake Geotechnical Engineering (Beijing 2022)*, 2022, pp. 971–979.

[171] M. Saleh, M. AlHamaydeh, and M. Zakaria, "Finite element analysis of reinforced concrete deep beams with square web openings using damage plasticity model," *Eng Struct*, vol. 278, p. 115496, 2023.

[172] A. S. Karzad, Z. A. Al-Sadoon, A. Sagheer, and M. AlHamaydeh, "Experimental and Nonlinear Finite Element Analysis Data for an Innovative Buckling Restrained Bracing System to Rehabilitate Seismically Deficient Structures," *Data (Basel)*, vol. 7, no. 12, p. 171, Nov. 2022, doi: 10.3390/data7120171.

[173] A. S. Karzad, Z. Al-Sadoon, A. Sagheer, and M. AlHamaydeh, "Dataset from Experimental and Nonlinear Finite Element Modeling Investigating an Innovative Buckling Restrained Bracing System for Rehabilitation of Seismic Deficient Structures," *Zenodo. http://doi.org/10.5281/zenodo.6795612*. 2022.

[174] M. E. Elkafrawy, A. Mohsen Khalil, W. Abuzaid, R. A. Hawileh, and M. AlHamaydeh, "Nonlinear Finite Element Analysis (NLFEA) of Prestressed RC Beams Reinforced with Iron-Based Shape Memory Alloy

(Fe-SMA)," in *2022 Advances in Science and Engineering Technology International Conferences (ASET)*, IEEE, Feb. 2022, pp. 1–7. doi: 10.1109/ASET53988.2022.9735110.

[175] G. Markou and M. Alhamaydeh, "3D finite element modeling of GFRP-reinforced concrete deep beams without shear reinforcement," *Int J Comput Methods*, vol. 15, no. 1, pp. 1–35, 2018.

[176] F. Abed, S. Barakat, and M. AlHamaydeh, "Nonlinear Finite Element Analysis of Buckling Capacity of Pretwisted Bars," in *The Engineering Mechanics Conference (EMI 2011)*, 2011.

[177] F. H. Abed, M. H. AlHamaydeh, and S. A. Barakat, "Nonlinear Finite-Element Analysis of Buckling Capacity of Pretwisted Steel Bars," *Journal of Engineering Mechanics, ASCE*, vol. 139, no. 7, pp. 791–801, 2013.

[178] F. Abed, S. Barakat, and M. AlHamaydeh, "Numerical simulation of buckling of pretwisted non-circular bars," in *The 4th International Conference on Modeling, Simulation and Applied Optimization (ICMSAO'11)*, 2011, pp. 1–6.

[179] M. AlHamaydeh, S. Barakat, and F. Abed, "Multiple Regression Modeling of Natural Rubber Seismic-Isolation Systems with Supplemental Viscous Damping for Near-Field Ground Motion," *Journal of Civil Engineering and Management*, 2013.

[180] M. AlHamaydeh, G. Markou, and D. Saadi, "Nonlinear FEA of Soil-Structure-Interaction Effects on RC Shear Wall Structures," pp. 3476–3490, 2017, doi: 10.7712/120117.5659.18218.

[181] M. AlHamaydeh and F. Amin, "Interaction Diagrams of Geopolymer FRC Slender Columns with Double-Layer Reinforcement_Dataset V1.," *Zenodo*, Feb. 2021, doi: 10.5281/ZENODO.4568644.

[182] M. AlHamaydeh and F. Amin, "Strength Curves of Slender Geopolymer Concrete Columns_Dataset," *Zenodo*, 2021, doi: 10.5281/zenodo.4568635.

[183] M. AlHamaydeh and F. M. Amin, "Strength curve data for slender geopolymer concrete columns with GFRP, steel and hybrid reinforcement," *Data Brief*, vol. 39, p. 107589, Dec. 2021, doi: 10.1016/j.dib.2021.107589.

[184] M. AlHamaydeh and F. Amin, "Data for Interaction Diagrams of Geopolymer FRC Slender Columns with Double-Layer GFRP and Steel Reinforcement," *Data (Basel)*, vol. 6, no. 5, p. 43, Apr. 2021, doi: 10.3390/data6050043.

[185] M. Elkafrawy, A. Alashkar, R. Hawileh, and M. Alhamaydeh, "FEA Investigation of Elastic Buckling for Functionally Graded Material (FGM) Thin Plates with Different Hole Shapes under Uniaxial Loading," *Buildings*, vol. 12, no. 6, 2022, doi: 10.3390/buildings12060802.

[186] A. Khalil, M. Elkafrawy, W. Abuzaid, R. Hawileh, and M. AlHamaydeh, "Flexural Performance of RC Beams Strengthened with Pre-Stressed Iron-Based Shape Memory Alloy (Fe-SMA) Bars: Numerical Study," *Buildings*, vol. 12, no. 12, p. 2228, Dec. 2022, doi: 10.3390/buildings12122228.

[187] M. Al Satari and J. Anderson, "Estimating Inelastic Seismic Demands by Elastic Analysis for Reinforced Concrete (RC) Framed Structures," in *The*

75th SEAOC Annual Convention, September 13-16, Long Beach, California, USA, 2006, pp. 153–167.

[188] F. Abed, M. AlHamaydeh, and S. Abdalla, "Experimental and numerical investigations of the compressive behavior of concrete filled steel tubes (CFSTs)," *J Constr Steel Res*, vol. 80, pp. 429–439, 2013.

[189] M. AlHamaydeh, H. Jarallah, and M. Ahmed, "Punching Shear Capacity of Two-Way Slabs Made with Macro Synthetic Fiber-Reinforced Concrete," *The 11th International Conference on Composite Science and Technology (ICCST-11), April 4-6*, 2017.

[190] M. AlHamaydeh, M. A. Orabi, M. Ahmed, S. Mohamed, A. Jabr, and M. K. Al Hariri, "Punching Shear Capacity of Macro Synthetic Fiber-Reinforced Concrete Two-Way Slabs with GFRP Rebars," *The 11th International Conference on Composite Science and Technology (ICCST-11), April 4-6*, 2017.

[191] M. AlHamaydeh, F. Afghan, R. Mithani, T. Besiso, and H. Al Salim, "Shear Strength of Circular Beams Made of Geopolymer Concrete and Reinforced with GFRP Rebars," *AIP Conf Proc*, vol. 2297, no. August, 2020, doi: 10.1063/5.0029862.

[192] M. AlHamaydeh and M. A. Orabi, "Experimental quantification of punching shear capacity for large-scale GFRP-reinforced flat slabs made of synthetic fiber-reinforced self-compacting concrete dataset," *Data Brief*, vol. 37, p. 107196, Aug. 2021, doi: 10.1016/j.dib.2021.107196.

[193] M. AlHamaydeh and M. Anwar Orabi, "Punching Shear Behavior of Synthetic Fiber-Reinforced Self-Consolidating Concrete Flat Slabs with GFRP Bars," *Journal of Composites for Construction*, vol. 25, no. 4, p.

(ASCE)CC.1943-5614.0001131, Aug. 2021, doi: 10.1061/(ASCE)CC.1943-5614.0001131.

[194] Z. A. Al-Sadoon, A. S. Karzad, A. Sagheer, and M. AlHamaydeh, "Proof-of-Concept and Experimental Qualification for a Repairable Buckling-Restrained Brace (BRB)," in *Coordinating Engineering for Sustainability and Resilience (CESARE22), Irbid, Jordan*, 2022, pp. 279–288.

[195] F. Abed, H. El-Chabib, and M. AlHamaydeh, "Shear characteristics of GFRP-reinforced concrete deep beams without web reinforcement," *Journal of Reinforced Plastics and Composites*, vol. 31, no. 16, pp. 1063–1073, Aug. 2012, doi: 10.1177/0731684412450350.

[196] A. E.-H. Khalil, E. Etman, A. Atta, and M. Essam, "Nonlinear behavior of RC beams strengthened with strain hardening cementitious composites subjected to monotonic and cyclic loads," *Alexandria Engineering Journal*, vol. 55, no. 2, 2016, doi: 10.1016/j.aej.2016.01.032.

[197] A. E.-H. Khalil, E. Etman, A. Atta, and M. Essam, "Ductility enhancement of RC beams strengthened with strain hardening cementi-tious composites," in *Proceedings of International Structural Engineering and Construction*, 2017. doi: 10.14455/ISEC.res.2017.225.

[198] A. E.-H. Khalil, E. Etman, A. Atta, and M. Essam, "Strengthening of RC beams subjected to cyclic load using ultra high-performance strain hardening cementitious composites," in *Proceedings of International Structural Engineering and Construction*, 2017. doi: 10.14455/ISEC.res.2017.215.

[199] A. E. H. Khalil, E. Etman, A. Atta, and M. Essam, "Behavior of RC beams strengthened with strain hardening cementitious composites (SHCC)

subjected to monotonic and repeated loads," *Eng Struct*, vol. 140, 2017, doi: 10.1016/j.engstruct.2017.02.049.

Appendix A

Table 17: Tall buildings gravity columns design summary.

Ref.Building	Floors	Column Type	Column Size (m × m)	Reinforcement	Ties in X and Y	ρ (%)
M1_10F_50RC	[1:5]	Corner	0.45 × 0.45	16 Φ 13	4 Legs-Φ 8 @ 16.00 cm	1.05
		Edge	0.45 × 0.45	16 Φ 13	4 Legs-Φ 8 @ 16.00 cm	1.05
		Interior	0.45 × 0.45	16 Φ 13	4 Legs-Φ 8 @ 16.00 cm	1.05
		Opening	0.45 × 0.45	16 Φ 13	4 Legs-Φ 8 @ 16.00 cm	1.05
	[6:10]	Corner	0.35 × 0.35	12 Φ 13	4 Legs-Φ 8 @ 16.00 cm	1.30
		Edge	0.35 × 0.35	12 Φ 13	4 Legs-Φ 8 @ 16.00 cm	1.30
		Interior	0.35 × 0.35	12 Φ 13	4 Legs-Φ 8 @ 16.00 cm	1.30
		Opening	0.35 × 0.35	12 Φ 13	4 Legs-Φ 8 @ 16.00 cm	1.30
M2_15F_50RC	[1:5]	Corner	0.45 × 0.45	16 Φ 13	4 Legs-Φ 8 @ 16.00 cm	1.05
		Edge	0.45 × 0.45	16 Φ 13	4 Legs-Φ 8 @ 16.00 cm	1.05
		Interior	0.45 × 0.45	16 Φ 16	4 Legs-Φ 8 @ 16.00 cm	1.59
		Opening	0.45 × 0.45	16 Φ 13	4 Legs-Φ 8 @ 16.00 cm	1.05
	[6:10]	Corner	0.35 × 0.35	12 Φ 13	4 Legs-Φ 8 @ 16.00 cm	1.30
		Edge	0.35 × 0.35	12 Φ 13	4 Legs-Φ 8 @ 16.00 cm	1.30
		Interior	0.35 × 0.35	12 Φ 13	4 Legs-Φ 8 @ 16.00 cm	1.30
		Opening	0.35 × 0.35	12 Φ 13	4 Legs-Φ 8 @ 16.00 cm	1.30
	[11:15]	Corner	0.35 × 0.35	12 Φ 13	4 Legs-Φ 8 @ 16.00 cm	1.30
		Edge	0.35 × 0.35	12 Φ 13	4 Legs-Φ 8 @ 16.00 cm	1.30
		Interior	0.35 × 0.35	12 Φ 13	4 Legs-Φ 8 @ 16.00 cm	1.30
		Opening	0.35 × 0.35	12 Φ 13	4 Legs-Φ 8 @ 16.00 cm	1.30
M3_20F_50RC	[1:5]	Corner	0.45 × 0.45	16 Φ 13	4 Legs-Φ 8 @ 16.00 cm	1.05
		Edge	0.45 × 0.45	16 Φ 13	4 Legs-Φ 8 @ 16.00 cm	1.05
		Interior	0.45 × 0.45	16 Φ 22	4 Legs-Φ 8 @ 16.00 cm	3.00
		Opening	0.45 × 0.45	16 Φ 16	4 Legs-Φ 8 @ 16.00 cm	1.59
	[6:10]	Corner	0.35 × 0.35	12 Φ 13	4 Legs-Φ 8 @ 16.00 cm	1.30
		Edge	0.35 × 0.35	12 Φ 13	4 Legs-Φ 8 @ 16.00 cm	1.30
		Interior	0.35 × 0.35	12 Φ 19	4 Legs-Φ 8 @ 16.00 cm	2.78
		Opening	0.35 × 0.35	12 Φ 13	4 Legs-Φ 8 @ 16.00 cm	1.30
	[11:15]	Corner	0.35 × 0.35	12 Φ 13	4 Legs-Φ 8 @ 16.00 cm	1.30
		Edge	0.35 × 0.35	12 Φ 13	4 Legs-Φ 8 @ 16.00 cm	1.30
		Interior	0.35 × 0.35	12 Φ 19	4 Legs-Φ 8 @ 16.00 cm	2.78
		Opening	0.35 × 0.35	12 Φ 13	4 Legs-Φ 8 @ 16.00 cm	1.30
	[16:20]	Corner	0.35 × 0.35	12 Φ 13	4 Legs-Φ 8 @ 16.00 cm	1.30
		Edge	0.35 × 0.35	12 Φ 13	4 Legs-Φ 8 @ 16.00 cm	1.30
		Interior	0.35 × 0.35	12 Φ 19	4 Legs-Φ 8 @ 16.00 cm	2.78
		Opening	0.35 × 0.35	12 Φ 13	4 Legs-Φ 8 @ 16.00 cm	1.30
M4_25F_60RC	[1:5]	Corner	0.45 × 0.45	16 Φ 13	4 Legs-Φ 8 @ 16.00 cm	1.05
		Edge	0.45 × 0.45	16 Φ 13	4 Legs-Φ 8 @ 16.00 cm	1.05
		Interior	0.45 × 0.45	16 Φ 25	4 Legs-Φ 8 @ 16.00 cm	3.88
		Opening	0.45 × 0.45	12 Φ 19	4 Legs-Φ 8 @ 16.00 cm	1.68

	[6:10]	Corner	0.35 × 0.35	12 Φ 13	4 Legs-Φ 8 @ 16.00 cm	1.30
		Edge	0.35 × 0.35	12 Φ 13	4 Legs-Φ 8 @ 16.00 cm	1.30
		Interior	0.35 × 0.35	12 Φ 22	4 Legs-Φ 8 @ 16.00 cm	3.72
		Opening	0.35 × 0.35	8 Φ 16	2 Legs-Φ 8 @ 16.00 cm	1.31
	[11:15]	Corner	0.35 × 0.35	12 Φ 13	4 Legs-Φ 8 @ 16.00 cm	1.30
		Edge	0.35 × 0.35	12 Φ 13	4 Legs-Φ 8 @ 16.00 cm	1.30
		Interior	0.35 × 0.35	12 Φ 22	4 Legs-Φ 8 @ 16.00 cm	3.72
		Opening	0.35 × 0.35	12 Φ 13	4 Legs-Φ 8 @ 16.00 cm	1.30
	[16:20]	Corner	0.35 × 0.35	12 Φ 13	4 Legs-Φ 8 @ 16.00 cm	1.30
		Edge	0.35 × 0.35	12 Φ 13	4 Legs-Φ 8 @ 16.00 cm	1.30
		Interior	0.35 × 0.35	12 Φ 22	4 Legs-Φ 8 @ 16.00 cm	3.72
		Opening	0.35 × 0.35	12 Φ 13	4 Legs-Φ 8 @ 16.00 cm	1.30
	[21:25]	Corner	0.35 × 0.35	12 Φ 13	4 Legs-Φ 8 @ 16.00 cm	1.30
		Edge	0.35 × 0.35	12 Φ 13	4 Legs-Φ 8 @ 16.00 cm	1.30
		Interior	0.35 × 0.35	12 Φ 22	4 Legs-Φ 8 @ 16.00 cm	3.72
		Opening	0.35 × 0.35	12 Φ 13	4 Legs-Φ 8 @ 16.00 cm	1.30
M5_30F_60RC	[1:5]	Corner	0.45 × 0.45	16 Φ 13	4 Legs-Φ 8 @ 16.00 cm	1.05
		Edge	0.45 × 0.45	16 Φ 16	4 Legs-Φ 8 @ 16.00 cm	1.59
		Interior	0.50 × 0.50	12 Φ 29	4 Legs-Φ 8 @ 16.00 cm	3.17
		Opening	0.45 × 0.45	16 Φ 22	4 Legs-Φ 8 @ 16.00 cm	3.00
	[6:10]	Corner	0.35 × 0.35	12 Φ 13	4 Legs-Φ 8 @ 16.00 cm	1.30
		Edge	0.35 × 0.35	12 Φ 13	4 Legs-Φ 8 @ 16.00 cm	1.30
		Interior	0.40 × 0.40	12 Φ 25	4 Legs-Φ 8 @ 16.00 cm	3.68
		Opening	0.35 × 0.35	12 Φ 19	4 Legs-Φ 8 @ 16.00 cm	2.78
	[11:15]	Corner	0.35 × 0.35	12 Φ 13	4 Legs-Φ 8 @ 16.00 cm	1.30
		Edge	0.35 × 0.35	12 Φ 13	4 Legs-Φ 8 @ 16.00 cm	1.30
		Interior	0.35 × 0.35	12 Φ 22	4 Legs-Φ 8 @ 16.00 cm	3.72
		Opening	0.35 × 0.35	12 Φ 19	4 Legs-Φ 8 @ 16.00 cm	2.78
	[16:20]	Corner	0.35 × 0.35	12 Φ 13	4 Legs-Φ 8 @ 16.00 cm	1.30
		Edge	0.35 × 0.35	12 Φ 13	4 Legs-Φ 8 @ 16.00 cm	1.30
		Interior	0.35 × 0.35	12 Φ 22	4 Legs-Φ 8 @ 16.00 cm	3.72
		Opening	0.35 × 0.35	12 Φ 19	4 Legs-Φ 8 @ 16.00 cm	2.78
	[21:25]	Corner	0.35 × 0.35	12 Φ 13	4 Legs-Φ 8 @ 16.00 cm	1.30
		Edge	0.35 × 0.35	12 Φ 13	4 Legs-Φ 8 @ 16.00 cm	1.30
		Interior	0.35 × 0.35	12 Φ 22	4 Legs-Φ 8 @ 16.00 cm	3.72
		Opening	0.35 × 0.35	12 Φ 19	4 Legs-Φ 8 @ 16.00 cm	2.78
	[26:30]	Corner	0.35 × 0.35	12 Φ 13	4 Legs-Φ 8 @ 16.00 cm	1.30
		Edge	0.35 × 0.35	12 Φ 13	4 Legs-Φ 8 @ 16.00 cm	1.30
		Interior	0.35 × 0.35	12 Φ 22	4 Legs-Φ 8 @ 16.00 cm	3.72
		Opening	0.35 × 0.35	12 Φ 19	4 Legs-Φ 8 @ 16.00 cm	2.78
M6_35F_60RC	[1:5]	Corner	0.45 × 0.45	16 Φ 13	4 Legs-Φ 8 @ 16.00 cm	1.05
		Edge	0.45 × 0.45	12 Φ 19	4 Legs-Φ 8 @ 16.00 cm	1.68
		Interior	1.10 × 1.10	32 Φ 36	6 Legs-Φ 8 @ 11.00 cm	2.69
		Opening	0.45 × 0.45	16 Φ 25	4 Legs-Φ 8 @ 16.00 cm	3.88
	[6:10]	Corner	0.35 × 0.35	12 Φ 13	4 Legs-Φ 8 @ 16.00 cm	1.30
		Edge	0.35 × 0.35	8 Φ 16	2 Legs-Φ 8 @ 16.00 cm	1.31

		Interior	1.00 × 1.00	28 Φ 32	6 Legs-Φ 8 @ 16.00 cm	2.25
		Opening	0.35 × 0.35	12 Φ 22	4 Legs-Φ 8 @ 16.00 cm	3.72
	[11:15]	Corner	0.35 × 0.35	12 Φ 13	4 Legs-Φ 8 @ 16.00 cm	1.30
		Edge	0.35 × 0.35	12 Φ 13	4 Legs-Φ 8 @ 16.00 cm	1.30
		Interior	0.90 × 0.90	24 Φ 29	4 Legs-Φ 8 @ 16.00 cm	1.96
		Opening	0.35 × 0.35	12 Φ 22	4 Legs-Φ 8 @ 16.00 cm	3.72
	[16:20]	Corner	0.35 × 0.35	12 Φ 13	4 Legs-Φ 8 @ 16.00 cm	1.30
		Edge	0.35 × 0.35	12 Φ 13	4 Legs-Φ 8 @ 16.00 cm	1.30
		Interior	0.80 × 0.80	20 Φ 25	4 Legs-Φ 8 @ 16.00 cm	1.53
		Opening	0.35 × 0.35	12 Φ 22	4 Legs-Φ 8 @ 16.00 cm	3.72
	[21:25]	Corner	0.35 × 0.35	12 Φ 13	4 Legs-Φ 8 @ 16.00 cm	1.30
		Edge	0.35 × 0.35	12 Φ 13	4 Legs-Φ 8 @ 16.00 cm	1.30
		Interior	0.70 × 0.70	16 Φ 22	4 Legs-Φ 8 @ 16.00 cm	1.24
		Opening	0.35 × 0.35	12 Φ 22	4 Legs-Φ 8 @ 16.00 cm	3.72
	[26:30]	Corner	0.35 × 0.35	12 Φ 13	4 Legs-Φ 8 @ 16.00 cm	1.30
		Edge	0.35 × 0.35	12 Φ 13	4 Legs-Φ 8 @ 16.00 cm	1.30
		Interior	0.60 × 0.60	16 Φ 19	4 Legs-Φ 8 @ 16.00 cm	1.26
		Opening	0.35 × 0.35	12 Φ 22	4 Legs-Φ 8 @ 16.00 cm	3.72
	[31:35]	Corner	0.35 × 0.35	12 Φ 13	4 Legs-Φ 8 @ 16.00 cm	1.30
		Edge	0.35 × 0.35	12 Φ 13	4 Legs-Φ 8 @ 16.00 cm	1.30
		Interior	0.50 × 0.50	12 Φ 16	4 Legs-Φ 8 @ 16.00 cm	0.97
		Opening	0.35 × 0.35	12 Φ 22	4 Legs-Φ 8 @ 16.00 cm	3.72
M7_40F_70RC	[1:5]	Corner	0.45 × 0.45	16 Φ 13	4 Legs-Φ 8 @ 16.00 cm	1.05
		Edge	0.45 × 0.45	12 Φ 19	4 Legs-Φ 8 @ 16.00 cm	1.68
		Interior	1.10 × 1.10	32 Φ 36	6 Legs-Φ 8 @ 11.00 cm	2.69
		Opening	0.45 × 0.45	16 Φ 25	4 Legs-Φ 8 @ 16.00 cm	3.88
	[6:10]	Corner	0.35 × 0.35	12 Φ 13	4 Legs-Φ 8 @ 16.00 cm	1.30
		Edge	0.35 × 0.35	8 Φ 16	2 Legs-Φ 8 @ 16.00 cm	1.31
		Interior	1.00 × 1.00	28 Φ 32	6 Legs-Φ 8 @ 16.00 cm	2.25
		Opening	0.35 × 0.35	12 Φ 22	4 Legs-Φ 8 @ 16.00 cm	3.72
	[11:15]	Corner	0.35 × 0.35	12 Φ 13	4 Legs-Φ 8 @ 16.00 cm	1.30
		Edge	0.35 × 0.35	12 Φ 13	4 Legs-Φ 8 @ 16.00 cm	1.30
		Interior	0.90 × 0.90	24 Φ 29	4 Legs-Φ 8 @ 16.00 cm	1.96
		Opening	0.35 × 0.35	12 Φ 22	4 Legs-Φ 8 @ 16.00 cm	3.72
	[16:20]	Corner	0.35 × 0.35	12 Φ 13	4 Legs-Φ 8 @ 16.00 cm	1.30
		Edge	0.35 × 0.35	12 Φ 13	4 Legs-Φ 8 @ 16.00 cm	1.30
		Interior	0.80 × 0.80	20 Φ 25	4 Legs-Φ 8 @ 16.00 cm	1.53
		Opening	0.35 × 0.35	12 Φ 22	4 Legs-Φ 8 @ 16.00 cm	3.72
	[21:25]	Corner	0.35 × 0.35	12 Φ 13	4 Legs-Φ 8 @ 16.00 cm	1.30
		Edge	0.35 × 0.35	12 Φ 13	4 Legs-Φ 8 @ 16.00 cm	1.30
		Interior	0.70 × 0.70	16 Φ 22	4 Legs-Φ 8 @ 16.00 cm	1.24
		Opening	0.35 × 0.35	12 Φ 22	4 Legs-Φ 8 @ 16.00 cm	3.72
	[26:30]	Corner	0.35 × 0.35	12 Φ 13	4 Legs-Φ 8 @ 16.00 cm	1.30
		Edge	0.35 × 0.35	12 Φ 13	4 Legs-Φ 8 @ 16.00 cm	1.30
		Interior	0.60 × 0.60	16 Φ 19	4 Legs-Φ 8 @ 16.00 cm	1.26
		Opening	0.35 × 0.35	12 Φ 22	4 Legs-Φ 8 @ 16.00 cm	3.72

	[31:35]	Corner	0.35 × 0.35	12 Φ 13	4 Legs-Φ 8 @ 16.00 cm	1.30
		Edge	0.35 × 0.35	12 Φ 13	4 Legs-Φ 8 @ 16.00 cm	1.30
		Interior	0.50 × 0.50	12 Φ 16	4 Legs-Φ 8 @ 16.00 cm	0.97
		Opening	0.35 × 0.35	12 Φ 22	4 Legs-Φ 8 @ 16.00 cm	3.72
	[36:40]	Corner	0.35 × 0.35	12 Φ 13	4 Legs-Φ 8 @ 16.00 cm	1.30
		Edge	0.35 × 0.35	12 Φ 13	4 Legs-Φ 8 @ 16.00 cm	1.30
		Interior	0.50 × 0.50	12 Φ 16	4 Legs-Φ 8 @ 16.00 cm	0.97
		Opening	0.35 × 0.35	12 Φ 22	4 Legs-Φ 8 @ 16.00 cm	3.72
M8_45F_70RC	[1:5]	Corner	0.45 × 0.45	16 Φ 13	4 Legs-Φ 8 @ 16.00 cm	1.05
		Edge	0.45 × 0.45	16 Φ 22	4 Legs-Φ 8 @ 16.00 cm	3.00
		Interior	1.10 × 1.10	32 Φ 36	6 Legs-Φ 8 @ 11.00 cm	2.69
		Opening	0.50 × 0.50	20 Φ 22	4 Legs-Φ 8 @ 16.00 cm	3.04
	[6:10]	Corner	0.35 × 0.35	12 Φ 13	4 Legs-Φ 8 @ 16.00 cm	1.30
		Edge	0.35 × 0.35	12 Φ 19	4 Legs-Φ 8 @ 16.00 cm	2.78
		Interior	1.00 × 1.00	28 Φ 32	6 Legs-Φ 8 @ 16.00 cm	2.25
		Opening	0.40 × 0.40	16 Φ 19	4 Legs-Φ 8 @ 16.00 cm	2.84
	[11:15]	Corner	0.35 × 0.35	12 Φ 13	4 Legs-Φ 8 @ 16.00 cm	1.30
		Edge	0.35 × 0.35	12 Φ 19	4 Legs-Φ 8 @ 16.00 cm	2.78
		Interior	0.90 × 0.90	24 Φ 29	4 Legs-Φ 8 @ 16.00 cm	1.96
		Opening	0.35 × 0.35	12 Φ 19	4 Legs-Φ 8 @ 16.00 cm	2.78
	[16:20]	Corner	0.35 × 0.35	12 Φ 13	4 Legs-Φ 8 @ 16.00 cm	1.30
		Edge	0.35 × 0.35	12 Φ 19	4 Legs-Φ 8 @ 16.00 cm	2.78
		Interior	0.80 × 0.80	20 Φ 25	4 Legs-Φ 8 @ 16.00 cm	1.53
		Opening	0.35 × 0.35	12 Φ 19	4 Legs-Φ 8 @ 16.00 cm	2.78
	[21:25]	Corner	0.35 × 0.35	12 Φ 13	4 Legs-Φ 8 @ 16.00 cm	1.30
		Edge	0.35 × 0.35	12 Φ 19	4 Legs-Φ 8 @ 16.00 cm	2.78
		Interior	0.70 × 0.70	16 Φ 22	4 Legs-Φ 8 @ 16.00 cm	1.24
		Opening	0.35 × 0.35	12 Φ 19	4 Legs-Φ 8 @ 16.00 cm	2.78
	[26:30]	Corner	0.35 × 0.35	12 Φ 13	4 Legs-Φ 8 @ 16.00 cm	1.30
		Edge	0.35 × 0.35	12 Φ 19	4 Legs-Φ 8 @ 16.00 cm	2.78
		Interior	0.60 × 0.60	16 Φ 19	4 Legs-Φ 8 @ 16.00 cm	1.26
		Opening	0.35 × 0.35	12 Φ 19	4 Legs-Φ 8 @ 16.00 cm	2.78
	[31:35]	Corner	0.35 × 0.35	12 Φ 13	4 Legs-Φ 8 @ 16.00 cm	1.30
		Edge	0.35 × 0.35	12 Φ 19	4 Legs-Φ 8 @ 16.00 cm	2.78
		Interior	0.50 × 0.50	12 Φ 16	4 Legs-Φ 8 @ 16.00 cm	0.97
		Opening	0.35 × 0.35	12 Φ 19	4 Legs-Φ 8 @ 16.00 cm	2.78
	[36:40]	Corner	0.35 × 0.35	12 Φ 13	4 Legs-Φ 8 @ 16.00 cm	1.30
		Edge	0.35 × 0.35	12 Φ 19	4 Legs-Φ 8 @ 16.00 cm	2.78
		Interior	0.50 × 0.50	12 Φ 16	4 Legs-Φ 8 @ 16.00 cm	0.97
		Opening	0.35 × 0.35	12 Φ 19	4 Legs-Φ 8 @ 16.00 cm	2.78
	[41:45]	Corner	0.35 × 0.35	12 Φ 13	4 Legs-Φ 8 @ 16.00 cm	1.30
		Edge	0.35 × 0.35	12 Φ 19	4 Legs-Φ 8 @ 16.00 cm	2.78
		Interior	0.50 × 0.50	12 Φ 16	4 Legs-Φ 8 @ 16.00 cm	0.97
		Opening	0.35 × 0.35	12 Φ 19	4 Legs-Φ 8 @ 16.00 cm	2.78
M9_50F_70RC	[1:5]	Corner	0.45 × 0.45	16 Φ 13	4 Legs-Φ 8 @ 16.00 cm	1.05
		Edge	0.45 × 0.45	16 Φ 22	4 Legs-Φ 8 @ 16.00 cm	3.00

		Interior	1.20 × 1.20	28 Φ 43	8 Legs-Φ 13 @ 7.00 cm	2.82
		Opening	1.10 × 1.10	32 Φ 36	6 Legs-Φ 8 @ 11.00 cm	2.69
	[6:10]	Corner	0.35 × 0.35	12 Φ 13	4 Legs-Φ 8 @ 16.00 cm	1.30
		Edge	0.35 × 0.35	12 Φ 19	4 Legs-Φ 8 @ 16.00 cm	2.78
		Interior	1.10 × 1.10	28 Φ 36	6 Legs-Φ 8 @ 16.00 cm	2.36
		Opening	1.00 × 1.00	28 Φ 32	6 Legs-Φ 8 @ 16.00 cm	2.25
	[11:15]	Corner	0.35 × 0.35	12 Φ 13	4 Legs-Φ 8 @ 16.00 cm	1.30
		Edge	0.35 × 0.35	12 Φ 19	4 Legs-Φ 8 @ 16.00 cm	2.78
		Interior	1.00 × 1.00	28 Φ 32	6 Legs-Φ 8 @ 16.00 cm	2.25
		Opening	0.90 × 0.90	24 Φ 29	4 Legs-Φ 8 @ 16.00 cm	1.96
	[16:20]	Corner	0.35 × 0.35	12 Φ 13	4 Legs-Φ 8 @ 16.00 cm	1.30
		Edge	0.35 × 0.35	12 Φ 19	4 Legs-Φ 8 @ 16.00 cm	2.78
		Interior	0.90 × 0.90	24 Φ 29	4 Legs-Φ 8 @ 16.00 cm	1.96
		Opening	0.80 × 0.80	20 Φ 25	4 Legs-Φ 8 @ 16.00 cm	1.53
	[21:25]	Corner	0.35 × 0.35	12 Φ 13	4 Legs-Φ 8 @ 16.00 cm	1.30
		Edge	0.35 × 0.35	12 Φ 19	4 Legs-Φ 8 @ 16.00 cm	2.78
		Interior	0.80 × 0.80	20 Φ 25	4 Legs-Φ 8 @ 16.00 cm	1.53
		Opening	0.70 × 0.70	16 Φ 22	4 Legs-Φ 8 @ 16.00 cm	1.24
	[26:30]	Corner	0.35 × 0.35	12 Φ 13	4 Legs-Φ 8 @ 16.00 cm	1.30
		Edge	0.35 × 0.35	12 Φ 19	4 Legs-Φ 8 @ 16.00 cm	2.78
		Interior	0.70 × 0.70	16 Φ 22	4 Legs-Φ 8 @ 16.00 cm	1.24
		Opening	0.60 × 0.60	16 Φ 19	4 Legs-Φ 8 @ 16.00 cm	1.26
	[31:35]	Corner	0.35 × 0.35	12 Φ 13	4 Legs-Φ 8 @ 16.00 cm	1.30
		Edge	0.35 × 0.35	12 Φ 19	4 Legs-Φ 8 @ 16.00 cm	2.78
		Interior	0.60 × 0.60	16 Φ 19	4 Legs-Φ 8 @ 16.00 cm	1.26
		Opening	0.50 × 0.50	12 Φ 16	4 Legs-Φ 8 @ 16.00 cm	0.97
	[36:40]	Corner	0.35 × 0.35	12 Φ 13	4 Legs-Φ 8 @ 16.00 cm	1.30
		Edge	0.35 × 0.35	12 Φ 19	4 Legs-Φ 8 @ 16.00 cm	2.78
		Interior	0.50 × 0.50	12 Φ 16	4 Legs-Φ 8 @ 16.00 cm	0.97
		Opening	0.50 × 0.50	12 Φ 16	4 Legs-Φ 8 @ 16.00 cm	0.97
	[41:45]	Corner	0.35 × 0.35	12 Φ 13	4 Legs-Φ 8 @ 16.00 cm	1.30
		Edge	0.35 × 0.35	12 Φ 19	4 Legs-Φ 8 @ 16.00 cm	2.78
		Interior	0.50 × 0.50	12 Φ 16	4 Legs-Φ 8 @ 16.00 cm	0.97
		Opening	0.50 × 0.50	12 Φ 16	4 Legs-Φ 8 @ 16.00 cm	0.97
	[46:50]	Corner	0.35 × 0.35	12 Φ 13	4 Legs-Φ 8 @ 16.00 cm	1.30
		Edge	0.35 × 0.35	12 Φ 19	4 Legs-Φ 8 @ 16.00 cm	2.78
		Interior	0.50 × 0.50	12 Φ 16	4 Legs-Φ 8 @ 16.00 cm	0.97
		Opening	0.50 × 0.50	12 Φ 16	4 Legs-Φ 8 @ 16.00 cm	0.97

Table 18: Modal analysis results for Tall Buildings.

Ref.Building	Mode	ψ (rad/s)^2	Ω (rad/s)	Frequency (Hrz)	Period (s)	Cumulative Mx (%)	Cumulative My (%)
M1_10F_50RC	1	31.9563	5.6530	0.8997	1.1115	69.73	1.55
	2	31.9563	5.6530	0.8997	1.1115	71.28	71.28
	3	478.3730	21.8717	3.4810	0.2873	73.69	83.58

121

	4	478.3730	21.8717	3.4810	0.2873	85.99	85.99
	5	2515.8200	50.1579	7.9829	0.1253	87.17	90.70
	6	2515.8200	50.1579	7.9829	0.1253	91.88	91.88
M2_15F_50RC	1	10.4694	3.2357	0.5150	1.9419	19.18	51.73
	2	10.4694	3.2357	0.5150	1.9419	70.91	70.91
	3	144.7320	12.0305	1.9147	0.5223	81.44	74.81
	4	144.7320	12.0305	1.9147	0.5223	85.35	85.35
	5	688.2620	26.2347	4.1754	0.2395	87.61	88.34
	6	688.2620	26.2347	4.1754	0.2395	90.60	90.60
M3_20F_50RC	1	5.9827	2.4460	0.3893	2.5688	67.33	0.00
	2	5.9827	2.4460	0.3893	2.5688	67.33	67.33
	3	90.9863	9.5387	1.5181	0.6587	83.21	67.33
	4	90.9863	9.5387	1.5181	0.6587	83.21	83.21
	5	447.2020	21.1472	3.3657	0.2971	89.19	83.21
	6	447.2020	21.1472	3.3657	0.2971	89.19	89.19
	7	1398.2700	37.3934	5.9513	0.1680	92.40	89.19
M4_25F_60RC	1	3.2444	1.8012	0.2867	3.4883	21.68	45.21
	2	3.2444	1.8012	0.2867	3.4883	66.88	66.88
	3	50.0966	7.0779	1.1265	0.8877	67.03	82.78
	4	50.0966	7.0779	1.1265	0.8877	82.93	82.93
	5	239.3500	15.4709	2.4623	0.4061	86.64	84.96
	6	239.3500	15.4709	2.4623	0.4061	88.68	88.68
	7	710.4360	26.6540	4.2421	0.2357	90.64	89.91
M5_30F_60RC	1	2.8015	1.6738	0.2664	3.7539	1.99	62.34
	2	2.8015	1.6738	0.2664	3.7539	64.33	64.33
	3	58.0003	7.6158	1.2121	0.8250	68.20	79.05
	4	58.0003	7.6158	1.2121	0.8250	82.91	82.91
	5	292.3150	17.0972	2.7211	0.3675	83.26	88.29
	6	292.3150	17.0972	2.7211	0.3675	88.64	88.64
	7	809.4020	28.4500	4.5280	0.2209	91.58	88.85
M6_35F_60RC	1	2.6395	1.6247	0.2586	3.8674	1.31	62.25
	2	2.6395	1.6247	0.2586	3.8674	63.56	63.56
	3	73.1778	8.5544	1.3615	0.7345	80.96	66.15
	4	73.1778	8.5544	1.3615	0.7345	83.56	83.56
	5	413.1640	20.3264	3.2351	0.3091	88.09	85.07
	6	413.1640	20.3264	3.2351	0.3091	89.60	89.60
	7	1173.2000	34.2520	5.4514	0.1834	92.43	89.62
M7_40F_70RC	1	1.9275	1.3884	0.2210	4.5257	0.87	61.15
	2	1.9275	1.3884	0.2210	4.5257	62.02	62.02
	3	56.0887	7.4892	1.1920	0.8390	77.26	66.47
	4	56.0887	7.4892	1.1920	0.8390	81.72	81.72
	5	327.3270	18.0922	2.8795	0.3473	81.75	88.18
	6	327.3270	18.0922	2.8795	0.3473	88.22	88.22
	7	937.5510	30.6194	4.8732	0.2052	90.84	88.85
M8_45F_70RC	1	1.2359	1.1117	0.1769	5.6518	15.61	44.55
	2	1.2359	1.1117	0.1769	5.6518	60.17	60.17

	3	31.0929	5.5761	0.8875	1.1268	63.92	75.70
	4	31.0929	5.5761	0.8875	1.1268	79.46	79.46
	5	172.1230	13.1196	2.0880	0.4789	80.27	85.33
	6	172.1230	13.1196	2.0880	0.4789	86.13	86.13
	7	503.9690	22.4492	3.5729	0.2799	87.47	88.62
M9_50F_70RC	1	0.8895	0.9431	0.1501	6.6619	33.81	26.31
	2	0.8895	0.9431	0.1501	6.6619	60.12	60.12
	3	24.1868	4.9180	0.7827	1.2776	79.38	60.23
	4	24.1868	4.9180	0.7827	1.2776	79.49	79.49
	5	143.9330	11.9972	1.9094	0.5237	80.08	85.64
	6	143.9330	11.9972	1.9094	0.5237	86.23	86.23
	7	452.9820	21.2834	3.3874	0.2952	88.73	87.49
	8	452.9820	21.2834	3.3874	0.2952	89.99	89.99

Table 19: Shear wall sections reinforcement for tall buildings archetypes.

Ref. Building	Floors	Wall Type	L (m)	T (m)	L_{BE} (m)	R_{BE}	$C_{BE,W}$	$C_{BE,L}$	R_{HW}	R_{VW}	ρ (%)
M1_10F_50RC	[1:5]	Edge	2	0.25	-	-	-	-	Φ 10 @ 16.00 cm	Φ 13 @ 16.00 cm	0.69
		Interior	2	0.25	-	-	-	-	Φ 10 @ 16.00 cm	Φ 13 @ 16.00 cm	0.69
	[6:10]	Edge	2	0.25	-	-	-	-	Φ 10 @ 16.00 cm	Φ 13 @ 16.00 cm	0.69
		Interior	2	0.25	-	-	-	-	Φ 10 @ 16.00 cm	Φ 13 @ 16.00 cm	0.69
M2_15F_50RC	[1:5]	Edge	2	0.25	-	-	-	-	Φ 10 @ 16.00 cm	Φ 13 @ 16.00 cm	0.69
		Interior	2	0.25	-	-	-	-	Φ 10 @ 16.00 cm	Φ 13 @ 16.00 cm	0.69
	[6:10]	Edge	2	0.25	-	-	-	-	Φ 10 @ 16.00 cm	Φ 13 @ 16.00 cm	0.69
		Interior	2	0.25	-	-	-	-	Φ 10 @ 16.00 cm	Φ 13 @ 16.00 cm	0.69
	[11:15]	Edge	2	0.25	-	-	-	-	Φ 10 @ 16.00 cm	Φ 13 @ 16.00 cm	0.69
		Interior	2	0.25	-	-	-	-	Φ 10 @ 16.00 cm	Φ 13 @ 16.00 cm	0.69
M3_20F_50RC	[1:5]	Edge	2.5	0.25	0.75	28 Φ 16	8 Φ 10 @ 7.00 cm	3 Φ 10 @ 7.00 cm	Φ 8 @ 14.00 cm	Φ 13 @ 11.00 cm	0.96
		Interior	2.5	0.3	0.75	32 Φ 16	8 Φ 8 @ 7.00 cm	5 Φ 8 @ 7.00 cm	Φ 8 @ 12.00 cm	Φ 13 @ 9.00 cm	1.08
	[6:10]	Edge	2.5	0.25	0.75	28 Φ 16	8 Φ 10 @ 7.00 cm	3 Φ 10 @ 7.00 cm	Φ 8 @ 14.00 cm	Φ 13 @ 11.00 cm	0.96
		Interior	2.5	0.25	0.75	28 Φ 16	8 Φ 10 @ 7.00 cm	3 Φ 10 @ 7.00 cm	Φ 8 @ 14.00 cm	Φ 13 @ 11.00 cm	0.96

	[11:15]	Edge	2.5	0.25	0.75	28 Φ 16	8 Φ 10 @ 7.00 cm	3 Φ 10 @ 7.00 cm	Φ 8 @ 14.00 cm	Φ 13 @ 11.00 cm	0.96
		Interior	2.5	0.25	0.75	28 Φ 16	8 Φ 10 @ 7.00 cm	3 Φ 10 @ 7.00 cm	Φ 8 @ 14.00 cm	Φ 13 @ 11.00 cm	0.96
	[16:20]	Edge	2.5	0.25	0.75	28 Φ 16	8 Φ 10 @ 7.00 cm	3 Φ 10 @ 7.00 cm	Φ 8 @ 14.00 cm	Φ 13 @ 11.00 cm	0.96
		Interior	2.5	0.25	0.75	28 Φ 16	8 Φ 10 @ 7.00 cm	3 Φ 10 @ 7.00 cm	Φ 8 @ 14.00 cm	Φ 13 @ 11.00 cm	0.96
M4_25F_60RC	[1:5]	Edge	2.5	0.3	0.75	32 Φ 16	8 Φ 8 @ 6.00 cm	5 Φ 8 @ 6.00 cm	Φ 8 @ 12.00 cm	Φ 13 @ 9.00 cm	1.08
		Interior	2.5	0.3	0.75	32 Φ 16	8 Φ 8 @ 6.00 cm	5 Φ 8 @ 6.00 cm	Φ 8 @ 12.00 cm	Φ 13 @ 9.00 cm	1.08
	[6:10]	Edge	2.5	0.25	0.75	28 Φ 16	8 Φ 10 @ 6.00 cm	3 Φ 10 @ 6.00 cm	Φ 8 @ 14.00 cm	Φ 13 @ 11.00 cm	0.96
		Interior	2.5	0.25	0.75	28 Φ 16	8 Φ 10 @ 6.00 cm	3 Φ 10 @ 6.00 cm	Φ 8 @ 14.00 cm	Φ 13 @ 11.00 cm	0.96
	[11:15]	Edge	2.5	0.25	0.75	28 Φ 16	8 Φ 10 @ 6.00 cm	3 Φ 10 @ 6.00 cm	Φ 8 @ 14.00 cm	Φ 13 @ 11.00 cm	0.96
		Interior	2.5	0.25	0.75	28 Φ 16	8 Φ 10 @ 6.00 cm	3 Φ 10 @ 6.00 cm	Φ 8 @ 14.00 cm	Φ 13 @ 11.00 cm	0.96
	[16:20]	Edge	2.5	0.25	0.75	28 Φ 16	8 Φ 10 @ 6.00 cm	3 Φ 10 @ 6.00 cm	Φ 8 @ 14.00 cm	Φ 13 @ 11.00 cm	0.96
		Interior	2.5	0.25	0.75	28 Φ 16	8 Φ 10 @ 6.00 cm	3 Φ 10 @ 6.00 cm	Φ 8 @ 14.00 cm	Φ 13 @ 11.00 cm	0.96
	[21:25]	Edge	2.5	0.25	0.75	28 Φ 16	8 Φ 10 @ 6.00 cm	3 Φ 10 @ 6.00 cm	Φ 8 @ 14.00 cm	Φ 13 @ 11.00 cm	0.96
		Interior	2.5	0.25	0.75	28 Φ 16	8 Φ 10 @ 6.00 cm	3 Φ 10 @ 6.00 cm	Φ 8 @ 14.00 cm	Φ 13 @ 11.00 cm	0.96
M5_30F_60RC	[1:5]	Edge	3	0.3	0.9	36 Φ 16	9 Φ 8 @ 6.00 cm	5 Φ 8 @ 6.00 cm	Φ 8 @ 12.00 cm	Φ 13 @ 9.00 cm	1.04
		Interior	3	0.3	0.9	36 Φ 16	9 Φ 8 @ 6.00 cm	5 Φ 8 @ 6.00 cm	Φ 8 @ 12.00 cm	Φ 13 @ 9.00 cm	1.04
	[6:10]	Edge	3	0.25	0.9	34 Φ 16	9 Φ 10 @ 8.00 cm	4 Φ 10 @ 8.00 cm	Φ 8 @ 14.00 cm	Φ 13 @ 11.00 cm	0.98
		Interior	3	0.25	0.9	34 Φ 16	9 Φ 10 @ 8.00 cm	4 Φ 10 @ 8.00 cm	Φ 8 @ 14.00 cm	Φ 13 @ 11.00 cm	0.98
	[11:15]	Edge	3	0.25	0.9	34 Φ 16	9 Φ 10 @ 8.00 cm	4 Φ 10 @ 8.00 cm	Φ 8 @ 14.00 cm	Φ 13 @ 11.00 cm	0.98
		Interior	3	0.25	0.9	34 Φ 16	9 Φ 10 @ 8.00 cm	4 Φ 10 @ 8.00 cm	Φ 8 @ 14.00 cm	Φ 13 @ 11.00 cm	0.98
	[16:20]	Edge	3	0.25	0.9	34 Φ 16	9 Φ 10 @ 8.00 cm	4 Φ 10 @ 8.00 cm	Φ 8 @ 14.00 cm	Φ 13 @ 11.00 cm	0.98
		Interior	3	0.25	0.9	34 Φ 16	9 Φ 10 @ 8.00 cm	4 Φ 10 @ 8.00 cm	Φ 8 @ 14.00 cm	Φ 13 @ 11.00 cm	0.98
	[21:25]	Edge	3	0.25	0.9	34 Φ 16	9 Φ 10 @ 8.00 cm	4 Φ 10 @ 8.00 cm	Φ 8 @ 14.00 cm	Φ 13 @ 11.00 cm	0.98

		Interior	3	0.25	0.9	34 Φ 16	9 Φ 10 @ 8.00 cm	4 Φ 10 @ 8.00 cm	Φ 8 @ 14.00 cm	Φ 13 @ 11.00 cm	0.98
	[26:30]	Edge	3	0.25	0.9	34 Φ 16	9 Φ 10 @ 8.00 cm	4 Φ 10 @ 8.00 cm	Φ 8 @ 14.00 cm	Φ 13 @ 11.00 cm	0.98
		Interior	3	0.25	0.9	34 Φ 16	9 Φ 10 @ 8.00 cm	4 Φ 10 @ 8.00 cm	Φ 8 @ 14.00 cm	Φ 13 @ 11.00 cm	0.98
M6_35F_60RC	[1:5]	Edge	3.5	0.3	1.05	42 Φ 16	10 Φ 8 @ 6.00 cm	5 Φ 8 @ 6.00 cm	Φ 8 @ 12.00 cm	Φ 13 @ 9.00 cm	1.02
		Interior	3	0.4	0.9	38 Φ 19	9 Φ 10 @ 9.00 cm	6 Φ 10 @ 9.00 cm	Φ 8 @ 10.00 cm	Φ 16 @ 11.00 cm	0.93
	[6:10]	Edge	3.5	0.3	1.05	42 Φ 16	10 Φ 8 @ 6.00 cm	5 Φ 8 @ 6.00 cm	Φ 8 @ 12.00 cm	Φ 13 @ 9.00 cm	1.02
		Interior	3	0.4	0.9	38 Φ 19	9 Φ 10 @ 9.00 cm	6 Φ 10 @ 9.00 cm	Φ 8 @ 10.00 cm	Φ 16 @ 11.00 cm	0.93
	[11:15]	Edge	3.5	0.3	1.05	42 Φ 16	10 Φ 8 @ 6.00 cm	5 Φ 8 @ 6.00 cm	Φ 8 @ 12.00 cm	Φ 13 @ 9.00 cm	1.02
		Interior	3	0.4	0.9	38 Φ 19	9 Φ 10 @ 9.00 cm	6 Φ 10 @ 9.00 cm	Φ 8 @ 10.00 cm	Φ 16 @ 11.00 cm	0.93
	[16:20]	Edge	3.5	0.3	1.05	42 Φ 16	10 Φ 8 @ 6.00 cm	5 Φ 8 @ 6.00 cm	Φ 8 @ 12.00 cm	Φ 13 @ 9.00 cm	1.02
		Interior	3	0.4	0.9	38 Φ 19	9 Φ 10 @ 9.00 cm	6 Φ 10 @ 9.00 cm	Φ 8 @ 10.00 cm	Φ 16 @ 11.00 cm	0.93
	[21:25]	Edge	3.5	0.3	1.05	42 Φ 16	10 Φ 8 @ 6.00 cm	5 Φ 8 @ 6.00 cm	Φ 8 @ 12.00 cm	Φ 13 @ 9.00 cm	1.02
		Interior	3	0.4	0.9	38 Φ 19	9 Φ 10 @ 9.00 cm	6 Φ 10 @ 9.00 cm	Φ 8 @ 10.00 cm	Φ 16 @ 11.00 cm	0.93
	[26:30]	Edge	3.5	0.3	1.05	42 Φ 16	10 Φ 8 @ 6.00 cm	5 Φ 8 @ 6.00 cm	Φ 8 @ 12.00 cm	Φ 13 @ 9.00 cm	1.02
		Interior	3	0.4	0.9	38 Φ 19	9 Φ 10 @ 9.00 cm	6 Φ 10 @ 9.00 cm	Φ 8 @ 10.00 cm	Φ 16 @ 11.00 cm	0.93
	[31:35]	Edge	3.5	0.3	1.05	42 Φ 16	10 Φ 8 @ 6.00 cm	5 Φ 8 @ 6.00 cm	Φ 8 @ 12.00 cm	Φ 13 @ 9.00 cm	1.02
		Interior	3	0.4	0.9	38 Φ 19	9 Φ 10 @ 9.00 cm	6 Φ 10 @ 9.00 cm	Φ 8 @ 10.00 cm	Φ 16 @ 11.00 cm	0.93
M7_40F_70RC	[1:5]	Edge	3.5	0.4	1.05	44 Φ 19	10 Φ 10 @ 7.00 cm	6 Φ 10 @ 7.00 cm	Φ 8 @ 10.00 cm	Φ 16 @ 11.00 cm	0.94
		Interior	3	0.5	0.9	42 Φ 19	9 Φ 10 @ 7.00 cm	8 Φ 10 @ 7.00 cm	Φ 8 @ 7.00 cm	Φ 16 @ 8.00 cm	1.01
	[6:10]	Edge	3.5	0.4	1.05	44 Φ 19	10 Φ 10 @ 7.00 cm	6 Φ 10 @ 7.00 cm	Φ 8 @ 10.00 cm	Φ 16 @ 11.00 cm	0.94
		Interior	3	0.45	0.9	40 Φ 19	9 Φ 10 @ 7.00 cm	7 Φ 10 @ 7.00 cm	Φ 8 @ 8.00 cm	Φ 16 @ 9.00 cm	1.05
	[11:15]	Edge	3.5	0.4	1.05	44 Φ 19	10 Φ 10 @ 7.00 cm	6 Φ 10 @ 7.00 cm	Φ 8 @ 10.00 cm	Φ 16 @ 11.00 cm	0.94
		Interior	3	0.4	0.9	38 Φ 19	9 Φ 10 @ 7.00 cm	6 Φ 10 @ 7.00 cm	Φ 8 @ 10.00 cm	Φ 16 @ 11.00 cm	0.93

	[16:20]	Edge	3.5	0.4	1.05	44 Φ 19	10 Φ 10 @ 7.00 cm	6 Φ 10 @ 7.00 cm	Φ 8 @ 10.00 cm	Φ 16 @ 11.00 cm	0.94
		Interior	3	0.4	0.9	38 Φ 19	9 Φ 10 @ 7.00 cm	6 Φ 10 @ 7.00 cm	Φ 8 @ 10.00 cm	Φ 16 @ 11.00 cm	0.93
	[21:25]	Edge	3.5	0.4	1.05	44 Φ 19	10 Φ 10 @ 7.00 cm	6 Φ 10 @ 7.00 cm	Φ 8 @ 10.00 cm	Φ 16 @ 11.00 cm	0.94
		Interior	3	0.4	0.9	38 Φ 19	9 Φ 10 @ 7.00 cm	6 Φ 10 @ 7.00 cm	Φ 8 @ 10.00 cm	Φ 16 @ 11.00 cm	0.93
	[26:30]	Edge	3.5	0.4	1.05	44 Φ 19	10 Φ 10 @ 7.00 cm	6 Φ 10 @ 7.00 cm	Φ 8 @ 10.00 cm	Φ 16 @ 11.00 cm	0.94
		Interior	3	0.4	0.9	38 Φ 19	9 Φ 10 @ 7.00 cm	6 Φ 10 @ 7.00 cm	Φ 8 @ 10.00 cm	Φ 16 @ 11.00 cm	0.93
	[31:35]	Edge	3.5	0.4	1.05	44 Φ 19	10 Φ 10 @ 7.00 cm	6 Φ 10 @ 7.00 cm	Φ 8 @ 10.00 cm	Φ 16 @ 11.00 cm	0.94
		Interior	3	0.4	0.9	38 Φ 19	9 Φ 10 @ 7.00 cm	6 Φ 10 @ 7.00 cm	Φ 8 @ 10.00 cm	Φ 16 @ 11.00 cm	0.93
	[36:40]	Edge	3.5	0.4	1.05	44 Φ 19	10 Φ 10 @ 7.00 cm	6 Φ 10 @ 7.00 cm	Φ 8 @ 10.00 cm	Φ 16 @ 11.00 cm	0.94
		Interior	3	0.4	0.9	38 Φ 19	9 Φ 10 @ 7.00 cm	6 Φ 10 @ 7.00 cm	Φ 8 @ 10.00 cm	Φ 16 @ 11.00 cm	0.93
M8_45F_70RC	[1:5]	Edge	4.5	0.4	1.35	56 Φ 19	13 Φ 10 @ 9.00 cm	7 Φ 10 @ 9.00 cm	Φ 8 @ 10.00 cm	Φ 16 @ 11.00 cm	0.96
		Interior	3	0.5	0.9	26 Φ 32	6 Φ 10 @ 6.00 cm	5 Φ 10 @ 6.00 cm	Φ 8 @ 7.00 cm	Φ 32 @ 9.00 cm	3.79
	[6:10]	Edge	4.5	0.4	1.35	56 Φ 19	13 Φ 10 @ 9.00 cm	7 Φ 10 @ 9.00 cm	Φ 8 @ 10.00 cm	Φ 16 @ 11.00 cm	0.96
		Interior	3	0.45	0.9	26 Φ 29	6 Φ 10 @ 6.00 cm	5 Φ 10 @ 6.00 cm	Φ 8 @ 8.00 cm	Φ 29 @ 9.00 cm	3.46
	[11:15]	Edge	4.5	0.4	1.35	56 Φ 19	13 Φ 10 @ 9.00 cm	7 Φ 10 @ 9.00 cm	Φ 8 @ 10.00 cm	Φ 16 @ 11.00 cm	0.96
		Interior	3	0.4	0.9	30 Φ 25	7 Φ 10 @ 6.00 cm	5 Φ 10 @ 6.00 cm	Φ 8 @ 10.00 cm	Φ 25 @ 8.00 cm	3.09
	[16:20]	Edge	4.5	0.4	1.35	56 Φ 19	13 Φ 10 @ 9.00 cm	7 Φ 10 @ 9.00 cm	Φ 8 @ 10.00 cm	Φ 16 @ 11.00 cm	0.96
		Interior	3	0.35	0.9	34 Φ 22	9 Φ 10 @ 6.00 cm	4 Φ 10 @ 6.00 cm	Φ 8 @ 11.00 cm	Φ 22 @ 9.00 cm	2.56
	[21:25]	Edge	4.5	0.4	1.35	56 Φ 19	13 Φ 10 @ 9.00 cm	7 Φ 10 @ 9.00 cm	Φ 8 @ 10.00 cm	Φ 16 @ 11.00 cm	0.96
		Interior	3	0.3	0.9	28 Φ 22	8 Φ 10 @ 6.00 cm	3 Φ 10 @ 6.00 cm	Φ 8 @ 12.00 cm	Φ 19 @ 10.00 cm	2.08
	[26:30]	Edge	4.5	0.4	1.35	56 Φ 19	13 Φ 10 @ 9.00 cm	7 Φ 10 @ 9.00 cm	Φ 8 @ 10.00 cm	Φ 16 @ 11.00 cm	0.96
		Interior	3	0.25	0.9	32 Φ 19	9 Φ 10 @ 6.00 cm	3 Φ 10 @ 6.00 cm	Φ 8 @ 14.00 cm	Φ 16 @ 11.00 cm	1.48
	[31:35]	Edge	4.5	0.4	1.35	56 Φ 19	13 Φ 10 @ 9.00 cm	7 Φ 10 @ 9.00 cm	Φ 8 @ 10.00 cm	Φ 16 @ 11.00 cm	0.96

		Interior	3	0.25	0.9	34 Φ 16	9 Φ 10 @ 7.00 cm	4 Φ 10 @ 7.00 cm	Φ 8 @ 14.00 cm	Φ 13 @ 11.00 cm	0.98
	[36:40]	Edge	4.5	0.4	1.35	56 Φ 19	13 Φ 10 @ 9.00 cm	7 Φ 10 @ 9.00 cm	Φ 8 @ 10.00 cm	Φ 16 @ 11.00 cm	0.96
		Interior	3	0.25	0.9	34 Φ 16	9 Φ 10 @ 7.00 cm	4 Φ 10 @ 7.00 cm	Φ 8 @ 14.00 cm	Φ 13 @ 11.00 cm	0.98
	[41:45]	Edge	4.5	0.4	1.35	56 Φ 19	13 Φ 10 @ 9.00 cm	7 Φ 10 @ 9.00 cm	Φ 8 @ 10.00 cm	Φ 16 @ 11.00 cm	0.96
		Interior	3	0.25	0.9	34 Φ 16	9 Φ 10 @ 7.00 cm	4 Φ 10 @ 7.00 cm	Φ 8 @ 14.00 cm	Φ 13 @ 11.00 cm	0.98
	[1:5]	Edge	5.5	0.45	1.65	66 Φ 19	15 Φ 10 @ 7.00 cm	7 Φ 10 @ 7.00 cm	Φ 8 @ 8.00 cm	Φ 16 @ 9.00 cm	1.02
		Interior	3	0.5	0.9	26 Φ 32	6 Φ 10 @ 6.00 cm	5 Φ 10 @ 6.00 cm	Φ 8 @ 7.00 cm	Φ 32 @ 9.00 cm	3.79
	[6:10]	Edge	5.5	0.45	1.65	66 Φ 19	15 Φ 10 @ 7.00 cm	7 Φ 10 @ 7.00 cm	Φ 8 @ 8.00 cm	Φ 16 @ 9.00 cm	1.02
		Interior	3	0.45	0.9	26 Φ 29	6 Φ 10 @ 6.00 cm	5 Φ 10 @ 6.00 cm	Φ 8 @ 8.00 cm	Φ 29 @ 9.00 cm	3.46
	[11:15]	Edge	5.5	0.45	1.65	66 Φ 19	15 Φ 10 @ 7.00 cm	7 Φ 10 @ 7.00 cm	Φ 8 @ 8.00 cm	Φ 16 @ 9.00 cm	1.02
		Interior	3	0.4	0.9	30 Φ 25	7 Φ 10 @ 6.00 cm	5 Φ 10 @ 6.00 cm	Φ 8 @ 10.00 cm	Φ 25 @ 8.00 cm	3.09
	[16:20]	Edge	5.5	0.45	1.65	66 Φ 19	15 Φ 10 @ 7.00 cm	7 Φ 10 @ 7.00 cm	Φ 8 @ 8.00 cm	Φ 16 @ 9.00 cm	1.02
M9_50F_70RC		Interior	3	0.35	0.9	34 Φ 22	9 Φ 10 @ 6.00 cm	4 Φ 10 @ 6.00 cm	Φ 8 @ 11.00 cm	Φ 22 @ 9.00 cm	2.56
	[21:25]	Edge	5.5	0.45	1.65	66 Φ 19	15 Φ 10 @ 7.00 cm	7 Φ 10 @ 7.00 cm	Φ 8 @ 8.00 cm	Φ 16 @ 9.00 cm	1.02
		Interior	3	0.3	0.9	28 Φ 22	8 Φ 10 @ 6.00 cm	3 Φ 10 @ 6.00 cm	Φ 8 @ 12.00 cm	Φ 19 @ 10.00 cm	2.08
	[26:30]	Edge	5.5	0.45	1.65	66 Φ 19	15 Φ 10 @ 7.00 cm	7 Φ 10 @ 7.00 cm	Φ 8 @ 8.00 cm	Φ 16 @ 9.00 cm	1.02
		Interior	3	0.25	0.9	32 Φ 19	9 Φ 10 @ 6.00 cm	3 Φ 10 @ 6.00 cm	Φ 8 @ 14.00 cm	Φ 16 @ 11.00 cm	1.48
	[31:35]	Edge	5.5	0.45	1.65	66 Φ 19	15 Φ 10 @ 7.00 cm	7 Φ 10 @ 7.00 cm	Φ 8 @ 8.00 cm	Φ 16 @ 9.00 cm	1.02
		Interior	3	0.25	0.9	34 Φ 16	9 Φ 10 @ 7.00 cm	4 Φ 10 @ 7.00 cm	Φ 8 @ 14.00 cm	Φ 13 @ 11.00 cm	0.98
	[36:40]	Edge	5.5	0.45	1.65	66 Φ 19	15 Φ 10 @ 7.00 cm	7 Φ 10 @ 7.00 cm	Φ 8 @ 8.00 cm	Φ 16 @ 9.00 cm	1.02
		Interior	3	0.25	0.9	34 Φ 16	9 Φ 10 @ 7.00 cm	4 Φ 10 @ 7.00 cm	Φ 8 @ 14.00 cm	Φ 13 @ 11.00 cm	0.98
	[41:45]	Edge	5.5	0.45	1.65	66 Φ 19	15 Φ 10 @ 7.00 cm	7 Φ 10 @ 7.00 cm	Φ 8 @ 8.00 cm	Φ 16 @ 9.00 cm	1.02
		Interior	3	0.25	0.9	34 Φ 16	9 Φ 10 @ 7.00 cm	4 Φ 10 @ 7.00 cm	Φ 8 @ 14.00 cm	Φ 13 @ 11.00 cm	0.98

| | [46:50] | Edge | 5.5 | 0.45 | 1.65 | 66 Φ 19 | 15 Φ 10 @ 7.00 cm | 7 Φ 10 @ 7.00 cm | Φ 8 @ 8.00 cm | Φ 16 @ 9.00 cm | 1.02 |
| | | Interior | 3 | 0.25 | 0.9 | 34 Φ 16 | 9 Φ 10 @ 7.00 cm | 4 Φ 10 @ 7.00 cm | Φ 8 @ 14.00 cm | Φ 13 @ 11.00 cm | 0.98 |

T: wall thickness; L_{BE}: boundary element length; R_{BE}: boundary element reinforcement; R_{VW}: shear wall vertical reinforcement; $C_{BE,W}$: boundary element confinement reinforcement perpendicular to wall; $C_{BE,L}$: boundary element confinement reinforcement parallel to wall; R_{HW}: shear wall horizontal reinforcement.

Table 20: Design of coupling beams for tall buildings archetypes.

Ref. Building	L (m)	Floors	Beam Size (m × m)	Top / Bottom Reinforcement	Transverse Reinforcement	Ties in Y Direction	ρ (%)
M1_10F_50RC	4.00	[1:5]	4.00 × 0.25	5 Φ 13	3 Φ 10	2 Legs - Φ 10 / 16.00 cm	0.18
		[6:10]	4.00 × 0.25	5 Φ 13	3 Φ 10	2 Legs - Φ 10 / 16.00 cm	0.18
M2_15F_50RC	4.00	[1:5]	4.00 × 0.25	5 Φ 13	3 Φ 10	2 Legs - Φ 10 / 16.00 cm	0.18
		[6:10]	4.00 × 0.25	5 Φ 13	3 Φ 10	2 Legs - Φ 10 / 16.00 cm	0.18
		[11:15]	4.00 × 0.25	5 Φ 13	3 Φ 10	2 Legs - Φ 10 / 16.00 cm	0.18
M3_20F_50RC	3.00	[1:5]	1.50 × 0.30	5 Φ 16	25 Φ 10	2 Legs - Φ 8 / 16.00 cm	1.32
		[6:10]	1.50 × 0.25	4 Φ 16	23 Φ 10	2 Legs - Φ 8 / 16.00 cm	1.39
		[11:15]	1.50 × 0.25	4 Φ 16	23 Φ 10	2 Legs - Φ 8 / 16.00 cm	1.39
		[16:20]	1.50 × 0.25	4 Φ 16	23 Φ 10	2 Legs - Φ 8 / 16.00 cm	1.39
M4_25F_60RC	3.00	[1:5]	1.50 × 0.30	5 Φ 16	25 Φ 10	2 Legs - Φ 8 / 16.00 cm	1.32
		[6:10]	1.50 × 0.25	4 Φ 16	23 Φ 10	2 Legs - Φ 8 / 16.00 cm	1.39
		[11:15]	1.50 × 0.25	4 Φ 16	23 Φ 10	2 Legs - Φ 8 / 16.00 cm	1.39
		[16:20]	1.50 × 0.25	4 Φ 16	23 Φ 10	2 Legs - Φ 8 / 16.00 cm	1.39
		[21:25]	1.50 × 0.25	4 Φ 16	23 Φ 10	2 Legs - Φ 8 / 16.00 cm	1.39
M5_30F_60RC	2.00	[1:5]	1.50 × 0.30	5 Φ 16	25 Φ 10	2 Legs - Φ 8 / 16.00 cm	1.32
		[6:10]	1.50 × 0.25	4 Φ 16	23 Φ 10	2 Legs - Φ 8 / 16.00 cm	1.39
		[11:15]	1.50 × 0.25	4 Φ 16	23 Φ 10	2 Legs - Φ 8 / 16.00 cm	1.39
		[16:20]	1.50 × 0.25	4 Φ 16	23 Φ 10	2 Legs - Φ 8 / 16.00 cm	1.39
		[21:25]	1.50 × 0.25	4 Φ 16	23 Φ 10	2 Legs - Φ 8 / 16.00 cm	1.39
		[26:30]	1.50 × 0.25	4 Φ 16	23 Φ 10	2 Legs - Φ 8 / 16.00 cm	1.39
M6_35F_60RC	2.00	[1:5]	1.50 × 0.40	6 Φ 16	25 Φ 10	2 Legs - Φ 8 / 16.00 cm	1.06
		[6:10]	1.50 × 0.40	6 Φ 16	25 Φ 10	2 Legs - Φ 8 / 16.00 cm	1.06
		[11:15]	1.50 × 0.40	6 Φ 16	25 Φ 10	2 Legs - Φ 8 / 16.00 cm	1.06
		[16:20]	1.50 × 0.40	6 Φ 16	25 Φ 10	2 Legs - Φ 8 / 16.00 cm	1.06
		[21:25]	1.50 × 0.40	6 Φ 16	25 Φ 10	2 Legs - Φ 8 / 16.00 cm	1.06
		[26:30]	1.50 × 0.40	6 Φ 16	25 Φ 10	2 Legs - Φ 8 / 16.00 cm	1.06
		[31:35]	1.50 × 0.40	6 Φ 16	25 Φ 10	2 Legs - Φ 8 / 16.00 cm	1.06
M7_40F_70RC	2.00	[1:5]	1.50 × 0.50	8 Φ 19	18 Φ 13	4 Legs - Φ 8 / 16.00 cm	1.24
		[6:10]	1.50 × 0.45	7 Φ 19	16 Φ 13	2 Legs - Φ 8 / 16.00 cm	1.22
		[11:15]	1.50 × 0.40	6 Φ 16	25 Φ 10	2 Legs - Φ 8 / 16.00 cm	1.06
		[16:20]	1.50 × 0.40	6 Φ 16	25 Φ 10	2 Legs - Φ 8 / 16.00 cm	1.06
		[21:25]	1.50 × 0.40	6 Φ 16	25 Φ 10	2 Legs - Φ 8 / 16.00 cm	1.06

		[26:30]	1.50 × 0.40	6 Φ 16	25 Φ 10	2 Legs - Φ 8 / 16.00 cm	1.06
		[31:35]	1.50 × 0.40	6 Φ 16	25 Φ 10	2 Legs - Φ 8 / 16.00 cm	1.06
		[36:40]	1.50 × 0.40	6 Φ 16	25 Φ 10	2 Legs - Φ 8 / 16.00 cm	1.06
M8_45F_70RC	2.00	[1:5]	1.50 × 0.50	8 Φ 13	25 Φ 13	4 Legs - Φ 8 / 16.00 cm	1.17
		[6:10]	1.50 × 0.45	7 Φ 13	25 Φ 13	2 Legs - Φ 8 / 16.00 cm	1.26
		[11:15]	1.50 × 0.40	6 Φ 13	25 Φ 13	2 Legs - Φ 8 / 16.00 cm	1.37
		[16:20]	1.50 × 0.35	5 Φ 13	25 Φ 13	2 Legs - Φ 8 / 16.00 cm	1.52
		[21:25]	1.50 × 0.30	5 Φ 13	19 Φ 13	2 Legs - Φ 8 / 16.00 cm	1.42
		[26:30]	1.50 × 0.25	4 Φ 10	25 Φ 10	2 Legs - Φ 8 / 16.00 cm	1.21
		[31:35]	1.50 × 0.25	4 Φ 16	23 Φ 10	2 Legs - Φ 8 / 16.00 cm	1.39
		[36:40]	1.50 × 0.25	4 Φ 16	23 Φ 10	2 Legs - Φ 8 / 16.00 cm	1.39
		[41:45]	1.50 × 0.25	4 Φ 16	23 Φ 10	2 Legs - Φ 8 / 16.00 cm	1.39
M9_50F_70RC	2.00	[1:5]	1.50 × 0.50	8 Φ 13	25 Φ 13	4 Legs - Φ 8 / 16.00 cm	1.17
		[6:10]	1.50 × 0.45	7 Φ 13	25 Φ 13	2 Legs - Φ 8 / 16.00 cm	1.26
		[11:15]	1.50 × 0.40	6 Φ 13	25 Φ 13	2 Legs - Φ 8 / 16.00 cm	1.37
		[16:20]	1.50 × 0.35	5 Φ 13	25 Φ 13	2 Legs - Φ 8 / 16.00 cm	1.52
		[21:25]	1.50 × 0.30	5 Φ 13	19 Φ 13	2 Legs - Φ 8 / 16.00 cm	1.42
		[26:30]	1.50 × 0.25	4 Φ 10	25 Φ 10	2 Legs - Φ 8 / 16.00 cm	1.21
		[31:35]	1.50 × 0.25	4 Φ 16	23 Φ 10	2 Legs - Φ 8 / 16.00 cm	1.39
		[36:40]	1.50 × 0.25	4 Φ 16	23 Φ 10	2 Legs - Φ 8 / 16.00 cm	1.39
		[41:45]	1.50 × 0.25	4 Φ 16	23 Φ 10	2 Legs - Φ 8 / 16.00 cm	1.39
		[46:50]	1.50 × 0.25	4 Φ 16	23 Φ 10	2 Legs - Φ 8 / 16.00 cm	1.39
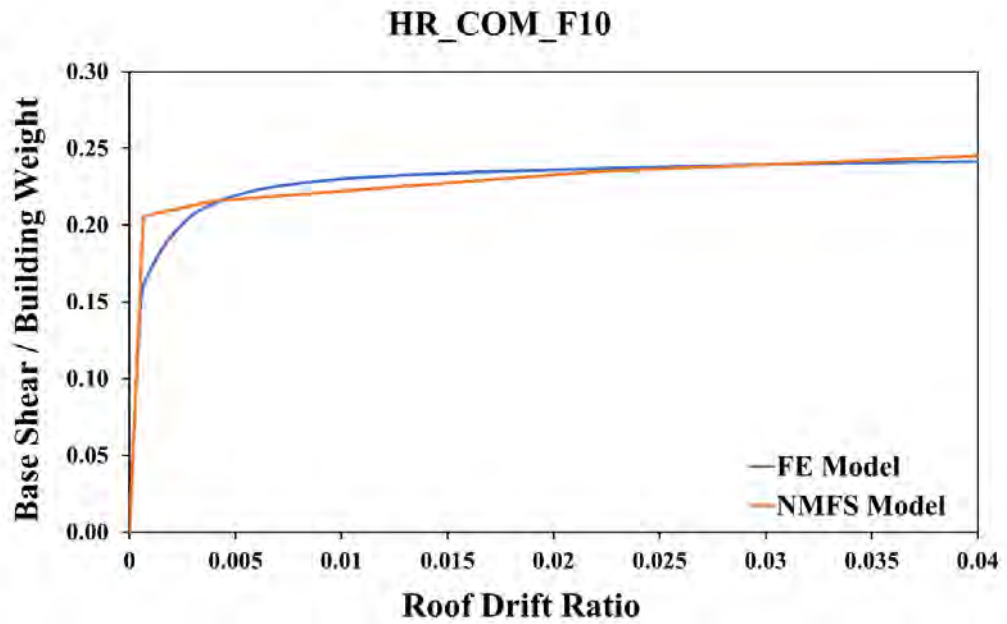
Figure 37: Detailed FE and NMFS models Pushover curves for "HR_COM_F10"

archetype.
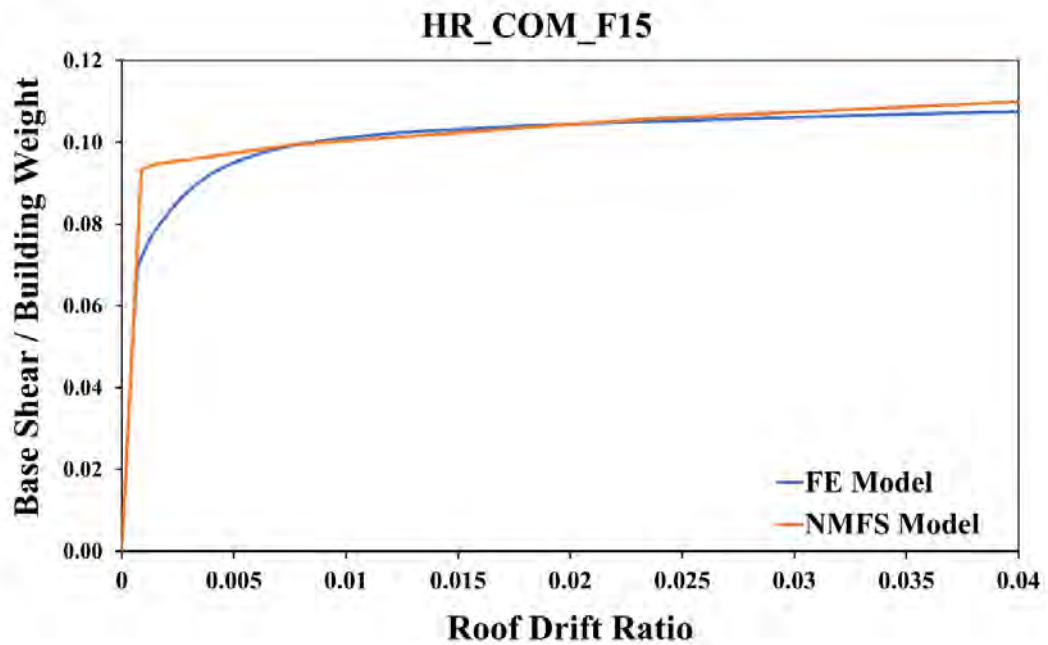
Figure 38: Detailed FE and NMFS models Pushover curves for "HR_COM_F15"

archetype.
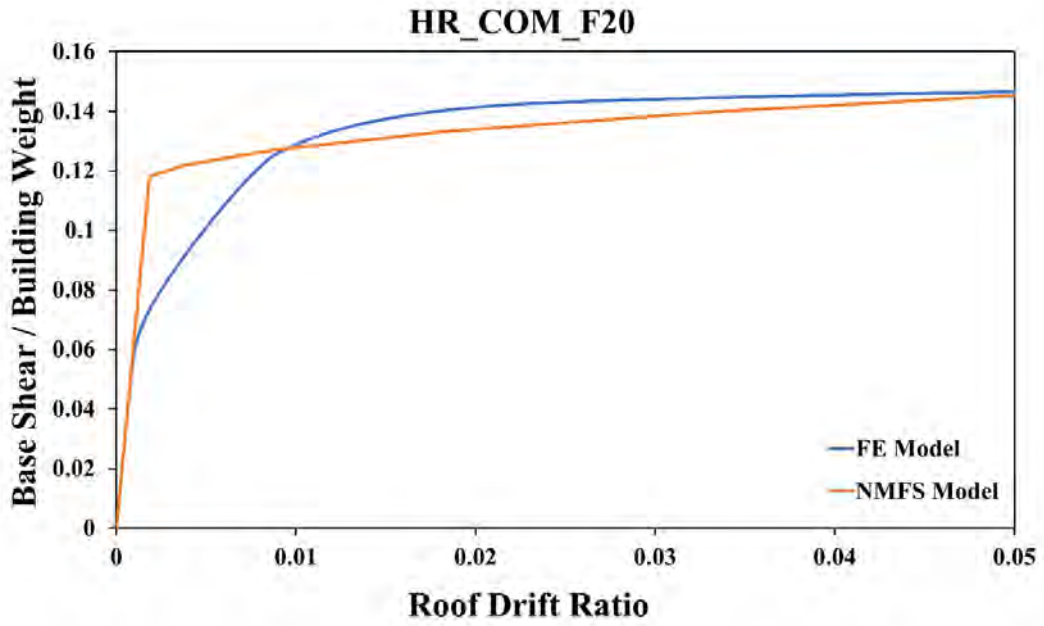
Figure 39: Detailed FE and NMFS models Pushover curves for "HR_COM_F20"

archetype.
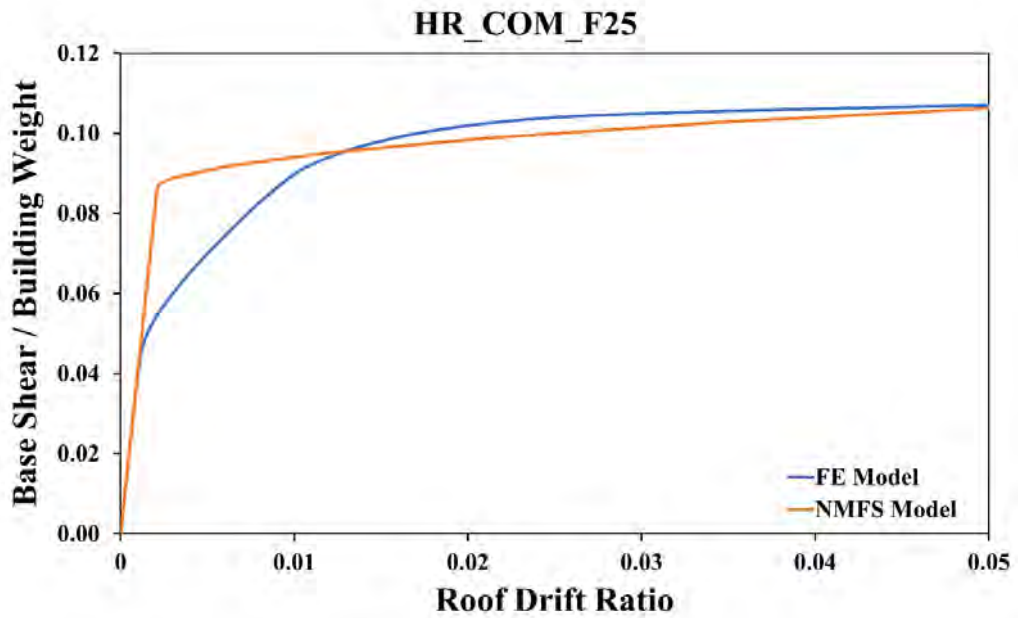
Figure 40: Detailed FE and NMFS models Pushover curves for "HR_COM_F25"

archetype.
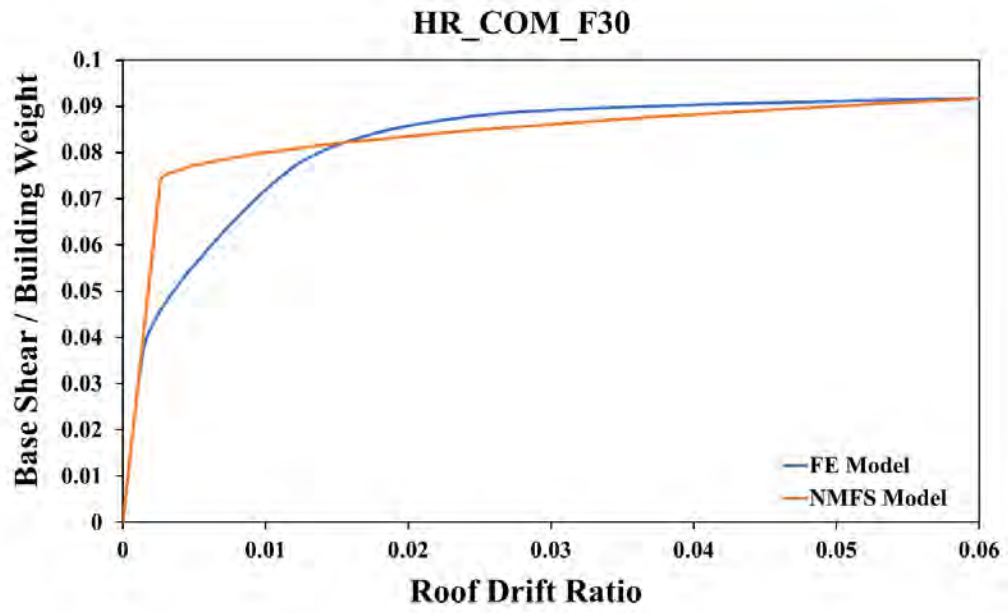
Figure 41: Detailed FE and NMFS models Pushover curves for "HR_COM_F30" archetype.
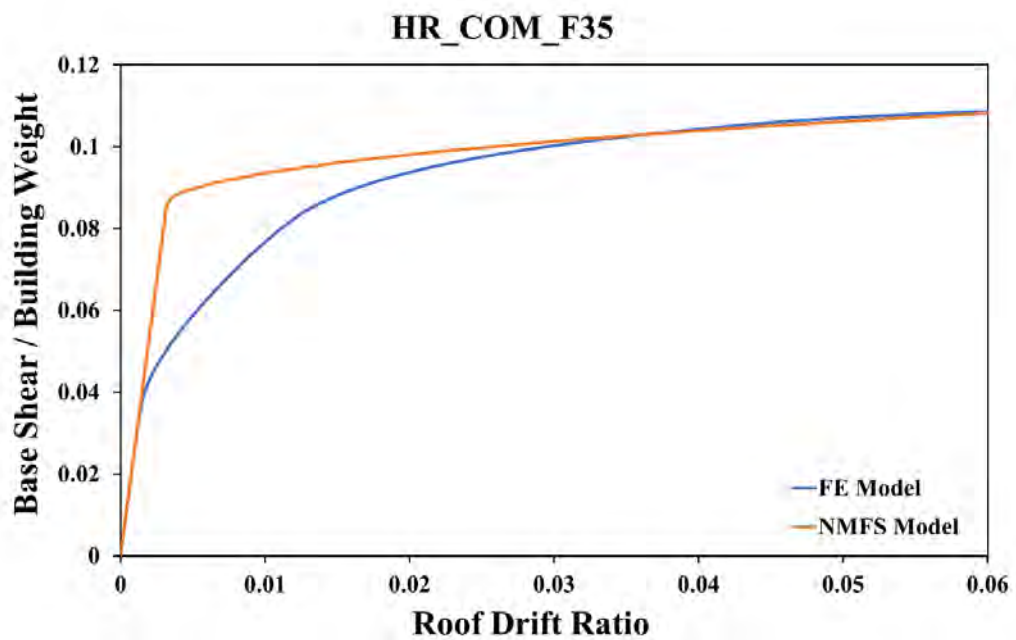
Figure 42: Detailed FE and NMFS models Pushover curves for "HR_COM_F35" archetype.
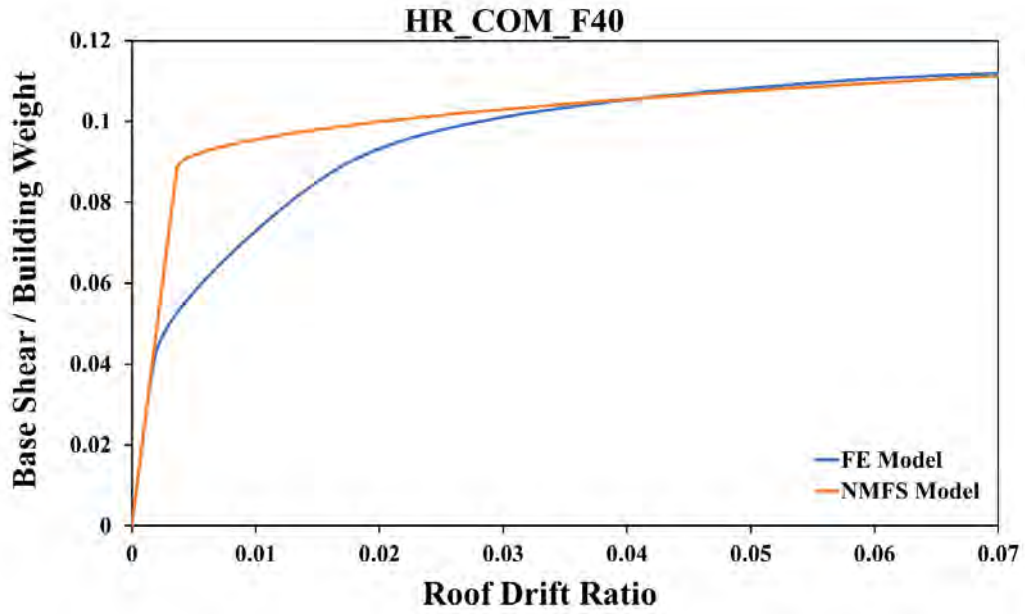
Figure 43: Detailed FE and NMFS models Pushover curves for "HR_COM_F40" archetype.
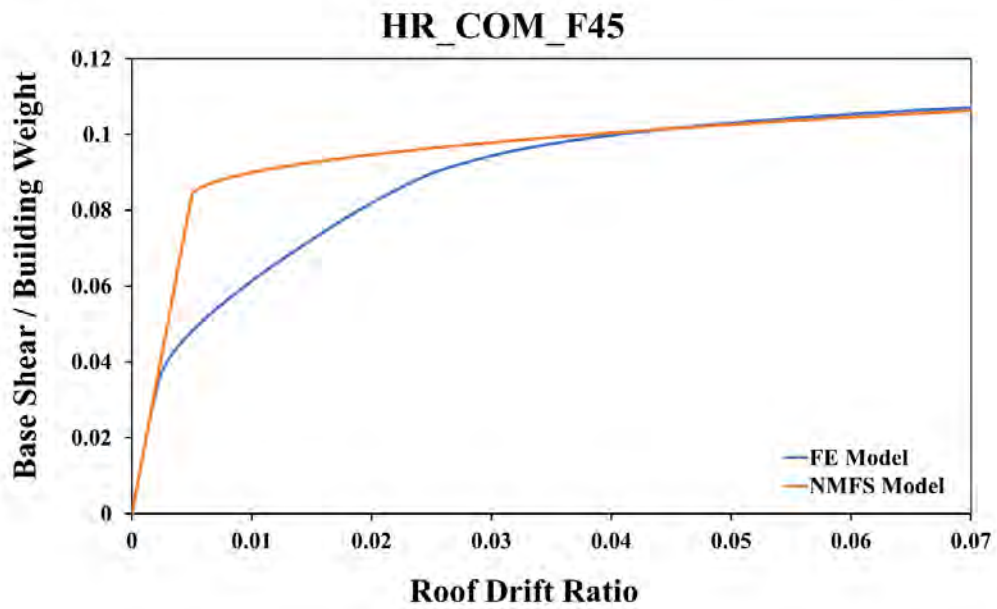
Figure 44: Detailed FE and NMFS models Pushover curves for "HR_COM_F45" archetype.
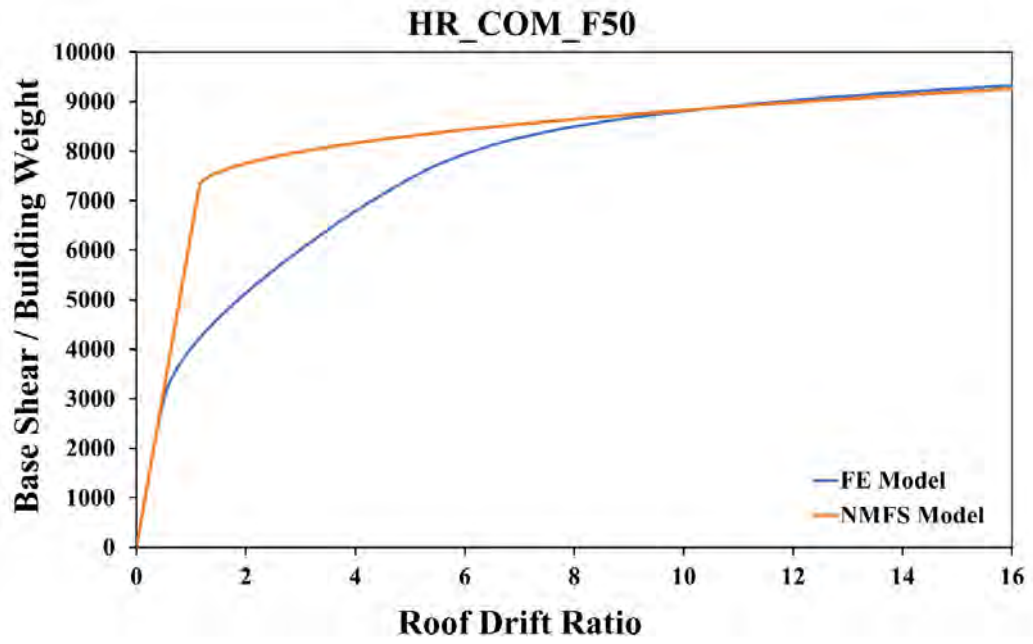
Figure 45: Detailed FE and NMFS models Pushover curves for "HR_COM_F50" archetype.

Table 21: Comparison among FE models and NFMS parameters.

Archetype		Peak Strength (KN)	Curve Area (KN.m)	No. FE Nodes	No. FE Elements	Time (milliseconds)	MSE
M1_10F_50RC	FE Model	4.6E+03	7.1E+03	440	440	6.32E+04	
	NFMS Model	4.7E+03	7.0E+03	11	20	1.92E+02	
	Relative Error	1.5E-02	-3.1E-03			3.04E-03	1.3E-03
M2_15F_50RC	FE Model	3.1E+03	7.0E+03	640	660	1.09E+05	
	NFMS Model	3.2E+03	7.1E+03	16	30	3.00E+02	
	Relative Error	2.3E-02	1.6E-02			2.75E-03	1.5E-03
M3_20F_50RC	FE Model	5.6E+03	2.0E+04	840	880	1.56E+05	
	NFMS Model	5.6E+03	2.0E+04	21	40	3.06E+02	
	Relative Error	-7.3E-03	-3.6E-03			1.96E-03	3.6E-03
M4_25F_60RC	FE Model	5.1E+03	2.3E+04	1040	1100	1.98E+05	
	NFMS Model	5.1E+03	2.3E+04	26	50	2.81E+02	
	Relative Error	-6.9E-03	1.3E-02			1.42E-03	3.9E-03
M5_30F_60RC	FE Model	5.3E+03	3.4E+04	1240	1320	2.83E+05	
	NFMS Model	5.3E+03	3.4E+04	31	60	3.27E+02	
	Relative Error	2.9E-05	1.6E-02			1.16E-03	4.0E-03
M6_35F_60RC	FE Model	7.3E+03	5.2E+04	1440	1540	4.24E+05	
	NFMS Model	7.2E+03	5.5E+04	36	70	4.62E+02	
	Relative Error	-3.0E-03	5.8E-02			1.09E-03	5.0E-03
M7_40F_70RC	FE Model	8.5E+03	8.1E+04	1640	1760	5.93E+05	
	NFMS Model	8.5E+03	8.6E+04	41	80	5.29E+02	
	Relative Error	-6.3E-03	6.0E-02			8.92E-04	4.9E-03
M8_45F_70RC	FE Model	9.2E+03	9.5E+04	1840	1980	6.78E+05	
	NFMS Model	9.1E+03	1.0E+05	46	90	5.06E+02	
	Relative Error	-7.6E-03	8.07E-02			7.47E-04	6.1E-03
M9_50F_70RC	FE Model	9.3E+03	1.22E+05	2040	2200	8.97E+05	
	NFMS Model	9.2E+03	1.32E+05	56	100	5.50E+02	
	Relative Error	-7.5E-03	7.88E-02			6.13E-04	5.7E-03

Appendix C

Table 22: Estimated loss results for overall Dubai's assets

Number of Assets	Parameter	Mean	σ	Min.	Max.
121871	Collapse probability (%)	3.571	-	0.000	60.000
	Total Repair Cost Ratio (%)	13.877	0.254	0.000	100.000
	(S) Repair Cost Ratio (%)	3.202	-	0.000	37.250
	(NSA) Repair Cost Ratio (%)	0.204	-	0.000	3.657
	(NSD) Repair Cost Ratio (%)	7.531	-	0.000	72.500
	Repair Time (Days)	21.833	51.693	0.000	407.400
	Injuries (SEV-1) (%)	0.948	-	0.000	37.700
	Injuries (SEV-2) (%)	0.357	-	0.000	17.980
	Injuries (SEV-3) (%)	0.073	-	0.000	4.356
	Injuries (SEV-4) (%)	0.146	-	0.000	8.706
	Total Injuries (%)	1.524	-	0.000	26.987

Table 23: Estimated loss results for different archetypes

Archetype Group	Number of Assets	Parameter	Mean	σ	Min.	Max.
RES (1-5)	53620	Collapse probability (%)	5.4845	-	0.000	60.000
		Total Repair Cost Ratio (%)	20.7564	0.3156	0.000	100.000
		(S) Repair Cost Ratio (%)	3.5388	-	0.000	25.448
		(NSA) Repair Cost Ratio (%)	0.0480	-	0.000	1.014
		(NSD) Repair Cost Ratio (%)	11.9226	-	0.000	72.500
		Repair Time (Days)	24.2823	56.4602	0.000	360.000
		Injuries (SEV-1) (%)	1.7562	-	0.000	37.700
		Injuries (SEV-2) (%)	0.6925	-	0.000	17.980
		Injuries (SEV-3) (%)	0.1480	-	0.000	4.356
		Injuries (SEV-4) (%)	0.2950	-	0.000	8.706
		Total Injuries (%)	2.8916	-	0.000	26.987
IND	1726	Collapse probability (%)	0	-	0.000	0.000
		Total Repair Cost Ratio (%)	26.0768	0.1344	0.000	40.715
		(S) Repair Cost Ratio (%)	14.5361	-	4.843	21.620
		(NSA) Repair Cost Ratio (%)	0.2153	-	0.000	0.280
		(NSD) Repair Cost Ratio (%)	11.3254	-	4.452	16.255
		Repair Time (Days)	222.5422	116.3931	0.000	348.000
		Injuries (SEV-1) (%)	4.4432	-	0.000	7.250
		Injuries (SEV-2) (%)	0.8762	-	0.000	1.450
		Injuries (SEV-3) (%)	0.0088	-	0.000	0.015
		Injuries (SEV-4) (%)	0.0088	-	0.000	0.015
		Total Injuries (%)	5.3369	-	1.786	8.016

COM (3-7)	30153	Collapse probability (%)	3.0624	-	0.000	40.000
		Total Repair Cost Ratio (%)	12.3864	0.2511	0.000	100.000
		(S) Repair Cost Ratio (%)	4.1303	-	0.000	37.250
		(NSA) Repair Cost Ratio (%)	0.0937	-	0.000	1.672
		(NSD) Repair Cost Ratio (%)	4.9967	-	0.000	41.025
		Repair Time (Days)	18.0647	47.4902	0.000	273.000
		Injuries (SEV-1) (%)	0.4367	-	0.000	14.861
		Injuries (SEV-2) (%)	0.1586	-	0.000	6.639
		Injuries (SEV-3) (%)	0.0325	-	0.000	1.533
		Injuries (SEV-4) (%)	0.0647	-	0.000	3.061
		Total Injuries (%)	0.6925	-	0.000	14.507
COM (10-20)	19200	Collapse probability (%)	2.0979	-	0.000	60.000
		Total Repair Cost Ratio (%)	6.0665	0.1556	0.000	100.000
		(S) Repair Cost Ratio (%)	2.0258	-	0.000	33.514
		(NSA) Repair Cost Ratio (%)	0.6571	-	0.000	3.657
		(NSD) Repair Cost Ratio (%)	4.2212	-	0.000	49.555
		Repair Time (Days)	15.6377	51.0589	0.000	407.400
		Injuries (SEV-1) (%)	0.0226	-	0.000	1.350
		Injuries (SEV-2) (%)	0.0032	-	0.000	0.270
		Injuries (SEV-3) (%)	0.0000	-	0.000	0.003
		Injuries (SEV-4) (%)	0.0000	-	0.000	0.003
		Total Injuries (%)	0.0258	-	0.000	0.641
COM (25-35)	8586	Collapse probability (%)	0.8269	-	0.000	40.000
		Total Repair Costs Ratio (%)	3.1758	0.0985	0.000	100.000
		(S) Repair Cost Ratio (%)	0.9314	-	0.000	23.777
		(NSA) Repair Cost Ratio (%)	0.4712	-	0.000	2.478
		(NSD) Repair Cost Ratio (%)	2.0363	-	0.000	40.000
		Repair Time (Days)	9.3575	30.9495	0.000	400.000
		Injuries (SEV-1) (%)	0.0042	-	0.000	0.403
		Injuries (SEV-2) (%)	0.0004	-	0.000	0.070
		Injuries (SEV-3) (%)	1.73E-06	-	0.000	0.001
		Injuries (SEV-4) (%)	1.73E-06	-	0.000	0.001
		Total Injuries (%)	0.0046	-	0.000	0.167
COM (40-50)	8586	Collapse probability (%)	0.1654	-	0.000	40.000
		Total Repair Cost Ratio (%)	1.8622	0.0658	0.000	100.000
		(S) Repair Cost Ratio (%)	0.4616	-	0.000	15.985
		(NSA) Repair Cost Ratio (%)	0.2873	-	0.000	1.676
		(NSD) Repair Cost Ratio (%)	1.1453	-	0.000	33.692
		Repair Time (Days)	5.7468	24.2888	0.000	328.500
		Injuries (SEV-1) (%)	0.0013	-	0.000	0.097
		Injuries (SEV-2) (%)	0.0001	-	0.000	0.010
		Injuries (SEV-3) (%)	1.46E-07	-	0.000	0.000
		Injuries (SEV-4) (%)	1.46E-07	-	0.000	0.000
		Total Injuries (%)	0.0014	-	0.000	0.043

Table 24: Estimated loss results for neighbor's classes

Neighbour Class	Number of Assets	Parameter	Mean	σ	Min.	Max.
Residential	105237	Collapse probability (%)	3.97408	-	0.000	60.000
		Total Repair Cost Ratio (%)	14.86016	0.2670	0.000	100.000
		(S) Repair Cost Ratio (%)	3.24054	-	0.000	25.448
		(NSA) Repair Cost Ratio (%)	0.18164	-	0.000	1.014
		(NSD) Repair Cost Ratio (%)	8.11268	-	0.000	72.500
		Repair Time (Days)	19.97349	51.9442	0.000	360.000
		Injuries (SEV-1) (%)	1.00249	-	0.000	37.700
		Injuries (SEV-2) (%)	0.39099	-	0.000	17.980
		Injuries (SEV-3) (%)	0.08310	-	0.000	4.356
		Injuries (SEV-4) (%)	0.16560	-	0.000	8.706
		Total Injuries (%)	1.64218	-	0.000	26.987
Commercial	13752	Collapse probability (%)	0.83770	-	0.000	0.000
		Total Repair Cost Ratio (%)	4.61879	0.1302	0.000	40.715
		(S) Repair Cost Ratio (%)	1.44486	-	4.843	21.620
		(NSA) Repair Cost Ratio (%)	0.38708	-	0.000	0.280
		(NSD) Repair Cost Ratio (%)	2.44312	-	4.452	16.255
		Repair Time (Days)	10.90260	32.8788	0.000	348.000
		Injuries (SEV-1) (%)	0.07446	-	0.000	7.250
		Injuries (SEV-2) (%)	0.02512	-	0.000	1.450
		Injuries (SEV-3) (%)	0.00506	-	0.000	0.015
		Injuries (SEV-4) (%)	0.01007	-	0.000	0.015
		Total Injuries (%)	0.11471	-	1.786	8.016
Industrial	2708	Collapse probability (%)	1.82422	-	0.000	40.000
		Total Repair Cost Ratio (%)	22.82854	0.2054	0.000	100.000
		(S) Repair Cost Ratio (%)	10.57043	-	0.000	37.250
		(NSA) Repair Cost Ratio (%)	0.16137	-	0.000	1.672
		(NSD) Repair Cost Ratio (%)	10.81302	-	0.000	41.025
		Repair Time (Days)	147.89089	98.7414	0.000	273.000
		Injuries (SEV-1) (%)	3.25084	-	0.000	14.861
		Injuries (SEV-2) (%)	0.72583	-	0.000	6.639
		Injuries (SEV-3) (%)	0.04215	-	0.000	1.533
		Injuries (SEV-4) (%)	0.07850	-	0.000	3.061
		Total Injuries (%)	4.09732	-	0.000	14.507
Unidentified	174	Collapse probability (%)	3.10345	-	0.000	60.000
		Total Repair Cost Ratio (%)	11.57281	0.1843	0.000	100.000
		(S) Repair Cost Ratio (%)	4.11806	-	0.000	33.514
		(NSA) Repair Cost Ratio (%)	0.11925	-	0.000	3.657
		(NSD) Repair Cost Ratio (%)	7.08645	-	0.000	49.555
		Repair Time (Days)	48.20813	50.2519	0.000	407.400
		Injuries (SEV-1) (%)	0.93075	-	0.000	1.350

Injuries (SEV-2) (%)	0.18842	-	0.000	0.270		
Injuries (SEV-3) (%)	0.00493	-	0.000	0.003		
Injuries (SEV-4) (%)	0.00812	-	0.000	0.003		
Total Injuries (%)	1.13221	-	0.000	0.641		

Table 25: Estimated loss results for different archetypes

Neighbour	Usage	Latitude	Longitude	Collapse probability (%)	Repair Cost Ratio (%)	Repair Time (Days)	Injuries
Jabal Ali Third	Residential	55.093	25.028	0.00	8.81	20.33	0.21
Nadd Shamma	Residential	55.384	25.217	0.00	7.95	28.63	1.62
Al Muteena	Commercial	55.323	25.274	0.00	2.41	2.96	0.00
Bu Kadra	Residential	55.326	25.177	9.64	18.39	24.09	2.00
EnKhali	Commercial	55.568	25.112	1.67	4.57	11.81	0.03
Warsan third	Residential	55.464	25.153	2.51	11.65	23.98	1.13
Ras Al Khor Ind. First	Residential	55.339	25.178	2.51	13.28	22.18	1.63
Grayteesah	Commercial	55.515	24.855	0.00	1.18	3.16	0.00
Hor Al Anz East	Commercial	55.347	25.283	0.00	1.53	5.86	0.00
Um Al Sheif	Residential	55.204	25.131	5.03	18.66	35.80	0.71
Muhaisneh 2nd	Commercial	55.422	25.264	1.67	10.39	26.63	0.25
Al yalayis 3	Commercial	55.346	24.973	0.00	0.96	2.65	0.01
Warsan first	Commercial	55.410	25.165	0.00	1.63	8.79	0.01
Margham	Residential	55.588	24.946	5.16	15.79	31.74	0.84
Saih Shuaib 3	Industrial	55.078	24.846	0.00	14.21	105.77	2.37
Al Qusais First	Commercial	55.372	25.278	0.00	9.23	12.30	0.83
Al Meryal	Residential	55.646	25.070	4.44	23.63	45.13	1.17
Remah	Commercial	55.671	24.838	0.00	6.89	28.00	0.03
Al Kifaf	Commercial	55.297	25.234	0.00	1.62	4.39	0.01
Saih Al Salam	Industrial	55.379	24.873	0.00	11.74	58.69	1.97
Ayal Nasir	Commercial	55.304	25.274	0.00	1.25	2.02	0.00
Oud Al Muteena Third	Commercial	55.448	25.275	3.33	7.97	12.27	0.10
Al Warqaa Second	Residential	55.409	25.203	6.70	13.01	8.60	0.90
Al Rega	Commercial	55.311	25.267	3.33	14.78	29.86	0.55
Umm Eselay	Commercial	55.598	24.866	5.00	8.87	16.10	0.09
Al Satwa	Commercial	55.273	25.220	0.00	2.81	8.52	0.03
Al Hathmah	Commercial	55.449	24.796	0.00	1.69	4.77	0.02
Al Murar	Commercial	55.310	25.277	5.00	12.37	22.52	0.28
Al Murqabat	Commercial	55.323	25.266	1.67	8.08	19.20	0.08
Al Qusais IND. First	Industrial	55.387	25.287	2.80	21.09	123.62	4.74
Al Barsha First	Commercial	55.195	25.111	0.00	4.11	16.24	0.04
Port Saeed	Commercial	55.333	25.251	0.00	4.91	20.03	0.02
Naif	Commercial	55.310	25.272	0.00	8.34	31.48	0.03
Al Rowaiyah first	Residential	55.431	25.126	4.21	9.91	17.38	0.21
Al Suq Al Kabeer	Commercial	55.294	25.262	0.00	1.79	4.20	0.00

139

Muhaisneh 5th	Industrial	55.433	25.279	6.67	37.96	202.47	6.72
Al Mezhar First	Residential	55.442	25.245	4.18	13.00	24.98	2.89
Al Hamriya Port	Industrial	55.333	25.298	0.75	19.77	125.34	4.02
Al Yufrah 2	Residential	55.379	24.978	0.00	6.06	19.20	0.27
Nad Al Shibba Third	Commercial	55.376	25.154	3.33	9.24	14.02	0.75
Wadi AlShabak	Industrial	55.484	25.176	3.85	27.41	180.74	4.27
Al Qouze IND. Third	Industrial	55.218	25.126	2.62	19.96	113.81	3.73
Lehbab First	Residential	55.608	25.060	1.65	15.79	33.90	0.93
Wadi Al Safa 5	Residential	55.352	25.078	7.66	22.56	2.84	2.20
Al Shandaga	Residential	55.289	25.267	10.60	20.59	11.71	2.76
Al Hamriya	Commercial	55.304	25.260	0.00	1.53	1.63	0.00
Oud al Muteena First	Commercial	55.445	25.264	6.67	8.42	1.86	0.11
Al Saffa First	Residential	55.238	25.176	0.00	5.85	20.70	0.12
Saih Al Dahal	Industrial	55.361	24.748	1.22	22.70	134.37	3.09
Al Layan 2	Commercial	55.156	24.750	0.00	1.16	3.19	0.01
Al Buteen	Commercial	55.300	25.269	1.67	8.61	10.56	0.82
Nadd Hessa	Industrial	55.386	25.122	2.08	30.22	207.12	6.09
Al Barsha Second	Residential	55.215	25.101	0.00	7.40	26.45	0.14
Jabal Ali IND. First	Industrial	55.124	24.999	0.00	10.27	65.44	1.29
Al Raffa	Commercial	55.288	25.254	0.00	1.82	3.25	0.01
Al Qusais IND. Fifth	Industrial	55.415	25.287	5.20	30.15	183.09	5.75
Mereiyeel	Commercial	55.512	25.099	0.00	1.52	4.60	0.01
Al Hebiah Third	Residential	55.260	25.020	0.00	7.54	14.98	1.56
Um Hurair First	Residential	55.312	25.254	2.53	8.98	15.30	0.64
Mirdif	Residential	55.422	25.223	4.17	21.62	28.21	2.48
Al Safouh Second	Commercial	55.162	25.104	1.67	5.17	14.49	0.03
Marsa Dubai	Commercial	55.139	25.080	0.00	4.80	14.33	0.06
Al Qouze IND. Second	Industrial	55.248	25.134	0.00	23.17	156.23	4.64
Al wasl	Residential	55.255	25.196	2.51	14.14	30.66	1.86
Al Karama	Commercial	55.305	25.245	1.67	5.97	12.31	0.22
Al Safouh First	Commercial	55.183	25.120	0.00	5.29	12.03	0.02
Wadi Al Safa 3	Residential	55.316	25.109	7.17	15.99	17.73	0.83
Al Layan 1	Commercial	55.122	24.793	0.00	0.30	1.13	0.00
Burj Khalifa	Commercial	55.272	25.187	0.00	0.84	3.52	0.01
Al Corniche	Residential	55.303	25.278	4.32	16.53	18.15	1.68
Mugatrah	Commercial	55.214	24.797	0.00	1.28	3.75	0.02
Al Thanyeh Third	Residential	55.166	25.085	5.02	13.76	32.61	0.53
Zaa'beel second	Residential	55.296	25.203	2.52	15.36	24.43	1.22
Corniche Deira	Commercial	55.318	25.287	0.00	0.97	0.87	0.00
Nakhlat Jumeira	Residential	55.134	25.117	0.00	12.24	25.89	1.53
Wadi Al Safa 6	Residential	55.272	25.051	0.00	2.54	9.65	0.03
Um Suqeim Second	Residential	55.204	25.151	4.18	8.74	12.40	0.25
Nakhlat Deira	Commercial	55.278	25.330	1.67	5.25	11.72	0.04
Al Selal	Commercial	55.276	24.891	0.00	0.26	0.15	0.00

Al Khairan Second	Industrial	55.364	25.192	1.33	16.00	105.68	2.41
Al yufrah 1	Commercial	55.433	25.002	0.00	2.12	7.86	0.00
Al Bada'	Commercial	55.269	25.225	0.00	1.52	5.76	0.02
Umm Nahad First	Commercial	55.385	25.064	0.00	1.09	1.92	0.00
Mushraif	Residential	55.450	25.211	4.34	11.58	9.45	0.90
Um Ramool	Residential	55.368	25.230	8.51	24.41	1.62	3.96
Saih Shuaib 1	Commercial	54.983	24.901	0.00	2.11	4.98	0.01
Al Hebiah fifth	Residential	55.239	25.008	9.18	13.90	13.19	0.64
Al Aweer First	Residential	55.572	25.199	0.00	6.50	19.42	0.05
Al Rowaiyah second	Commercial	55.398	25.105	0.00	0.89	4.15	0.00
Al Qusais IND. Second	Industrial	55.393	25.282	2.06	28.03	202.26	4.85
Um Suqaim Third	Residential	55.194	25.138	2.52	17.57	30.98	2.01
Al Khawaneej Second	Residential	55.521	25.231	8.40	17.79	35.95	0.31
Al Qusais Second	Commercial	55.387	25.269	16.67	22.87	9.34	0.75
Al Hebiah fourth	Residential	55.220	25.032	11.67	28.66	35.56	2.69
Al Qusais Third	Commercial	55.400	25.262	1.67	11.59	24.91	0.44
Al Ttay	Industrial	55.545	25.238	4.04	19.70	100.53	2.59
Ras Al Khor Ind. Second	Industrial	55.358	25.178	2.45	21.23	130.22	3.93
Saih Shuaib 2	Residential	55.059	24.870	2.51	11.82	17.87	1.78
Al Qouz Third	Commercial	55.241	25.160	0.00	2.69	5.96	0.02
Hor Al Anz	Commercial	55.337	25.277	0.00	3.91	5.66	0.37
Umm Nahad Second	Commercial	55.339	25.056	0.00	2.86	10.43	0.01
Al Qusais IND. Fourth	Industrial	55.400	25.294	4.49	29.37	164.51	4.58
Trade Center First	Commercial	55.279	25.219	0.00	1.00	3.00	0.01
Ras Al Khor IND. Third	Industrial	55.382	25.174	2.62	29.65	196.12	5.14
Al Yalayis 2	Residential	55.290	24.997	0.00	0.71	2.39	0.01
Yaraah	Commercial	55.672	24.762	0.00	2.78	7.63	0.02
Al Lesaily	Residential	55.445	24.919	0.00	3.69	16.18	0.15
Al Nahda Second	Residential	55.378	25.291	5.83	19.97	12.71	2.92
Al Hudaiba	Residential	55.279	25.243	4.18	10.46	13.74	0.71
Al Aweer Second	Residential	55.586	25.164	7.57	17.97	18.95	1.06
Al Twar Third	Residential	55.396	25.250	4.30	19.63	12.80	2.38
Al Garhoud	Residential	55.350	25.242	0.00	3.86	15.08	0.05
Al Hebiah Second	Commercial	55.246	25.035	0.00	1.53	6.65	0.02
Mankhool	Commercial	55.295	25.249	1.67	2.31	0.92	0.05
Wadi Alamradi	Residential	55.491	25.203	1.70	15.55	15.08	3.07
Al Khbeesi	Residential	55.338	25.269	1.69	13.87	19.34	1.98
Al Barsha South Fourth	Residential	55.209	25.058	1.67	8.19	25.00	0.14
Oud Metha	Commercial	55.312	25.238	1.67	3.92	9.18	0.02
Jumaira Third	Residential	55.229	25.183	0.00	2.86	10.05	0.03

141

Riggat Al Buteen	Commercial	55.319	25.259	0.00	1.59	3.90	0.00
Hadaeq Sheikh Mohammed Bin Rahisd	Residential	55.269	25.099	2.57	6.35	3.38	0.81
Zaa'beel first	Residential	55.305	25.224	1.69	19.34	20.86	3.56
Al Thanyah First	Residential	55.176	25.098	9.18	19.11	25.58	3.46
Al Qusais IND. Third	Industrial	55.392	25.297	2.04	29.30	166.13	5.24
Al Nahda First	Residential	55.364	25.290	2.50	12.71	17.35	1.62
Al Barsha South Fifth	Residential	55.187	25.045	2.52	17.07	27.34	3.43
Jabal Ali First	Commercial	55.133	25.034	0.00	2.54	7.33	0.02
Al Mezhar Second	Residential	55.460	25.243	2.51	12.27	19.49	3.56
Al Barsha South Third	Residential	55.237	25.061	0.00	7.77	26.53	0.31
Le Hemaira	Industrial	55.482	25.022	0.00	21.38	161.01	4.58
Muhaisanah Third	Residential	55.404	25.272	3.52	15.75	16.10	3.11
Warsan Second	Residential	55.437	25.159	9.59	16.21	15.95	0.80
Al Maha	Commercial	55.660	24.921	0.00	5.94	11.38	0.22
Al Warqaa Third	Residential	55.422	25.191	6.87	20.99	21.02	2.36
Margab	Residential	55.609	24.811	0.00	8.32	22.96	0.20
Al Manara	Residential	55.214	25.144	5.04	8.16	12.16	0.29
Umm Al Daman	Residential	55.457	25.060	5.30	13.82	25.04	3.25
Al O'Shoosh	Unidentified	55.355	24.683	6.21	13.58	41.84	1.32
Abu Hail	Commercial	55.329	25.285	0.00	1.58	5.86	0.01
Nad Al Shibba Second	Residential	55.348	25.159	2.59	12.78	12.65	1.27
Al Qouz Fourth	Residential	55.254	25.151	7.53	18.79	30.78	0.73
Al Wajeha Bahriah	Commercial	54.908	24.989	0.00	3.20	11.28	0.02
Hefair	Unidentified	55.250	24.694	0.00	9.56	54.58	0.94
Al Sabkha	Residential	55.302	25.269	2.53	8.95	15.59	0.58
Dubai International Airport	Commercial	55.368	25.252	1.67	5.65	12.81	0.03
Al Qouze IND Fourth	Industrial	55.233	25.116	0.00	18.94	146.37	3.07
Al Baraha	Commercial	55.320	25.281	0.00	2.33	9.15	0.01
Al Wohoosh	Commercial	55.623	25.119	3.33	11.94	27.81	0.04
Me'Aisem Second	Residential	55.218	24.996	2.65	14.49	31.75	0.25
Nazwah	Residential	55.647	25.024	2.65	10.14	20.67	3.20
AL Mamzar	Residential	55.349	25.296	2.51	16.06	12.67	3.18
AL Hebiah First	Residential	55.238	25.047	0.00	13.01	26.46	1.09
Wadi Al Safa 4	Commercial	55.318	25.077	0.00	3.90	8.73	0.23
Al Khairan First	Commercial	55.353	25.200	0.00	1.67	5.41	0.01
Hatta	Residential	56.135	24.809	5.00	25.00	36.57	1.40
Al Marmoom	Residential	55.452	24.976	6.02	14.82	25.06	1.12
Al warqaa fourth	Residential	55.437	25.186	3.34	16.40	8.83	3.50
Mena Jabal Ali	Commercial	55.077	24.974	0.00	0.66	3.08	0.01
Jabal Ali IND third	Industrial	55.057	24.921	0.00	21.29	156.83	4.85

Al Ayas	Residential	55.537	25.211	2.65	10.53	22.70	0.31
Al Twar Second	Residential	55.382	25.261	4.17	18.29	16.44	2.03
Madinat Dubai Al Melahiyeh	Commercial	55.272	25.267	0.00	1.39	3.46	0.00
Al Jadaf	Commercial	55.328	25.216	3.33	8.51	14.24	0.26
Wadi Al Safa 7	Residential	55.286	25.040	0.00	5.00	13.91	0.07
Warsan Fourth	Residential	55.403	25.142	5.06	8.49	8.57	0.47
Wadi Al Safa 2	Residential	55.353	25.100	4.18	21.74	14.32	4.09
Dubai Investment Park First	Commercial	55.165	24.988	1.67	3.78	8.72	0.03
Al Thanyah Fourth	Commercial	55.174	25.063	0.00	5.18	11.48	0.41
Al Yalayis 5	Commercial	55.266	24.972	0.00	1.12	3.44	0.01
Nakhlat Jabal Ali	Commercial	54.989	25.008	1.67	6.49	15.11	0.12
Me'aisem First	Residential	55.188	25.020	5.00	12.61	18.54	0.87
Al Waheda	Commercial	55.337	25.291	0.00	1.79	5.99	0.00
Jumeira Island Second	Residential	55.227	25.206	4.44	20.75	9.74	3.88
Umm Al Mo'meneen	Commercial	55.512	24.991	0.00	1.47	5.79	0.01
Muhaisna First	Residential	55.417	25.244	6.70	15.75	21.36	1.05
Madinat al Matar	Commercial	55.154	24.906	0.00	0.87	1.65	0.00
Nad Al Shiba First	Residential	55.316	25.147	0.00	4.41	14.29	0.04
Hessyan First	Residential	55.022	24.957	2.53	9.68	9.37	2.01
Al Rass	Commercial	55.295	25.268	0.00	2.67	6.14	0.01
Al Qouz Second	Residential	55.271	25.152	2.52	8.14	15.84	0.28
Trade Center Second	Commercial	55.287	25.223	0.00	1.32	2.96	0.01
Al Warqaa fifth	Commercial	55.454	25.180	1.67	10.91	24.88	0.29
Al Fagaa'	Residential	55.533	24.733	6.99	27.74	42.18	1.92
Umm Nahad Third	Residential	55.403	25.027	5.98	13.90	20.08	0.89
Dubai Investment Park Second	Commercial	55.210	24.974	0.00	0.55	1.94	0.01
Al Dhagaya	Commercial	55.300	25.273	0.00	0.63	0.90	0.00
Jumeira Second	Residential	55.242	25.200	0.00	10.22	28.75	0.15
Al Saffa Second	Residential	55.225	25.160	2.51	6.09	17.00	0.27
Al Thanyah Second	Residential	55.191	25.080	1.69	11.62	13.44	3.50
Al Twar First	Residential	55.363	25.272	3.50	24.28	33.89	3.18
Al Yalayis 1	Residential	55.310	25.018	5.20	11.43	19.59	0.28
Al Merkadh	Residential	55.291	25.170	6.77	18.56	44.23	0.55
Al Kheeran	Residential	55.360	25.218	2.53	6.34	13.21	0.06
Al Warqaa first	Residential	55.403	25.188	5.00	18.71	16.93	1.28
Jabal Ali Second	Residential	55.115	25.054	2.57	13.86	22.21	2.16
Al Qouze IND. First	Industrial	55.232	25.144	0.74	19.05	137.07	3.82
Al Jafliya	Residential	55.287	25.238	0.00	11.50	28.30	1.80
Ghadeer Barashy	Commercial	55.323	24.806	0.00	0.76	1.40	0.00
Al Barsha Third	Residential	55.199	25.092	0.00	7.95	22.42	0.38

Al Thanyah fifth	Residential	55.154	25.053	10.85	27.68	21.83	4.64
Saih Shuaib 4	Residential	55.096	24.824	0.00	7.45	18.74	0.30
Umm Suqeim First	Residential	55.216	25.166	1.67	6.94	12.34	0.38
Al Khawaneej First	Residential	55.487	25.245	4.18	13.94	9.72	1.71
Saih Shua'alah	Commercial	55.423	24.668	0.00	2.81	8.85	0.02
Nad Al Hamar	Commercial	55.386	25.198	0.00	3.81	10.58	0.05
Al Rowaiyah third	Residential	55.464	25.116	6.70	11.74	20.52	0.36
Al Barsha South Second	Residential	55.233	25.074	0.00	6.94	21.49	0.24
Al Barsha South First	Residential	55.231	25.087	0.00	7.30	29.46	0.30
Muhaisanah Fourth	Residential	55.409	25.279	1.33	16.31	12.03	1.61
Um Hurair second	Residential	55.324	25.236	4.21	9.85	13.54	0.08
Oud al Muteena second	Residential	55.464	25.264	7.82	20.79	7.87	3.10
Hessyan Second	Residential	54.964	24.936	13.98	18.47	13.57	0.60
Umm Nahad Fourth	Industrial	55.349	25.025	0.80	28.92	204.46	5.10
Jumeira First	Residential	55.258	25.221	7.53	13.72	12.49	0.61
Lehbab Second	Residential	55.572	25.025	2.55	7.47	11.96	0.26
Ras Al Khor	Residential	55.327	25.193	6.99	21.97	25.83	1.70
Al yalayis 4	Industrial	55.320	24.966	1.20	17.12	121.33	2.96
Nad Al Shibba Fourth	Residential	55.364	25.136	7.47	19.23	25.89	2.19
Al Rashidiya	Commercial	55.392	25.224	1.67	7.96	20.06	0.23
Al Qouz first	Commercial	55.253	25.169	1.67	7.83	14.79	0.08
Jabal Ali IND. Second	Industrial	55.105	24.955	0.73	24.79	189.38	4.52

Vita

Ahmed Mansour Maky was born in 1993, in Aswan, Egypt and he also received his primary and secondary education there. He received his B.Sc. degree in Civil Engineering Engineering from Aswan University in 201. From 2019 to 2020, he worked as a Research and Development Engineer in Elibre DMCC, Cairo.

In September 2020, he joined the Civil Engineering master's program in the American University of Sharjah as a graduate research and teaching assistant. During his master's study, he co-authored 3 papers that were presented in international conferences and journals. His research interests are in (e.g.Finite Elements Analysis, Computational Science and Earthquake Engineering).